Université de Sherbrooke

Évaluation du potentiel radiosensibilisateur ou radioprotecteur/antioxydant de quelques composés sélectionnés par dosimétrie par gel de polyacrylamide et dosimètre de Fricke, et utilisation de la filamentation par impulsion laser infrarouge femtoseconde comme un nouveau et puissant faisceau pour la radiothérapie du cancer

Par

Ridthee MEESAT
Département de médecine nucléaire et de radiobiologie

Thèse présentée à la Faculté de médecine et des sciences de la santé
en vue de l'obtention du grade de philosophiae doctor (Ph.D.)
en Sciences des radiations et imagerie biomédicale
Sherbrooke (Québec) J1H 5N4, Canada

Mars 2012

Membres du jury d'évaluation

Pr Léon Sanche	*Président,* Département de médecine nucléaire et radiobiologie, Faculté de médecine et des sciences de la santé, Université de Sherbrooke
Pr Kim B. McAuley	*Examinateur,* Department of chemical engineering, Faculty of engineering and applied science, Queen's University
Pr Yue Zhao	*Examinateur,* Département de chimie, Faculté des sciences, Université de Sherbrooke
Pr Daniel Houde	*Examinateur,* Département de médecine nucléaire et radiobiologie, Faculté de médecine et des sciences de la santé, Université de Sherbrooke
Pr Martin Lepage	*Directeur de recherche*, Département de médecine nucléaire et de radiobiologie, Faculté de médecine et des sciences de la santé, Université de Sherbrooke
Pr Abdelouahed Khalil	*Directeur de recherche*, Département de médecine (Service de gériatrie), Faculté de médecine et des sciences de la santé, Université de Sherbrooke
Pr Jean-Paul Jay-Gerin	*Directeur de recherche*, Département de médecine nucléaire et radiobiologie, Faculté de médecine et des sciences de la santé, Université de Sherbrooke

Library and Archives Canada

Published Heritage Branch

395 Wellington Street
Ottawa ON K1A 0N4
Canada

Bibliothèque et Archives Canada

Direction du Patrimoine de l'édition

395, rue Wellington
Ottawa ON K1A 0N4
Canada

Your file Votre référence
ISBN: 978-0-494-89650-1

Our file Notre référence
ISBN: 978-0-494-89650-1

Abstract

Evaluation of the radiosensitizing or radioprotective/antioxidant potential of some selected compounds by polyacrylamide gel dosimetry and Fricke dosimeter, and utilization of the femtosecond infrared laser pulse filamentation as a novel, powerful beam for cancer radiotherapy

by

Ridthee MEESAT

Département de médecine nucléaire et radiobiologie
Faculté de médecine et des sciences de la santé, Université de Sherbrooke
Sherbrooke (Québec) J1H 5N4, Canada

Thesis submitted to the Faculty of Medicine and Health Sciences for the Degree of Philosophiae Doctor (Ph.D.) in Radiation Sciences and Biomedical Imaging

In radiation treatment, a sufficiently high radiation dose must be delivered to the tissue volumes containing the tumor cells while the lowest possible dose should be deposited in surrounding healthy tissue. We developed an original approach that is fast and easy to implement for the early assessment of the efficiency of radiation sensitizers and protectors. In addition, we characterized a new femtosecond laser pulse irradiation technique. We are able to deposit a considerable dose with a very high dose rate inside a well-controlled macroscopic volume without deposition of energy in front or behind the target volume.

The radioprotective efficiency was measured by irradiation of the Fricke solution incorporating a compound under study and measuring the corresponding production of ferric ions $G(Fe^{3+})$. The production of ferric ions is most sensitive to the radical species produced in the radiolysis of water. We studied experimentally and simulated with a full Monte-Carlo computer code the radiation-induced chemistry of Fricke/cystamine solutions. Results clearly indicate that the protective effect of cystamine originates from its radical-capturing ability, which allows this compound to compete with the ferrous ions for the various free radicals – especially $^{\bullet}OH$ radicals and $H^{\bullet}$ atoms – formed during irradiation of the surrounding water.

The sensitizing capacity of radiation sensitizers was measured by irradiation of a polyacrylamide gel (PAG) dosimeter incorporating a compound under study and measuring the corresponding increase in the gradient between spin-spin relaxation rate (R_2) and absorbed dose. We measured an irradiation energy-dependent increase in R_2-dose sensitivity for halogenated compounds or a decrease for radioprotectors.

Finally, we studied a novel laser irradiation method called "filamentation". We showed that this phenomenon results in an unprecedented deposition of energy and the dose rate thus achieved exceeds by orders of magnitude values previously reported for the most intense clinical radiotherapy systems. Moreover, the length of the dose-free entrance region was adjusted by selecting the duration of femtosecond laser pulses. In addition, we provided evidence that the biological damage caused by this irradiation was similar to other ionizing radiation sources.

Keywords: Radiotherapy, radiosensitization, radioprotection, laser, filamentation, dosimetry

Résumé

Évaluation du potentiel radiosensibilisateur ou radioprotecteur/antioxydant de quelques composés sélectionnés par dosimétrie par gel de polyacrylamide et dosimètre de Fricke, et utilisation de la filamentation par impulsion laser infrarouge femtoseconde comme un nouveau et puissant faisceau pour la radiothérapie du cancer

par

Ridthee MEESAT

Département de médecine nucléaire et radiobiologie
Faculté de médecine et des sciences de la santé, Université de Sherbrooke
Sherbrooke (Québec) J1H 5N4, Canada

Thèse présentée à la Faculté de médecine et des sciences de la santé en vue de l'obtention du grade de Philosophiae Doctor (Ph.D.) en Sciences des radiations et imagerie biomédicale

La radiothérapie repose essentiellement sur le dépôt d'une dose de radiation létale suffisamment élevée à un volume tumoral, tout en minimisant celle délivrée aux tissus sains environnants. Ainsi, une approche originale a été développée, permettant l'évaluation simple et rapide de l'efficacité de composés ayant des propriétés radiosensibilisatrices ou radioprotectrices. En parallèle à cette étude, nous nous sommes intéressés à la caractérisation d'une nouvelle technique d'irradiation utilisant des impulsions laser femtosecondes. Nous avons démontré le dépôt d'une dose considérable avec un débit de dose très élevé au sein d'un volume bien déterminé, sans dépôt d'énergie en amont et en aval du volume cible.

L'efficacité de la radioprotection a été mesurée à l'aide du dosimètre de Fricke via le rendement de production en ions ferrique $G(Fe^{3+})$. Ce dernier est particulièrement sensible aux espèces radicalaires produites au cours de la radiolyse de l'eau. Ainsi, le rendement $G(Fe^{3+})$ dans une solution de Fricke diminue en présence de radioprotecteurs. Sur ce principe, nous étudié expérimentalement et nous avons développé un code Monte-Carlo pour comprendre le mécanisme d'action de la cystamine, un radioprotecteur bien connu.

L'action de radiosensibilisateurs peut être mesurée par la variation du gradient du taux de relaxation spin-spin (R_2) en fonction de la dose absorbée. La présente étude repose sur l'utilisation du dosimètre à gel de polymère afin d'estimer quantitativement les capacités d'ions halogénures et de la thiourée à titre respectivement de radiosensibilisateurs et de radioprotecteur. Nous avons mesuré une dépendence énergétique de la sensibilité R_2-dose.

Parallèlement, nous avons étudié le processus de filamentation laser comme une nouvelle source d'irradiation. Il en résulte un dépôt d'énergie considérable et un débit de dose qui surpasse de plusieurs ordres de grandeurs les valeurs précédemment rapportées pour les systèmes de radiothérapie clinique les plus intenses. De plus, il est possible d'ajuster la longueur de la zone libre de tout dépôt de dose à l'entrée du milieu irradié en jouant sur la durée de l'impulsion laser femtoseconde incidente. Finalement, nous nous sommes efforcés d'établir l'équivalence d'un point de vue radiobiologique (dommages induits à un système d'intérêt biologique) entre ce type d'irradiation et d'autres sources de radiations ionisantes plus conventionnelles.

Mots-clés: Radiothérapie, radiosensibilisation, radioprotection, laser, filamentation, dosimétrie

การประเมินศักย์ภาพทางการเพิ่มประสิทธิภาพรังสี การปกป้องรังสีและการต้านอนุมูลอิสระของสารประกอบบางชนิดด้วยระบบการวัดรังสีแบบโพลีอะครีลาไมด์เจลและมาตรวัดรังสีแบบฟริกกี และการใช้วิธีการแบบใหม่ของเฟมโตเซกันอินฟาเรดเลเซอร์พลัสฟิลาเมนต์เตชั่นสำแสงสมรรถณะสูงสำหรับรังสีรักษามะเร็ง

โดย

นายฤทธี มีสัตย์

Département de médecine nucléaire et de radiobiologie, Faculté de médecine et des sciences de la santé, Université de Sherbrooke, Sherbrooke (Québec) J1H 5N4, Canada

วิทยานิพนธ์นี้เป็นส่วนหนึ่งของการศึกษาระดับปริญญาดุษฎีบัณฑิต (Ph.D.) สาขา Radiation Sciences and Biomedical Imaging ของคณะ Medicine and Health Sciences

ในการรักษามะเร็งด้วยรังสี ปริมาณรังสีที่ใช้ในตำแหน่งเนื้อเยื่อที่เป็นมะเร็งจะต้องสูงเพียงพอต่อการทำลายเซลล์มะเร็ง ในขณะที่จะต้องควบคุมปริมาณรังสีที่ตำแหน่งเนื้อเยื่อปกติให้ได้รับปริมาณรังสีที่น้อยที่สุดเท่าที่จะเป็นไปได้ สารเพิ่มประสิทธิภาพรังสีและสารปกป้องอันตรายรังสีมีความสำคัญในการรักษามะเร็งด้วยรังสี ในวิทยานิพนธ์นี้ได้พัฒนาวิธีการแบบใหม่ที่สะดวกและรวดเร็วในการประเมินประสิทธิภาพของสารเพิ่มประสิทธิภาพรังสีและสารปกป้องรังสี นอกจากนี้ในการศึกษานี้ได้ทำการศึกษาลักษณะเฉพาะของเทคนิคใหม่ของการฉายรังสีด้วยเทคนิคเฟมโตเซกันอินฟาเรดเลเซอร์พลัสฟิลาเมนต์เตชั่น ด้วยวิธีการนี้เราสามารถที่จะส่งปริมาณรังสีที่มีอัตราปริมาณรังสีสูงไปยังตำแหน่งเป้าหมายในตัวกลาง โดยปราศจากพลังงานที่ถ่ายเทให้กับตัวกลางที่ตำแหน่งด้านหน้าและหลังของตำแหน่งเป้าหมาย

ประสิทธิภาพของสารปกป้องรังสีสามารถวัดได้ด้วยการใช้มาตรวัดรังสีแบบฟริกกี โดยพิจารณาจากผลผลิตของเฟอริกไอออน ($G(Fe^{3+})$) ภายหลังจากการฉายรังสีสารละลายฟริกกี ที่มีสารปกป้องรังสีผสมอยู่แล้ว ปริมาณของเฟอริกไอออนขึ้นอยู่กับอนุมูลอิสระทั้งหลายที่เกิดขึ้นจากกระบวนการสลายตัวของน้ำโดยใช้รังสี การวิจัยนี้ได้ใช้ทั้งการทดลองและการใช้แบบจำลอง Monte-Carlo คอมพิวเตอร์ เพื่อใช้ศึกษาประสิทธิภาพของสารซีสตามีน (cystamine) ในสารละลายฟริกกี ผลการศึกษาได้แสดงให้เห็นอย่างชัดเจนว่า ประสิทธิภาพการปกป้องรังสีของสารนี้เป็นผลมาจากการความสามารถในการทำปฏิกิริยากับอนุมูลอิสระ ซึ่งสารซีสตามีนสามารถแข่งขันกับเฟอร์รัสไอออนเพื่อทำปฏิกิริยากับอนุมูลอิสระทั้งหลายโดยเฉพาะอย่างยิ่ง $^{\bullet}OH$ และ $H^{\bullet}$ ที่เกิดจากกระบวนการสลายตัวของน้ำด้วยรังสี

การประเมินขีดจำกัดของสารเพิ่มประสิทธิภาพรังสีสามารถวัดได้จากการใช้มาตรวัดรังสีแบบโพลีอะครีลาไมด์เจล โดยพิจารณาจากการเปลี่ยนแปลงของความชันของความสัมพันธ์เชิงเส้นระหว่างค่าการผ่อนคลายแบบสปินสปิน (spin-spin relaxation หรือ R_2) กับปริมาณรังสี ภายหลังจากการฉายมาตรวัดรังสีโพลีอะครีลาไมด์เจล (PAG) ที่มีสารเพิ่มประสิทธิภาพผสมอยู่แล้ว ในการศึกษานี้เราสามารถวัดการเพิ่มขึ้นของความชัน (R_2-dose sensitivity) สำหรับสารประกอบของไอโอดีนทั้งหลาย และการลดลงของความชันสำหรับสารปกป้องรังสี

สุดท้ายในวิทยานิพนธ์นี้ได้ศึกษาวิธีการฉายรังสีแบบใหม่โดยใช้เลเซอร์ที่เรียกว่า "ฟิลาเมนต์เตชั่น (filamentation)" ในการศึกษานี้ได้แสดงให้เห็นแล้วว่าปรากฏการณ์นี้ก่อให้เกิดพลังงานที่ถ่ายเทกับตัวกลางด้วยอัตราปริมาณที่สูงมากกว่าที่เคยใช้ในรังสีรักษามาก่อน มากกว่านั้นด้วยการฉายรังสีแบบนี้ยังปราศจากพลังงานที่ถ่ายเทให้กับตัวกลางทั้งทางด้านหน้าและด้านหลังของตำแหน่งเป้าหมายที่ฉายรังสีอีกด้วย น้องจากนี้งานวิจัยนี้ได้แสดงหลักฐานความเสียหายทางด้านชีววิทยาของการฉายรังสีด้วยเลเซอร์นี้คล้ายกันกับการความเสียหายที่เกิดจากรังสีก่อไอออนทั้งหลายอีกด้วย

Table of contents

List of illustrations (Tables and Figures)

Acronyms, abbreviation and symbols

e^-_{aq}	Hydrated electron
ΔE_{ab}	Absorption energy
ΔE_l	Lost energy
ΔE_{tr}	Transfer energy
ΔX	Thickness
AA	Acrylamide
BIS	*N,N'*-methylene-bis-acrylamide
BNCT	Boron-neutron capture therapy
C	Molar concentration
CEDR	Ceric effective dose rate
CF	Conversion factor
CNS	Central nervous system
DER	Dose enhancement ratio
DNA	Deoxyribonucleic acid
DSB	Double stand break
E	Energy
EDR	Effective microscopic dose rate
ET	Effective time
eV	Electronvolt
fs	Femto-second
***g*(X)**	calculation 100-eV yield of the final product X
***G*(X)**	Experimental 100-eV yield of the final product X
G_x	Primary yield of radiolytic species X
HPLC	High-performance liquid chromatography
I_0	Incident intensity
ICA	Iodinated contrast agent
IR	Infrared
IRT	Independent reaction times

I_X	Transmitted intensity
k	Rate constant reaction
keV	Kilo-electronvolt
LEE	low-energy secondary electron
LET	Linear energy transfer
MC7-L1	Mouse mammary carcinoma cell
MeV	Mega-electronvolt
molec./100 eV	Molecule/100 eV
MRI	Magnetic resonance imaging
NaX	Sodium halides (X= Cl, Br, I)
OD	Optical density
PAG	Polyacrylamide gel dosimeter
R_2	Spin-spin relaxation rate
ROI	Region of interest
RSSR	Cystamine
SEM	Standard error of mean
SSB	Single stand break
T_2	Spin-spin relaxation time
THPC	Tetrakis (hydroxymethyl) phosphonium chloride
X-ray	X radiation
Z	Atomic number
Z_x	Projectile charge number
ε	Molar extinction coefficient
α	Alpha particle
γ	Gamma radiation
μ	Linear attenuation coefficient
ρ	Density
$\frac{\mu}{\rho}$	Mass attenuation coefficient

I. Introduction

I. 1. Interaction of the photons

Radiation therapy is the most widely used modern cancer treatment and continues to play a major role in the management of an array of potentially curable malignancies (IAEA, 2008). It is vital to deliver the highest radiation dose to the tumor volume while sparing surrounding normal tissues. This is an important challenge to modern radiotherapy since high-energy photons result in a significant entrance dose in front of the tumor and a non-negligible exit dose behind the tumor. Unfortunately, conventional radiation sources (γ or X rays, electrons) used over the decades, even with methods using multiple or modulated beams, inevitably deposit the majority of their dose in front or behind the tumor, thereby damaging healthy tissue, and causing secondary cancers years after treatment (Hall and Phill, 2006).

Radiation-sensitizers and radioprotectors are staring to play an important role in clinical radiotherapy (Wardman 2007; Nair et al., 2001). Antioxidants have been shown to prevent diseases and promote health (Garewal, 1997; Valko et al., 2007). It is therefore important to understand the mechanisms of action of such compounds at the chemical level in order to help better control and optimize their biological effects. For example, a chemical compound designed at protecting DNA from radiation damage needs not only to reach its cellular target location but also retain its radioprotecting activity to produce an effective response. Using clonogenic assays, the radiation survival of cells can be measured, but this only provides information on the addition of these two properties. If a compound proves to be less effective than anticipated, is it because it is in fact not a good radioprotector, or is it that it did not reach its target location? This project aims at characterizing compounds at the molecular or chemical level, such that this information can aid in the design and the optimization of compounds that will be therapeutically useful *in vivo*.

Radiosensitizers are intended to enhance tumor cell killing while having much less effect on normal tissues. Chemical radioprotectors are, of course, the reverse of radiosensitizers: the aim is to decrease radiosensitivity, especially of normal tissues.

(Dunne-Daly, 1999). Thus, it is important to understand their interaction with ionizing radiation.

When an ionizing radiation interacts with biological systems or other absorbing matter, a complex series of events takes place as shown in Figure 1. (Alpen, 1998). Typically, absorption of radiation is characterized by an energy transfer from the radiation beam to the medium (Anderson, 1984). The absorption of photon arises from the interaction of the radiation with electrons of the absorber molecule (Bensasson, 1993). In fact, ionizing radiations can be divided into "*direct ionizing radiations*" and "*indirect ionizing radiations*". The former are charged particles such as electrons, protons and alpha particles which can ionize by means of particle to particle Coulomb forces. The latter are uncharged species, such as electromagnetic radiations (*e.g.*, gamma and X-ray) and neutrons which can release energetic charged particles after interaction (Anderson, 1984). Ionization depends on the energy of these radiations. For photons, the energy must exceed the lower limit for ionization (or "ionization potential"). The ionization potential is the minimum energy required to eject an electron from an atom or molecule, values for selected compounds are shown in Table 1.

Table 1. Ionization potentials of selected molecules (Anderson, 1984)

Molecule	Ionization potential (eV)	Molecule	Ionization potential (eV)
H_2	15.4	CO_2	13.8
N_2	15.6	CH_4	13.0
O_2	12.1	C_2H_4	10.5
H_2O	12.6	C_6H_6	9.3

The probability of ionization depends on the photon energy as well. However, a large ionization potential is not necessarily found whenever the available energy exceeds the ionization potential. In general, the probability of ionization is described by an "*interaction coefficient*" or a "*cross section*", which is discussed later in the section.

In case of photon interaction, the photon energy ($E = h\nu$, h is Planck's constant (6.626×10^{-34} Js and ν is the light frequency) is converted into kinetic energy of high speed charged particles (electron or positrons), whereas some part of this energy is radiated from the medium as scattering radiation (Johns and Cunningham, 1969; Alpen, 1998).

When a radiation beam passes though biological materials or other absorbing media, energy is lost from the incident beam. The radiation can transfer energy to an absorber; this energy is called energy transferred (ΔE_{tr}). The medium absorbs some part of the radiation energy, which is called energy absorbed (ΔE_{ab}), while some of it leaves the volume of interaction which is called energy lost (ΔE_l). The total energy transfer is the sum of energy absorbed and energy lost as follows: (Alpen, 1998).

$$\Delta E_{tr} = \Delta E_{ab} + \Delta E_l.$$

The three main interactions of photons play an important role: *photoelectric effect*, *Compton scattering effect* and *pair production*. All these processes result in the partial or complete transfer of the photon energy to electron energy (Knoll, 2000). The fundamentals of the photon interaction are shown in Figure 2. Absorption of the ionizing radiation by matter follows the fundamental Lambert-Beer law (Hughes, 1973).

$$I_x = I_0 e^{-\mu x},$$

where I_0, I_x are the intensities of the incident and transmitted radiation respectively, x is the thickness of the absorber and μ is the linear attenuation coefficient (see Figure 2). In general, the thickness of the absorber is in cm, μ will be expressed in cm^{-1}. Thus, the linear attenuation coefficient depends on the density of the attenuator. The coefficient is expressed in terms of a mass attenuation coefficient ($\frac{\mu}{\rho}$), where ρ is the density of the material. The total attenuation coefficient is the sum of the coefficients for the three interactions. Figure 3 shows the total mass attenuation coefficient of H_2O, Br and I as a function of the photon incident energy (Hubbell and Seltzer, 2010).

Photoelectric effect

In the photoelectric effect, the entire energy of the ionizing photon (*e.g.* X-ray or gamma radiation) is transferred to an orbital electron of an atom with the consequent ejection of the electron which is then called photoelectron, typically from the K-shell (Johns and Cunningham, 1969; Hughes, 1973; Alpen, 1998; Knoll, 2000). In this case, the incoming photon disappears and the photoelectron is ejected from its orbital position. Interactions of this kind may occur with electrons in the K, L or M shell as well. The energy of the incoming radiation must be equal to or exceed the binding energy or absorption edges of the electron in the atom. The binding energies range from ~100 eV for low atomic weight absorbers to ~100 keV for high atomic weight absorbers. The photo interaction leads to a vacancy of an inner electronic orbital of the atom. This vacancy is quickly filled by an outer electron of the atom. With this process, the outer electron transfers excess energy by emitting a photon called a characteristic X-ray (or "fluorescent X-ray"). Similarly, this X-ray can eject other orbital electrons, and so on. The phenomenon is known as the "Auger effect" which is characterized by an electron avalanche or an Auger electron cascade sequence. The photoelectric interaction is the predominant mode of interaction for photon radiation (gamma rays or X-rays) of relatively low energy. The effect can be enhanced for absorber materials of high atomic number (Z) (Johns and Cunningham, 1969; Knoll, 2000).

Thus, at energies above the lowest absorption edge of an atom, photoelectric absorption leads to additional photoelectric effect, this ultimately results in the production of a photoelectron, characteristic X-ray photons, and Auger electrons. In the photoelectric interaction, the process leads to increase radiation absorbed dose in the medium (Johns et al., 1954; Murthy et al., 1976; Fairchild et al., 1982; Regulla et al., 1998) since the cross-section for absorption of electrons is larger than that for photons. In the point of view of medical application, the phenomenon can be applied to enhance radiation dose in a target tissue, a process called "photon activation therapy" (Corde et al., 2004). Applications of this principle led to the evaluation of the sensitizing effect of heavy atoms for example halogen compounds (*e. g.*, bromine and iodine) (Myers et al., 1977; Feinendegen, 1975; Happen et al., 1978; Fairchild et al., 1982; Dawson et al., 1987; Humm and Charlton, 1988; Meesat et al., 2009) and transition elements (*e. g.*, gold) (Regulla et al., 1998; Herold et al., 2000; Hua

et al., 2001). It should be noted that most authors have been used biological effects as an end point to evaluate the dose enhancing effects of these compounds.

Compton effect

In the Compton effect, the interaction process occurs between the incident ionizing photon and an electron in the absorbing material. The photon radiation provides only part of its energy to an orbital electron. The electron will be free or still bound in an atom. In the former case, the electron will be ejected from atom which is called a *recoil electron* and the incident photon will be scattered at an angle with respect to its original direction. The energy transferred to the electron can vary from zero to a large fraction of the radiation energy. The Compton interaction depends only on the number of electrons of the absorber. The number of electrons can be expressed in terms of electron density *i.e.* number of electrons per unit volume of material. The Compton absorption is more significant for high energy photons (>1 MeV) (Johns and Cunningham, 1969; Hughes, 1973; Anderson, 1984; Alpen, 1998; Knoll, 2000). In this energy range (1-25 MeV), photons mainly interact with biological tissue by Compton scattering effect. (Corde et al., 2004).

Pair production effect

In the pair production process, the energy of photons must be superior to 1.02 MeV. It is due to the fact that the energy of the radiation will produce a positron-electron pair where the rest mass energy of the particles is 0.511 MeV. In the mechanism of the interaction, the photon, moving close to the nucleus of an atom, is subjected to strong field effects from the nucleus; it may suddenly be converted to become a negative and positive electron pair. The cross section of this interaction continues to increase when the energy of photon increases, while the cross sections for the photoelectric effect and the Compton scattering effect decrease with increase in energy. In the high range energy of photons (~25-100 MeV), the pair production interaction in soft tissue is the most important type of absorption (Johns and Cunningham, 1969; Hughes, 1973; Anderson, 1984; Alpen, 1998; Knoll, 2000).

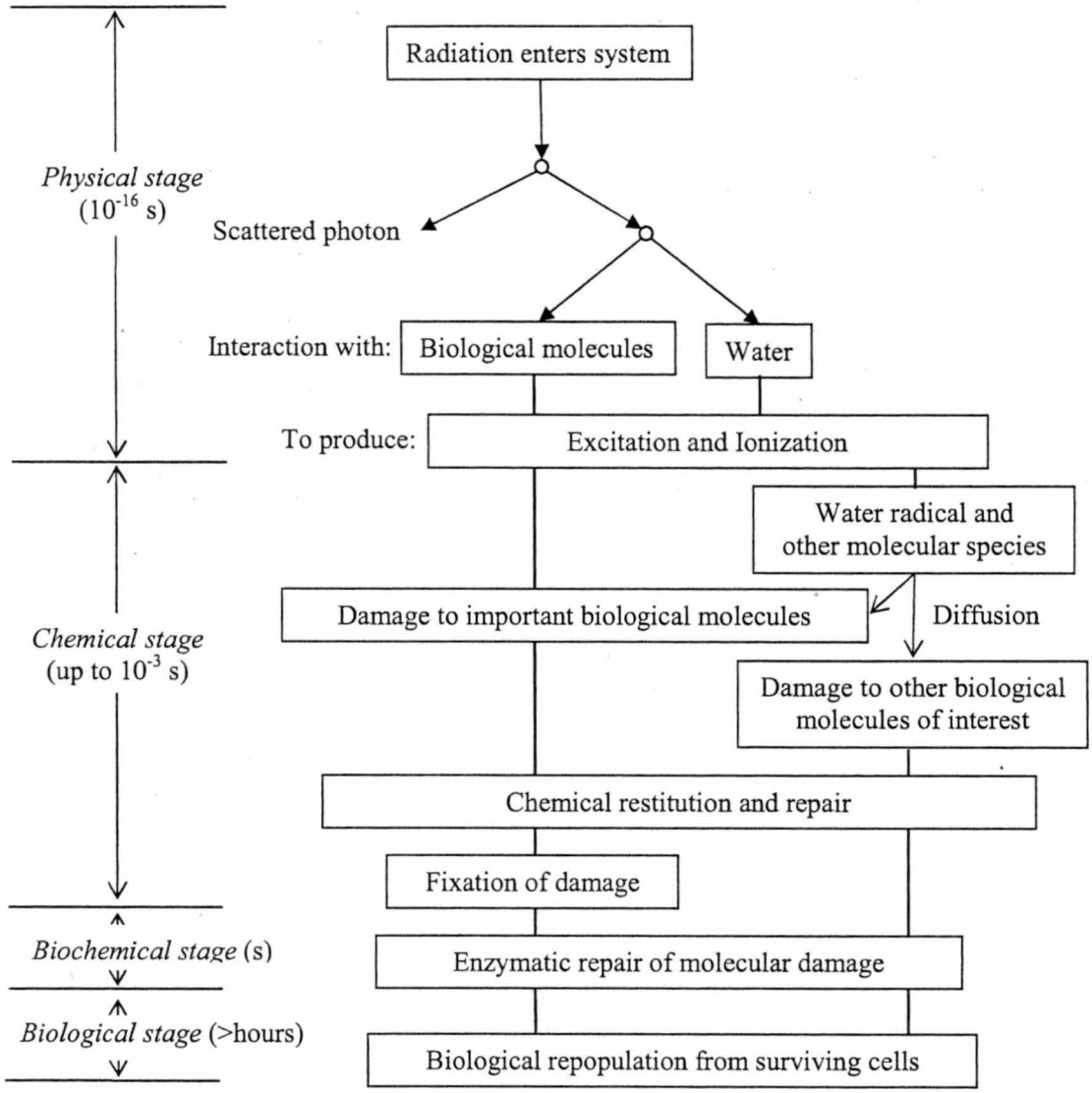

Figure 1. A diagrammatic representation of the processes from energy transfer to final biological damage. (Adapted from Alpen, 1998. *Radiation Biophysics 2nd ed.* Academic Press, San Diego.)

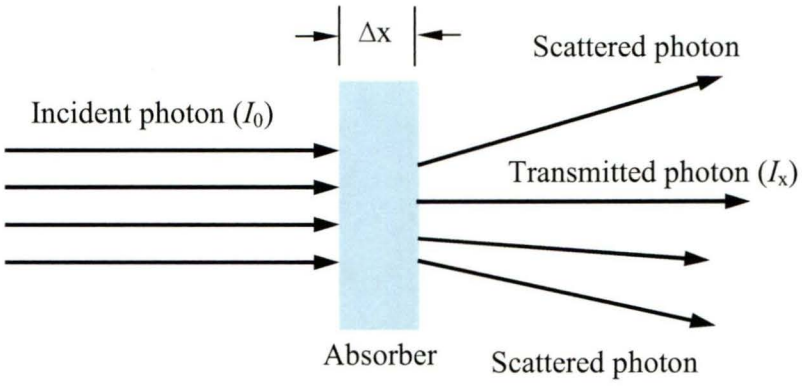

Figure 2 Diagram showing transmission of photon through an absorber of thickness Δx (Johns and Cunningham, 1969; Alpen, 1998).

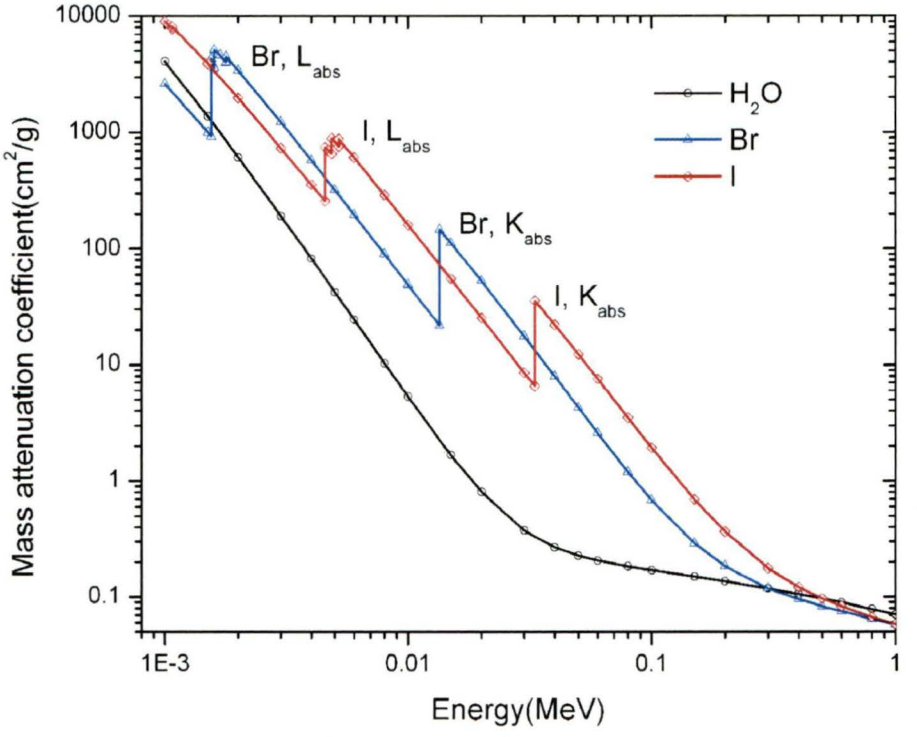

Figure 3 Mass attenuation coefficients for H_2O, Br and I (Adapted from Hubbel and Seltzer, 2010).

I. 2. Radiolysis of water

The biological effect of ionizing radiations can be illustrated by the schematic shown in Figure 1. Assume that the radiation beam is incident on a living system. The boxes represent stages in a time scale; the arrows indicate particles or molecular species present during the sequence. As an example, suppose radiation photons undergo scattering or absorption processes in the first step, and a high speed electron is ejected. In traveling through the tissue, the fast electron generates a track in which biological or water molecules are ionized and excited. Eventually, all of these processes lead to biological damage (Johns and Cunningham, 1969; Hughes, 1973; Anderson, 1984; Alpen, 1998; Knoll, 2000). Interactions may be separated in *direct* and *indirect* effects. The direct mode of action (often termed the *target theory*) exerts its effect directly on vital target molecules within the cell (such as DNA) in form of ionization and excitation. By contrast, the indirect action involves transfer of energy to water molecules with prompt formation of highly reactive species (through the *radiolysis of water* as shown in Figure 4) (Meesungnoen and Jay-Gerin, 2010) which, in turn, induce damage to the target molecules (Tubiana and Wambersie, 1990). In addition, the biological damage depends not only on the radiation absorbed dose but on the quality of radiation applied as well, a measure of which is given by the "linear energy transfer" or LET[1], which represents, to a first approximation, the nonhomogeneity of the energy deposition on a sub-microscopic scale. The LET is usually expressed in keV/μm of specific energy traversing the distance (Meesungnoen and Jay-Gerin, 2010).

Figure 4 shows the overall process of radiolysis of water by low LET radiation at ambient temperature and pressure. The process begins with the interaction of water by the ionizing radiation and terminates with the re-establishment of chemical equilibrium. The radiolysis events can be separated into three temporal stages, "physical stage", "physicochemical stage" and "chemical stage" (Meesungnoen and Jay-Gerin, 2010).

---

[1] The LET is defined for charged particle in any medium as the quotient of dE_l/dl, where dE is the average energy by a charge particle of specific energy traversing a distance *dl* (ICRU Report 16 1970). In this way, the (sometimes termed "energy-unrestricted", i.e., when all permissible energy transfers are included) LET is equivalent to the "stopping power" (which is commonly used in the domain of radiation physics) of the medium traversed (Anderson, 1984). Usually, LET values are in units of keV/μm (the conversion to SI units is: 1 keV/μm $\approx 1.602 \times 10^{-19}$ J/nm) (Meesungnoen and Jay-Gerin, 2010).

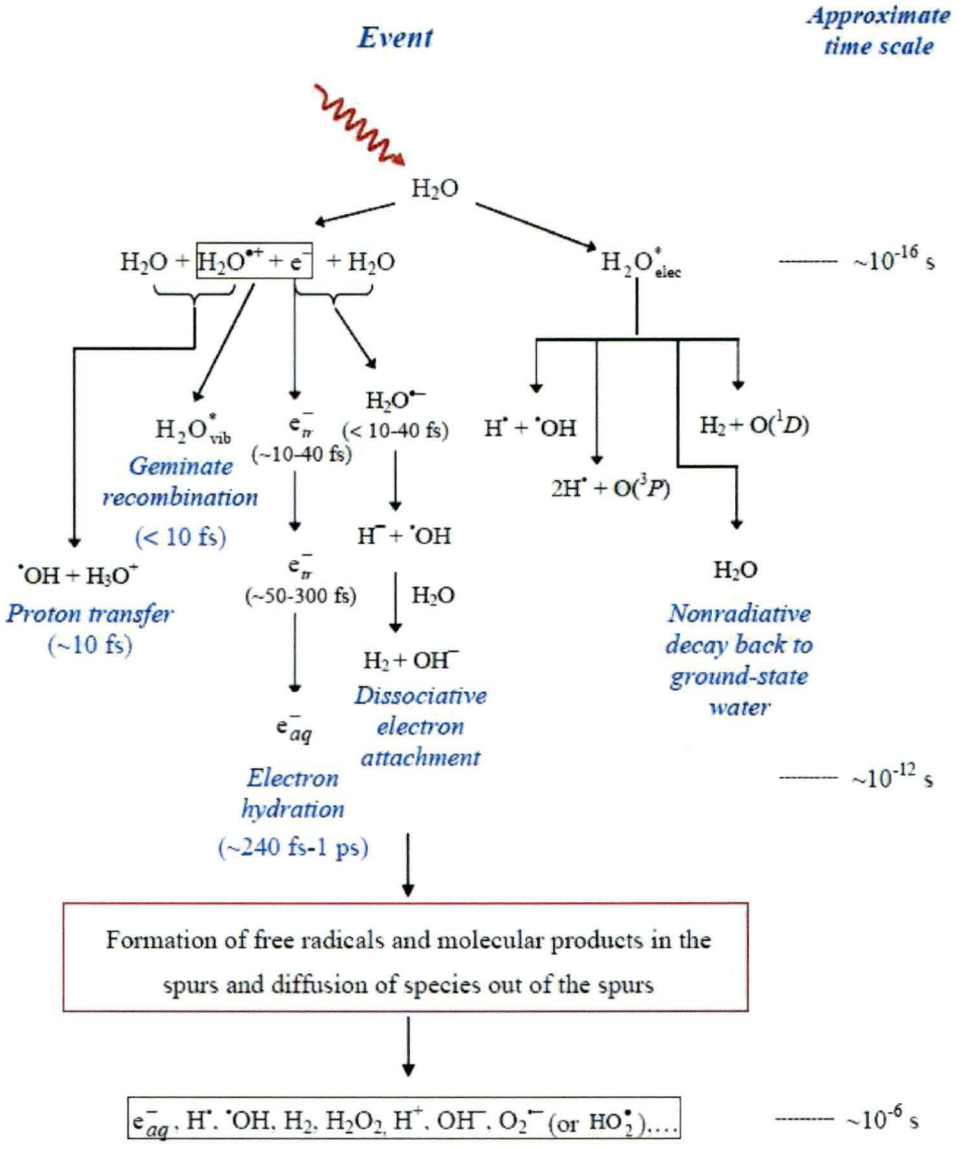

Figure 4. Radiolysis of water by the low-LET radiation. (J. Meesungnoen and J.-P. Jay-Gerin 2010)

(1) In the physical stage, the passage of ionizing radiation through liquid water leads to the production of free atoms and radicals in an initially nonhomogenous distribution. The duration of this stage is of the order of about 10^{-15} s or less (Draganić and Draganić, 1971). The result of the radiation interaction is the production, along the path of the radiation, of a large number of ionized and electronically excited water molecules (denoted $H_2O^{\bullet+}$ and H_2O^*, respectively) (Meesungnoen and Jay-Gerin, 2010) and secondary electrons. Note that H_2O^* represents here the many excited states (Meesungnoen and Jay-Gerin, 2010). The earliest phenomena in the water radiolysis are:

$$H_2O \sim\sim\rightarrow e^- + H_2O^{\bullet+},$$

$$H_2O \sim\sim\rightarrow H_2O^*_{elec}.$$

In general, the ejected electrons from ionization process have sufficient energy to ionize or excite one or more other water molecules in the vicinity, and this phenomenon results in, as explained above, to the formation of tracks, or spurs, that are composed of the products of the events. Thus, these secondary electrons of this cascade go on to lead to additional ionization and excitation events resulting in the production of radiation chemical spurs (Mozumder and Magee, 1966; Buxton, 2004; Meesungnoen and Jay-Gerin, 2010).

(2) The physicochemical stage is the period where thermal equilibrium is reached in the system. Its duration is usually taken to be of the order $\sim 10^{-12}$ s or less. During this period, the ejected electron (secondary electron) moves away from an ionized water molecule. The secondary electron can transfer energy to neighbouring molecules with which it collides and eventually reaches thermal equilibrium with the liquid. Once it has slowed down to the thermal energy (e^-_{th}), it can be localized or trapped (e^-_{tr}) in a preformed potential energy well of appropriate depth in the liquid, before it reaches a fully relaxed, hydrated state (e^-_{aq}) as the dipoles of the surrounding molecules orient in response to the negative charge of the electron (Meesungnoen and Jay-Gerin, 2010). All of these events (thermalization, trapping, and hydration) can then follow in quick succession (less than $\sim 10^{-12}$ s) (Mozumder, 1999; and Meesungnoen and Jay-Gerin, 2010):

$e^- \rightarrow e^-_{th} \rightarrow e^-_{tr} \rightarrow e^-_{aq}$.

Moreover, the ejected electron can attach temporarily to a surrounding water molecule to form H^- and $^{\bullet}OH$ according to

$e^- + H_2O \rightarrow H_2O^{\bullet -} \rightarrow H^- + {}^{\bullet}OH$.

Such a process, called "dissociative electron attachment (DEA)", is well known in water vapour and amorphous solid water at low temperature for incident electrons between ~5-15 eV (Sanche, 1992; Dugal et al., 1999; Pimblott and Mozumder, 2004). A product of the reaction, hydride anion (H^-), can react with another water molecule through a fast proton transfer as the following reaction: (Meesungnoen and Jay-Gerin, 2010)

$H^- + H_2O \rightarrow H_2 + OH^-$.

Additionally, in the physicochemical stage, the ejected electron can be recombined to $H_2O^{\bullet +}$ radical ions. It is due to the fact that Coulomb attraction between electron and the water positive ion tends to draw them back together to undergo electron-cation "geminate" recombination. As the electron is recaptured, the parent ion is transformed into a (vibrationally) excited neutral molecule. (Meesungnoen and Jay-Gerin, 2010)

$e^- + H_2O^{\bullet +} \rightarrow H_2O^*_{vib}$.

Ionized water molecules ($H_2O^{\bullet +}$), are unstable. There are electron transfers from neighboring water molecules to the $H_2O^{\bullet +}$ molecules. This period can occur in a very short lifetime (~10^{-14} s) (Mozumder and Magee, 1975). The species produced by the reaction are hydronium ion (H_3O^+) and hydroxyl radical according to

$H_2O + H_2O^{\bullet +} \rightarrow H_3O^+ + {}^{\bullet}OH$,

where H_3O^+ (or equivalently, H^+_{aq}) represents the hydrated hydrogen ion. Lampe *et al.* (Lampe et al, 1957) have estimated that this reaction takes place in ~1.6×10^{-14} s.

There are many possible pathways for the decay of the excited molecules (H_2O^*). The excited molecules may be produced directly as $H_2O^*_{elec}$ or in directly as $H_2O^*_{vib}$ (Meesungnoen and Jay-Gerin, 2010). However, we have little knowledge about the decomposition of excited water molecules in the liquid phase and the branching ratios associated with each of them (Buxton, 2004). Fortunately, the contribution of the excited compounds to primary yields of radical and molecular species in the radiolysis of water is of relatively minor importance in comparison with that of the ionization processes, such that the lack of information about their decomposition has only limited consequences (Meesungnoen and Jay-Gerin, 2010). Accordingly, they are generally assumed to be essentially the same as those in the water vapour or gas phase (Buxton, 2004) (note that the same decay processes have been reported to occur for the electronically and vibrationally excited water molecules in the gas phase (Meesungnoen and Jay-Gerin, 2010), namely (Cobut et al., 1998; Meesungnoen and Jay-Gerin, 2005):

$$H_2O^* \rightarrow H^\bullet + {}^\bullet OH,$$

$$H_2O^* \rightarrow H_2 + O(^1D),$$

$$H_2O^* \rightarrow 2H^\bullet + O(^3P),$$

$$H_2O^* \rightarrow H_2O + \text{release of thermal energy},$$

where $O(^1D)$ and $O(^3P)$ represent oxygen atoms in their singlet ^1D excited state and triplet ^3P ground state respectively (see Figure 4).

(3) In the nonhomogeneous chemical stage, the water reactive species (*e.g.*, e^-_{aq}, $^\bullet OH$, $H^\bullet$, H_2, H_3O^+, OH^-, $^\bullet O^\bullet$) will diffuse and react with each other, resulting in the re-establishment of chemical equilibrium. These products are present at 10^{-12} s in the spur after the passage of the radiation and then begin to diffuse away from the region where they were originally produced according to macroscopic diffusion principles. They can react with

themselves or with dissolved solutes (if any) present at the time of irradiation, until all spur or track reactions are complete (Meesungnoen and Jay-Gerin, 2010). Radical-radical reactions lead to form molecular products such as H_2, H_2O_2 and H_2O, while the remaining radicals will diffuse out into the bulk of the solution. The lifetime of the spur in liquid water for completion of the spur expansion is generally taken to be about 10^{-7} s (Klassen, 1987.). The yield of radicals and molecular products that escape into the bulk solution at this time are known as the "primary" or "escape" yields. The important reactions and reaction rate constants occurring while the spurs expand are shown in Table 2 (Meesungnoen and Jay-Gerin, 2010).

In mammalian cells, water makes up ~80 % of the cellular mass (Bensasson, et al., 1993) so that, in general, the indirect action of X or γ-rays (low-LET radiation) will predominate as mentioned previously. Various species are released during water radiolysis, the most important being the free radicals e_{aq}^-, $HO^\bullet$, $H^\bullet$ and $HO_2^\bullet/O_2^{\bullet-}$ ($pK_a = 4.8$), and the molecular products H_2O_2 and H_2 (Spinks and Woods, 1990). The formations of these reactive species are typically expressed as a radiation-chemical yield (G). The G-value is the number of species produced per 100 eV absorbed radiation dose. In general, the product yield is always the yield of "primary reaction", which is called primary yield. The primary yields (at ~10^{-6} s after energy deposition) of these radiolytic species in neutral water irradiated by ^{60}Co γ-rays or high-energy electrons (~0.3 keV/μm) are (Ferradini and Jay-Gerin, 2000):

$$G_{e_{aq}^-} = 2.65 \quad G_{H^\bullet} = 0.60 \quad G_{H_2} = 0.45,$$
$$G_{HO^\bullet} = 2.80 \quad G_{H_2O_2} = 0.68 \quad G_{-H_2O} = 4.15.$$

For acidic solution (0.4 M H_2SO_4), these values are (Ferradini and Jay-Gerin, 2000):

$$G_{e_{aq}^-} + G_{H^\bullet} = 3.7 \quad G_{H_2} = 0.45,$$
$$G_{HO^\bullet} = 2.90 \quad G_{H_2O_2} = 0.80 \quad G_{-H_2O} = 4.50.$$

These primary products can then react with solutes to form transient species of interest (Wishart, 1998). In a living system, these species will react with cellular macromolecules (such as DNA, proteins, membrane, etc.) and may cause pathological cell

changes and mortality (Nair et al., 2001). This is especially the case for the hydroxyl radical, which is responsible for about 60-70% of total DNA damage in mammalian cells (with low-LET radiation) (Lehnert, 2008).

Table 2. Main reaction scheme and rate constants (k) used in the radiolysis of pure liquid water at ambient temperature (25 °C) (J. Meesungnoen and J.-P. Jay-Gerin 2010).

Reaction	k (M^{-1} s^{-1})	Reaction	k (M^{-1} s^{-1})
$H^{\bullet} + H^{\bullet} \rightarrow H_2$	5.03×10^9	$e^-_{aq} + e^-_{aq} \rightarrow H_2 + 2\ OH^-$	5.0×10^9
$H^{\bullet} + {}^{\bullet}OH \rightarrow H_2O$	1.55×10^{10}	$e^-_{aq} + H^+ \rightarrow H^{\bullet}$	2.11×10^{10}
$H^{\bullet} + H_2O_2 \rightarrow H_2O + {}^{\bullet}OH$	3.5×10^7	$e^-_{aq} + O_2^{\bullet-} \rightarrow H_2O_2 + 2\ OH^-$	1.3×10^{10}
$H^{\bullet} + e^-_{aq} \rightarrow H_2 + OH^-$	2.5×10^{10}	$e^-_{aq} + HO_2^- \rightarrow O^{\bullet-} + OH^-$	3.51×10^9
$H^{\bullet} + OH^- \rightarrow H_2O + e^-_{aq}$	2.51×10^7	$e^-_{aq} + O^{\bullet-} \rightarrow 2\ OH^-$	2.31×10^{10}
$H^{\bullet} + O_2 \rightarrow HO_2^{\bullet}$	2.1×10^{10}	$e^-_{aq} + H_2O \rightarrow H^{\bullet} + OH^-$	15.8
$H^{\bullet} + HO_2^{\bullet} \rightarrow H_2O_2$	1.0×10^{10}	$e^-_{aq} + O_2 \rightarrow O_2^{\bullet-}$	1.74×10^{10}
$H^{\bullet} + O_2^{\bullet-} \rightarrow HO_2^-$	1.0×10^{10}	$e^-_{aq} + HO_2^{\bullet} \rightarrow HO_2^-$	1.28×10^{10}
$H^{\bullet} + HO_2^- \rightarrow {}^{\bullet}OH + OH^-$	1.46×10^9	$e^-_{aq} + O(^3P) \rightarrow O^{\bullet-}$	2.0×10^{10}
$H^{\bullet} + O(^3P) \rightarrow {}^{\bullet}OH$	2.02×10^{10}	$e^-_{aq} + O_3 \rightarrow O_3^{\bullet-}$	3.6×10^{10}
$H^{\bullet} + O^{\bullet-} \rightarrow OH^-$	2.0×10^{10}	$H^+ + O^{\bullet-} \rightarrow {}^{\bullet}OH$	4.78×10^{10}
$H^{\bullet} + O_3 \rightarrow O_2 + {}^{\bullet}OH$	3.7×10^{10}	$H^+ + O_2^{\bullet-} \rightarrow HO_2^{\bullet}$	4.78×10^{10}
$H^{\bullet} + O_3^{\bullet-} \rightarrow OH^- + O_2$	1.0×10^{10}	$H^+ + OH^- \rightarrow H_2O$	1.12×10^{11}
${}^{\bullet}OH + {}^{\bullet}OH \rightarrow H_2O_2$	5.5×10^9	$H^+ + O_3^{\bullet-} \rightarrow {}^{\bullet}OH + O_2$	9.0×10^{10}
${}^{\bullet}OH + H_2O_2 \rightarrow HO_2^{\bullet} + H_2O$	2.87×10^7	$H^+ + HO_2^- \rightarrow H_2O_2$	5.0×10^{10}
${}^{\bullet}OH + H_2 \rightarrow H^{\bullet} + H_2O$	3.28×10^7	$OH^- + O(^3P) \rightarrow HO_2^-$	4.2×10^8
${}^{\bullet}OH + e^-_{aq} \rightarrow OH^-$	2.95×10^{10}	$OH^- + HO_2^{\bullet} \rightarrow O_2^{\bullet-} + H_2O$	6.3×10^9
${}^{\bullet}OH + OH^- \rightarrow O^{\bullet-} + H_2O$	6.3×10^9	$O_2 + O^{\bullet-} \rightarrow O_3^{\bullet-}$	3.7×10^9
${}^{\bullet}OH + HO_2^{\bullet} \rightarrow O_2 + H_2O$	7.9×10^9	$O_2 + O(^3P) \rightarrow O_3$	4.0×10^9
${}^{\bullet}OH + O_2^{\bullet-} \rightarrow O_2 + OH^-$	1.07×10^{10}	$HO_2^{\bullet} + O_2^{\bullet-} \rightarrow HO_2^- + O_2$	9.7×10^7
${}^{\bullet}OH + HO_2^- \rightarrow HO_2^{\bullet} + OH^-$	8.32×10^9	$HO_2^{\bullet} + HO_2^{\bullet} \rightarrow H_2O_2 + O_2$	8.3×10^5
${}^{\bullet}OH + O(^3P) \rightarrow HO_2^{\bullet}$	2.02×10^{10}	$HO_2^{\bullet} + O(^3P) \rightarrow O_2 + {}^{\bullet}OH$	2.02×10^{10}
${}^{\bullet}OH + O^{\bullet-} \rightarrow HO_2^-$	1.0×10^9	$HO_2^{\bullet} + H_2O \rightarrow H^+ + O_2^{\bullet-}$	1.29×10^4
${}^{\bullet}OH + O_3^{\bullet-} \rightarrow O_2^{\bullet-} + HO_2^{\bullet}$	8.5×10^9	$O_2^{\bullet-} + O^{\bullet-} \rightarrow O_2 + 2\ OH^-$	6.0×10^8
${}^{\bullet}OH + O_3 \rightarrow O_2 + HO_2^{\bullet}$	1.11×10^8	$O_2^{\bullet-} + H_2O \rightarrow HO_2^{\bullet} + OH^-$	0.075
$H_2O_2 + e^-_{aq} \rightarrow OH^- + {}^{\bullet}OH$	1.1×10^{10}	$O_2^{\bullet-} + O_3 \rightarrow O_3^{\bullet-} + O_2$	1.5×10^9
$H_2O_2 + OH^- \rightarrow HO_2^- + H_2O$	4.75×10^8	$HO_2^- + H_2O \rightarrow H_2O_2 + OH^-$	3.83×10^4
$H_2O_2 + O(^3P) \rightarrow HO_2^{\bullet} + {}^{\bullet}OH$	1.6×10^9	$HO_2^- + O^{\bullet-} \rightarrow O_2^{\bullet-} + OH^-$	3.5×10^8
$H_2O_2 + O^{\bullet-} \rightarrow HO_2^{\bullet} + OH^-$	5.55×10^8	$HO_2^- + O(^3P) \rightarrow O_2^{\bullet-} + {}^{\bullet}OH$	5.3×10^9
$H_2 + O(^3P) \rightarrow H^{\bullet} + {}^{\bullet}OH$	4.77×10^3	$O^{\bullet-} + O^{\bullet-} \rightarrow H_2O_2 + 2\ OH^-$	1.0×10^8
$H_2 + O^{\bullet-} \rightarrow H^{\bullet} + OH^-$	1.21×10^8	$O^{\bullet-} + O_3^{\bullet-} \rightarrow 2\ O_2^{\bullet-}$	7.0×10^8
$O(^3P) + O(^3P) \rightarrow O_2$	2.2×10^{10}	$O^{\bullet-} + H_2O \rightarrow {}^{\bullet}OH + OH^-$	1.02×10^6
$O(^3P) + H_2O \rightarrow 2\ {}^{\bullet}OH$	1.9×10^3	$O_3^{\bullet-} + H_2O \rightarrow O^{\bullet-} + O_2$	48.0

I. 3. Radiation protector/antioxidant

A radioprotector is a chemical compound that can reduce the toxicity of ionizing radiation (Tubiana et al., 1990). Chemical radioprotectors play a significant role by scavenging water free radicals before they can damage DNA, thus reducing the biological consequences of radiation (Bensasson et al., 1993). In addition, some compounds (*e.g.*, those containing SH groups) also have radioprotective effects by hydrogen-atom donation to radiation-induced radicals to facilitate direct chemical repair at sites of DNA damage (Bump, 1997; Hall, 2000).

Antioxidants are one class of radioprotectors (Weiss, and Landauer, 2003). Thus, their mechanisms of action are similar, although their intended use is different. The former are used in conjunction with a radiation treatment (administered before radiation exposure), while the latter are used to protect tissues from the deleterious action of reactive species such as reactive oxygen species (ROS) and reactive nitrogen species (RNS) (Valko et al., 2007; Halliwell, and Gutteridge, 1999) that can be produced during normal cellular metabolism. The major ROS and RNS species (at physiological pH) are $HO^{\bullet}$, $O_2^{\bullet-}$, H_2O_2, $^{\bullet}NO$ and $ONOO^{-}$.

Indirect damage of ionizing radiations originates from reactions of the main radicals of water radiolysis (*e.g.*, $H^{\bullet}$, $^{\bullet}OH, e_{aq}^{-}$, etc.) with biological target molecules. It is useful to note that a commonly therapeutic radiation dose (~2 Gy) can produce approximately 2 μM these free radicals (von Sonntag, 1987; Bump, 1997). The hydroxyl radical is a strongly oxidizing species whereas the hydrated electron and the H radical are reducing species (Adams, 1970; von Sonntag, 1987). In cellular radiobiological damage, the OH radical and e_{aq}^{-} obviously are primary sources because of their high yield (Kiefer, 1990). The cellular radiation effects are potential or mitigated depending on many factors such as for example the presence of oxygen, sulfhydryl compounds (RSH) and other molecule in the cellular milieu (Nair et al., 2001). In presence of oxygen, reaction of oxygen molecules with hydrogen radicals and solvated electrons (e_{aq}^{-}) results in other reactive radical species such as superoxide radical ions ($O_2^{\bullet-}$) and hydroperoxyl radicals ($HO_2^{\bullet}$). These species play a significant role in oxygen conditions (von Sonntag, 1987; Bump, 1997).

$$e^-_{aq} + O_2 \rightarrow O_2^{\bullet -},$$

$$H^\bullet + O_2 \rightarrow HO_2^\bullet.$$

However, the radicals $HO_2^\bullet$ and $O_2^{\bullet -}$ are in equilibrium. In neutral water the pKa of $HO_2^\bullet$ is 4.8 (Ferradini and Jay-Gerin, 2000).

$$HO_2^\bullet \leftrightarrow H^+ + O_2^{\bullet -}.$$

Most living tissues naturally contain many sulphur-containing compounds such as amino acids, glutathione, methionine and cysteine (Kiefer, 1990; Kamarnisky et al., 2003). Glutathione is the principal nonprotein thiol (Bump, and Brown, 1990) which is the intracellular reducing compound of highest concentration in mammalian cells (Chaudière, 1994). The thiol-containing molecules (RSH) are generally good radical scavengers (Gilbert, and Colton, 1999) especially OH radicals (Kock, 1998). Moreover, the most important feature of their chemistry is probably that they are involved in many cellular redox reactions, illustrated by the general reaction:

$$2RSH \leftrightarrow RSSR + 2e^- + 2H^+.$$

This process most likely proceeds via thiyl free radicals, $RS^\bullet$, as intermediates which are known to readily form disulfides (RSSR) if they lack suitable partners for other reactions (Asmus, 1993). The RSH can react with other radicals through hydrogen atom abstraction, as an example of the following reaction (Murray, 1998; Wardman, 2007):

$$DNA^\bullet + RSH \rightarrow DNA + RS^\bullet.$$

In radiation biology, the process is commonly known as "repair reaction" (Asmus, 1993).

However, the chemical action of these radiation protectors is not well understood. In this project, we study the protecting effect of a disulfide compound, cystamine (RSSR) using Fricke and polyacrylamide gel dosimetry. The Fricke system has the advantage that it can be simulated by Monte Carlo techniques such that the mechanism of action of cystamine can be investigated.

I. 4. Radiosensitizers

Nowadays, radiation therapy is well established and is an important technique for localized cancer treatment (Blattmann et al., 2005). The basic idea of the radiation treatment is to maximize the absorbed dose to the tumour area while minimizing exposure to normal, healthy cells (Tilikidis et al., 1994). Unfortunately, in this case, the radiation dose is often limited by normal tissue tolerance (Viala et al., 1999; Young et al., 1996). Using a radiation-sensitizing agent is one strategy in order to increase the absorbed dose in the tumor.

Thus, radiosensitizers are intended to enhance tumor cell killing while having much less effect on normal tissues. The enhancement of the radiation damage by radiosensitizers (also called "dose enhancers") originates from the direct action of radiation on the sensitizing compounds. This mechanism of radiosensitization can be generated into three categories: production of free-radical species (Wardman, 1987), nuclear reaction sensitizer (Barth et al., 2005), and heavy element sensitizers (Ertl et al.,1970). The radiation sensitizer that can be used to produce free-radicals is called "electron-affinic radiosensitizer" because the efficiency of sensitization, which is defined by the concentration required to produce a given degree of sensitization, is related to the electron-affinities or the reduction potential of compounds (Adams, 1979; Wardman, 1987), for example, nitroimidazoles (Adams, 1979) and gadolinium (III) texaphyrin (Viala et al., 1999; Young et al., 1996). The radiation-sensitizing properties of these compounds are similar to that of molecular oxygen (also called "oxygen mimetic radiosensitizer"). Oxygen is itself a free radical, the prototypical radiosensitizer, but it has two unpaired electrons resulting in rapidly reacting with other species and producing new reactive radicals (Wardman, 1987). The electron-affinic molecules can react with water-radiolytic species especially solvated electrons (e^-_{aq}). This process forms aggressive radicals as shown in the following reaction.

$$S + e^-_{aq} \rightarrow S^{\bullet},$$

where, S is radiosensitizer. However, the main drawback of these compounds is their toxicity and the observation that they do not adequately sensitize the entire tumour cell population (Young et al., 1996).

An example of nuclear reaction sensitizer is "boron-neutron capture therapy (BNCT)" (Coderra and Morris, 1999; Barth et al., 2005). In this method, the nuclear reaction of low energy (thermal) neutrons (~0.025 eV) (Knoll, 2000) with boron has a high cross section. This interaction generates low LET alpha particles and charged fragments. The main idea is that the neutron by itself has little effect on tumor or normal tissue; the slow neutrons have not sufficient energy to make damage to tissue (Coderra and Morris, 1999). Meanwhile the high-LET radiations released in the tumor area by the nuclear interaction of ^{10}B with the thermal neutrons, $^{10}B(n,\alpha)^{7}Li$, can be sufficient to kill or sterilize the tumor cells. The nuclear reaction is the following (Coderra and Morris, 1999):

$$^{10}_{5}B+^{1}_{0}n\rightarrow^{11}_{5}B\rightarrow^{4}_{2}He+^{7}_{3}Li, \qquad 2.792\,MeV.$$

The boron drugs that have been investigated are composed of *p*-boronophenylalanine (BPA) and sulfhydryl borane (BSH) (Coderra and Morris, 1999 and Barth et al., 2005).

For heavy element sensitizers, bombardment with proper photon energy can generate secondary radiation such as secondary electrons, Auger electron cascades and characteristic X-rays. The example sensitizers of this group are halogen compounds (*e.g.,* Br and I) (Humm and Charlton, 1988. and Meesat et al., 2009) and transition metals (*e.g.*, Ga (Viala et al., 1999) and gold (Herold et al., 2000)). The concept of this technique is to use optimal energy of the ionizing radiation to induce photoelectric process of these radiation-sensitizing targets. At energies above the K-edge absorption and close to the binding energy of the absorber (sensitizer), the photoelectric interaction will be dominant, leading to an additional photoelectric process; this ultimately results in the production of secondary radiation generation such as X-ray fluorescence and Auger electrons. In fact, the characteristic X-rays originate from electron transitions between the inner shells of atoms as shown in Fig. 5. The energy of an X-ray is equal to the energy difference between the binding energies of the electron shells involved in the transition. The Auger effect is competitive to the X-ray emission phenomenon. It can be explained as a reabsorption of an excited characteristic X-ray photon internal to the atom resulting in a so-called "internal conversion" (Knoll, 2000) as shown in Fig. 5.

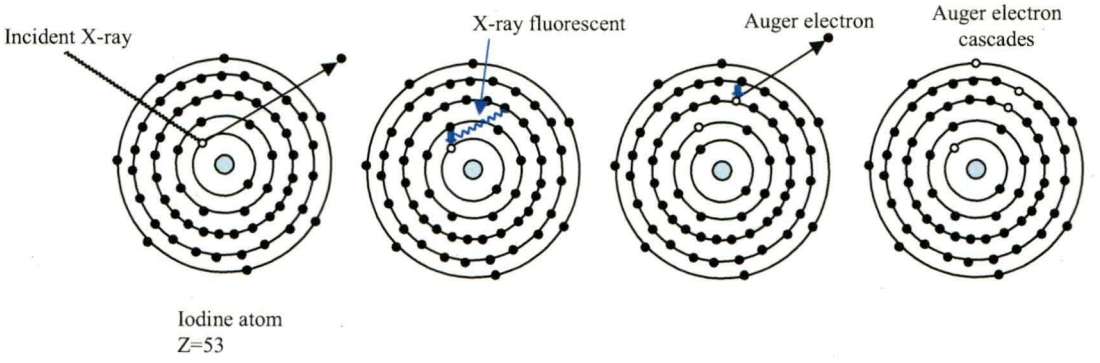

Figure 5. Diagrammatic representation of the absorption of an incident X-ray photon by an iodine atom.

These radiation-sensitizing products can damage critical cellular targets such as DNA, RNA, proteins or lipids, increasing the extent of initial radiation injury and thus improving tumor killing.

Radiation sensitizers/protectors and antioxidants are very important in different health-related problems. The effects of these compounds have mostly been measured by using *in vitro* techniques, including protection against clonogenic or apoptotic cell death, modulation of cell differentiation and mutagenesis, and protection against radiation-induced lipid peroxidation or other biochemical changes (Weiss and Landauer, 2003). A well-established general method is the cell survival to a radiation treatment by a clonogenic assay. However, this technique requires reliable cell growth in culture media, and can be difficult and time consuming (Slavotinek et al., 1998).

In this project, we have developed an alternative method, fast and easy to apply, to assess the efficiencies of radiation sensitizers and protectors, based on the use of Fricke and polyacrylamide gel dosimeters.

I. 5. Fricke dosimetry

Of the chemical systems, the ferrous sulfate dosimeter (referred to as the "Fricke dosimeter" after Hugo Fricke who first published accounts of its properties in 1927-1929) is, at the present time, the best understood and the most widely accepted chemical dosimeter (Spinks and Woods, 1990). It is easy to use, gives absolute dose measurements (the usual

dose range is limited to ~400 Gy), and its accuracy is high (with care, Fricke dosimetry is capable of 0.1% precision for ^{60}Co γ-rays and high-energy X-rays and electrons). The standard Fricke dosimeter solution contains 1 m*M* $FeSO_4$ (or ferrous ammonium iron(II) sulfate ($[NH_4]_2[Fe][SO_4]_2.6H_2O$), 0.4 *M* H_2SO_4 (pH 0.46) (note that this sulfuric acid concentration was originally chosen as being radiologically equivalent to biological tissue (Shalek et al., 1962) and is saturated with air (~0.25 m*M* O_2 at 25 °C (Halliwell and Gutteridge, 1999). The reaction involved in the Fricke dosimeter is the radiation-induced oxidation of ferrous (Fe^{2+}) ion to ferric (Fe^{3+}) ion at low pH and in the presence of oxygen. Determination of the ferric ion concentration is most conveniently carried out by direct spectrophotometric measurement at 304 nm (assuming Beer's law is obeyed). The ferric ion yield $G(Fe^{3+})$ is then obtained from the equation $C = \rho DG$, where C is the Fe^{3+} concentration, ρ (= 1.024 g/cm^3) is the density of the dosimeter solution and D is the absorbed dose. Practically, for the standard Fricke dosimeter, the accepted value of $G(Fe^{3+})$ for ^{60}Co γ-rays or high-energy electrons is 15.6 ± 0.3 molecules/100 eV (Spinks and Woods, 1990). In the presence of a radioprotector, this value will be less than 15.6 (Jayson and Wilbraham, 1968; Lalitha, and Mittal, 1971). On the contrary, the presence of a radiosensitizer will lead to increased ferric yields (Herold et al., 2000).

Using this method, Jayson and Wilbraham (Jayson and Wilbraham, 1968) and Lalitha and Mittal (Lalitha and Mittal, 1971) have studied the protective action of cystamine, a well-known biological radiation-protective compound. The result shows that cystamine can prevent oxidation of Fe^{2+}, which lowers the yield of Fe^{3+}. In this case, cystamine and Fe^{2+} competed in the reaction with oxidizing radicals. More recently, Herold *et al.* (Herold et al., 2000) have also used the Fricke dosimeter to measure dose enhancement from gold microspheres in solutions irradiated with 200 kV_p X-rays and ^{137}Cs γ-rays. Undoubtly, these studies suggest that the Fricke dosimeter can be used to evaluate the efficiency of radiation sensitizers/protectors and antioxidants.

In this work, we have determined *G*-values of the Fricke dosimeter to investigate the effect of cystamine on the ferric ion yield in the presence and in the absence of oxygen. Furthermore, based on our current knowledge of the radiation chemistry of cystamine, we have developed a full Monte Carlo code to simulate the radiation-induced chemistry of the studied Fricke/cystamine solutions. This computer code proposes reaction mechanisms and

incorporates specific reactions describing the radiolysis of cystamine in both aerated and deaerated Fricke solutions that are obtained from various literature sources and that lead to the observed quantitative chemical yields. Thus, this is the first time that Monte Carlo simulation techniques have been used to study a complex system such as the radiolysis of a sulfur-containing molecular system.

I. 6. Monte Carlo simulations

Monte Carlo simulation techniques can be used to model the complex succession of events that are generated in liquid water and aqueous solution after absorption of ionizing radiation (Clifford et al, 1982.; Cobut et al., 1998; Frongillo et al., 1998). If we consider the complicated series of events that follow the irradiation of a biological system (Figure 1), it is convenient to separate the events into three phases: (1) the physical stage, approximately 10^{-16} to 10^{-12} s, when the radiant energy is absorbed and chemically reactive species are formed as a result of ionization and excitation, (2) the chemical stage, about 10^{-12} to 1 s, when these highly reactive species-free radicals- react with each other and with environmental molecules, (3) the biological stage, beyond a minutes and so, when the biological system responds to chemical products of irradiation (Wardman, 1983). Monte Carlo methods are used to simulate the events of water radiolysis which can be divided into the first three of these stages. The computer simulations are based on stochastic phenomena and two important approaches have been extensively used: (1) "step-by-step" (or random flights Mote Carlo simulation) method, in which the trajectories of the diffusing species of the system are modeled by time-discredited random flights and in which reaction takes place when reactants undergo pairwise encounters, and (2) "independent reaction times (IRT)" (or random reaction times (Clifford et al., 1986.), which allows the calculation of reaction times without having to follow the trajectories of the diffusing species. Full random flights simulations are certainly the most reliable among the stochastic approaches; it is therfore generally considered as a measure of reality. However, the method can be exceedingly consuming in calculating time when large systems (such as complete radiation tracks or track segments) are studied. The IRT method, a computer efficient stochastic simulation technique, has been devised to achieve much faster realisations than are possible with the full Monte Carlo model. In essence, it relies on the approximation that the distances

between pairs of reactants evolve independently of each other, and therefore the reaction times of the various potentially reactive pairs are independent of the presence of other reactants in the system. For every pair, a reaction time is stochastically sampled according to the time-dependent survival function (Goulet and Jay-Gerin, 1992; Frongillo et al., 1998) that is appropriate for the type of reaction considered. This function depends on the initial (or zero-time) distance separating the species, their diffusion coefficients, their Coulomb interaction, their reaction radius, and the probability of reaction during one of their encounters. The first reaction time is found by taking the minimum of the resulting ensemble of reaction times and allowing the corresponding pair of species to react at this time. This procedure for modeling reaction is continued either until all reactions are completed or until a pre-defined cut-off time is reached. The IRT simulation technique also allows one to incorporate in a simple way pseudo first-order reactions of the radiolytic products with various scavengers that are homogeneously distributed in the medium (such as H^+, OH^-, and H_2O itself, or more generally any solutes for which the relevant reaction rates are know). The ability of the IRT methods to give accurate time-dependent chemical yields has been well validated by comparison with full random flights Monte Carlo simulation (Goulet et al., 1998).

Computer code simulations have been continually developed by the Sherbrooke group since 1990. The Monte Carlo codes have been used to simulate the track structure of ionizing particles in water, the yield of the various ionized and excited species, and the subsequent reactions of these species in time with one another or with available solutes (Frongillo et al., 1998; Meesungnoen and Jay-Gerin 2005; Autsavapromporn et al., 2007; Tippayamontri et al. 2009; Meesungnoen and Jay-Gerin, 2010). A most recent version of the Sherbrooke laboratory, called IONLYS-IRT (Meesungnoen and Jay-Gerin 2005; Autsavapromporn et al., 2007; Tippayamontri et al. 2009; Meesungnoen and Jay-Gerin, 2010), was used in the present work. The IONLYS step-by-step program is used to model all of the events of the physical and physicochemical stages in the track development. To reproduce the effects of ^{60}Co gamma radiolysis or of fast electrons, we use short (~100 μm) segments of one hundred fifty 300-MeV proton tracks, over which the LET is essentially constant and equal to ~0.3 keV/μm at 25 °C. Such an analysis thus gives the track segment yields at a well-defined LET (Muroya et al., 2002). Autsavapromporn et al. and

Tippayamontri et al. have used the Monte Carlo simulations to investigate yields of ferric ions produced in the radiolysis of Fricke solutions (Autsavapromporn et al., 2007 and Tippayamontri et al. 2009).

In this study, to help assess the radiation-protective mechanism of cystamine, the full Monte-Carlo computer code, IONLYS-IRT (Autsavapromporn et al., 2007 and Tippayamontri et al., 2009), was used to simulate in complete detail the radiolysis of the Fricke/cystamine (0-0.1 M) solutions. Benefiting from the fact that the radiation chemistry of cystamine is reasonably well characterized, this computer model incorporates specific reaction mechanisms describing the radiolysis of cystamine in oxygenated and deoxygenated Fricke solutions that lead to the observable quantitative chemical yields. To our knowledge, this is the first study of the radiolysis of a sulfur molecular system that uses such a computational approach. In brief, all the events of the early physical and physicochemical stages are handled, on an event by event basis, by the IONLYS simulation program. The subsequent nonhomogeneous chemical stage is covered by the IRT program. This program employs the IRT method to simulate the chemical reactions that take place in the irradiated solutions. To reproduce the effect of ^{60}Co γ-radiolysis, short (~100 μm) segments of 300-MeV proton tracks, over which the LET is nearly constant (~0.3 keV/μm at 25 °C), were used. The evolution of radiation-induced yields was followed until 200 s.

I. 7. Polyacrylamide gel (PAG) dosimetry

The acrylamide gel dosimeter is a three-dimensional radiation dosimeter (Maryanski et al., 1993) that is composed of two monomers, acrylamide (AA) and *N,N'*-methylene-bis-acrylamide (BIS) dissolved in an aqueous gelatin matrix. The PAG dosimeter can be divided into "hypoxic" or "anoxic" gel dosimeters and "normoxic" gel dosimeters (Baldock et al., 2010). The former must be prepared in a deoxygenated condition (Maryanski et al., 1994) (normally under an argon or a nitrogen atmosphere), while the latter can be manufactured in normal atmospheric condition by using an oxygen scavenger (*e.g.*, ascorbic acid (De Deene et al., 2002) and tetrakis (hydroxymethyl) phosphonium chloride (THPC) (De Deene et al., 2002). Conventionally, the gel dosimeter is water (Sellakumar et al., 2007) and tissue equivalent (Venning et al., 2005). This is linked to the percentage of water in the dosimeter (almost 90%) and the absence of heavy elements. Thus, the main interaction of

an ionizing radiation is with water molecules. The interaction process of ionizing radiation leads to form radical and molecular species as mentioned in the previous section. The basic principle of the dosimeter is based on the radiation-induced polymerization of the two monomers, which is initiated by the water free radicals (Lepage et al., 2001a) as provided in Figure 6 (Lepage and Jordan, 2010). It should be noted that the main radical species ($R^{\bullet}$) that can initiate the polymerization are e^{-}_{aq}, $^{\bullet}OH$ and $H^{\bullet}$ (Meesat et al., 2010). Figure 6 shows a general schematic of the different chemical reactions that occur in a polyacrylamide gel dosimeter. When a water free radical reacts with a monomer, a process which is called "initiation", a monomer radical is formed, which can react with another monomer, forming a polymer radical, and so on in a process called "propagation". The rate of initiation is controlled by the rate of formation of the initiating fragments, because of addition to the double bonds occurs rapidly (Lepage et al., 2001a; Baldock et al., 2010). Consequently, the propagation process results in the formation of high molecular weight polymers. In this case, several articles show that BIS is consumed more efficiently than AA during polymerization (Baldock et al., 1998; Lepage et al., 2001b). Lepage *et al.* 2001 have estimated that the degree of the polymerization reaction (*i.e.*, the number of repeating monomer units in a polymer chain) was of the order of $\sim 10^4$ (Lepage et al., 2001b). In this system, the resultant high molecular weight copolymer is insoluble in the aqueous environment and precipitates from solution. As a result a proportion of growing macroradicals will become less accessible and undergo slow reaction with monomer species, and eventually terminate (Lepage et al., 2001a.) The polymerization chain reaction of polyacrylamide gel dosimeter can be summarized as follows:

$$H_2O \rightsquigarrow R^{\bullet}(e^{-}_{aq}, H^{\bullet} \text{ and } {}^{\bullet}OH) + \text{molecular species} \quad \text{(water radiolysis)},$$

$$R^{\bullet} + M \rightarrow RM^{\bullet} \quad \text{(initiation step)},$$

$$RM^{\bullet} + M \rightarrow RMM^{\bullet} \quad \text{(propagation step)},$$

$$RM^{\bullet} + RM^{\bullet} \rightarrow \textit{dead polymer} \quad \text{(termination step)}.$$

The termination reaction is not only taking place by the combination reaction of two radicals. Oxygen can react with water free radicals and monomer radicals to form a peroxide-radical; this termination process is (Baldock et al., 2010):

$$R^{\bullet} + O_2 \rightarrow ROO^{\bullet},$$

$$M^{\bullet} + O_2 \rightarrow MOO^{\bullet}.$$

In addition, it is possible that termination will occur through reaction with small radical fragments from water or gelatin, or by scavenging by gelatin molecules (Lepage et al., 2001a).

Obviously, the polymerization process is a chain reaction, leading to form polymer in the gel matrix. The amount of polymer produced in the dosimeter is related to the absorbed radiation dose. Several techniques can be used to evaluate the radiation-induced chemical changes in the dosimeter gels, such as optical techniques including FT-Raman spectroscopy and laser attenuation, as well as ultrasound, X-ray computed tomography and magnetic resonance imaging (MRI) (Lepage et al., 2001c). The latter method provides the highest sensitivity (Lepage et al., 2000). Generally, in the evaluation of polymer gel dosimeters by MRI, the spin-spin relaxation time (T_2) of protons in the gel following irradiation is determined in two or three dimensions. The quasi-linear relationship between the inverse of T_2 (R_2) and the absorbed dose, at low doses, is called the "R_2-dose sensitivity" (Lepage et al., 2001a).

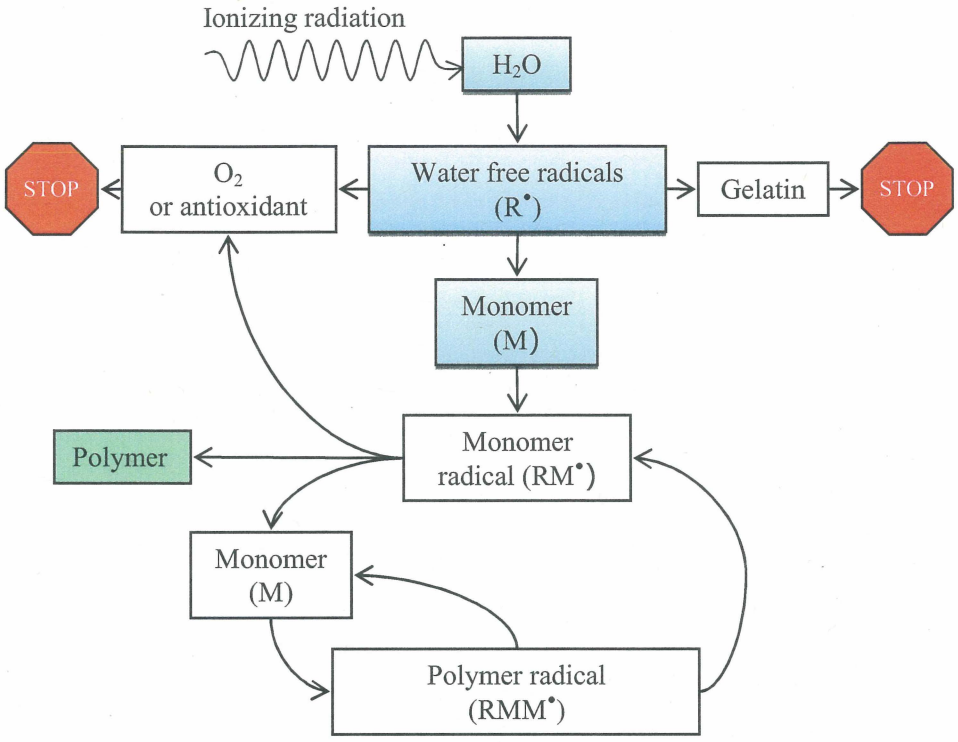

Figure 6. Schematic representation of the interaction between different chemicals in a polyacrylamide gel dosimeter. (From Lepage and Jordan 2010. *J. Phys.: Conf. Ser.* 250, 012055, reproduced with permission.)

In this project, in order to exclude reactions with oxygen, the action of radiation protectors and radiation sensitizers were studied with anoxic PAG. When a radiosensitizer (or "dose enhancer") is added to the gel dosimeter, the effect of radiation on the sensitizing compound results in more radical species and this should increase the extent of polymerization for a given dose. Under these conditions, the R_2-dose sensitivity will be higher than without the sensitizer. With this technique, Farajollahi et al. (Farajollahi et al., 2000) have shown the dose increasing effect of boron by thermal neutron capture therapy. In a recent study, Boudou et al. (Boudou et al., 2007) have used this method to measure the dose enhancement in polymer gels doped with iodine (a high-Z element). Unlike radiosensitizers, radioprotectors and antioxidants can scavenge radiation-induced water free radicals, so that we expect their presence will lead to a decrease in the R_2-dose sensitivity (Meesat et al., 2009).

I. 8. Femtosecound laser pulse fillamentation

In this project, we studied the potential of pulsed femtosecond laser irradiation as a radiation therapy. Lasers have already been exploited in a number of biomedical applications. For cancer therapeutic modalities, the effects of laser light on tissue can be separated into thermal and chemical effects. The former is called *photothermal therapy* (Bown, 1983), whereby light absorption leads to a local temperature increase resulting in damage to tumor cells. The latter is called *photodynamic therapy* (Wilson and Patterson, 1986; Bonnett, 1995; Stilts et al., 2000; Van lier et al., 2009) which involves using a chemical sensitizer that generates reactive oxygen species and results in damage to the vasculature or to tumor cells. Here, we attested whether pulsed laser light could create water radiolysis species in view of its potential medical and biological applications.

Basically, low-energy secondary electrons (LEEs) are generated in massive amounts from the degradation of the high-energy ionizing radiations like X rays, γ photons or charged particles (accelerated electrons or heavier charged particles) (Pimblott and Laverne, 2007). These electrons define the geometry of the radiation track (Paretzke, 1986; Magee and Chatterjee, 1986), with ionization energy deposition of secondary electrons with energies between ~1 and 20 eV (~5 x 10^4 per MeV) (Paretzke, 1986). In this energy range, the electron penetration range in water is of the order of 10 nm (Meesungnoen et al., 2002). Films of biological molecules in ultrahigh vacuum condition have clearly demonstrated the induction of strand breaks in DNA plasmids by such LEEs (Boudaïffa et al., 2000).

Here, we used intense ultra-short laser pulses in water, leading to self-focusing and filamentation (Chin et al., 2005; Chin, 2006; Couairon and Mysyrowicz, 2007). These processes lead to generate a plasma of LEEs in the medium. In case of optical breakdown, experimental studies have suggested that the plasma in water is very similar to that in transparent ocular and other biological media (Yablonovitch and Bloembergen, 1972; Chin, and Lagacé, 1996; Vogel, and Venugopalan, 2003). The phenomenon results in the generation of free electrons and ions, the electrons in a liquid are either bound to a particular molecule or "quasi-free" when they possess sufficient kinetic energy to move without being captured by local molecular energy potentials (Vogel and Venugopalan, 2003.).

The physical origin of the formation of filaments is well understood (Chin et al., 2005; Chin, 2006; Couairon and Mysyrowicz, 2007). Even if many physical effects come into play during the propagation of the pulse in the filament, the process of its formation can be described by the action of mainly two nonlinear physical effects: firstly, the optical Kerr effect acts against diffraction and tends to focus the beam on itself (Couairon and Mysyrowicz, 2007). It should be noted that the Kerr effect is an electric perturbation of the refractive index of a material. Secondly, multiphoton absorption limits the intensity (Couairon and Mysyrowicz, 2007). The ensuing ionization of the atmosphere reduces the local refraction index of the medium and leads to beam defocusing as shown in Figure 7.

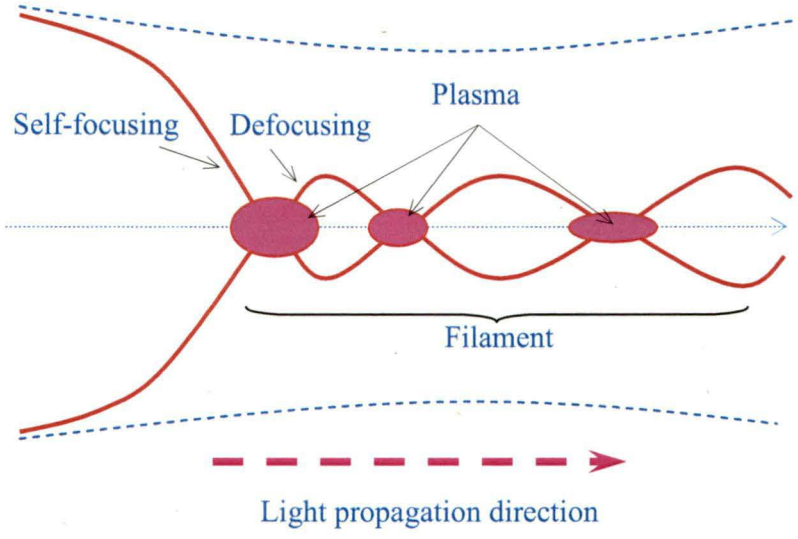

Figure 7. Schematic representation of the focusing-defocusing cycles sustaining a long range propagation of light filaments (Adapted from Couairon, and Mysyrowicz, 2007. *Phys Rep* **441**, 47-189).

Briefly, self-focusing is an induced lens effect. It results from wavefront distortion inflicted on the beam by itself while traversing an optically nonlinear medium. It is useful to note that the "nonlinear absorption" means that the absorption coefficient of a medium depends on the intensity of the incident light (Vogel, 1997). In other words, the absorption probability is a nonlinear function of the laser intensity; the absorption can be confined to the bulk of a transparent sample by tightly focusing the laser beam inside the sample,

producing much higher laser intensity in the focal volume than at the surface. It plays a dominant role in interactions of high-power laser beams with matter (Vogel, 1997). Consequently, as the beam travels in the medium, the original plane wavefront of the beam becomes progressively more distorted.

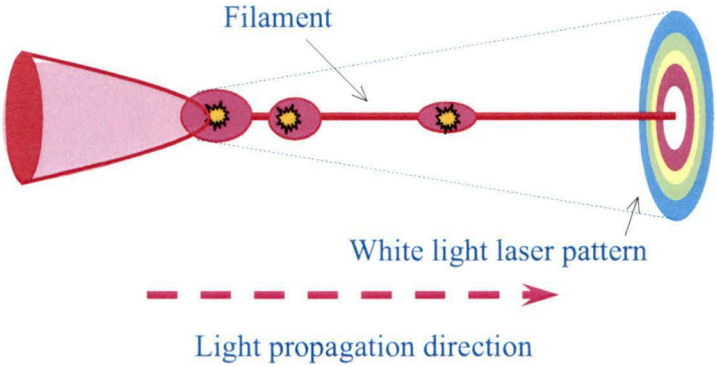

Figure 8. A schematic diagram of the evolution of a femtosecond laser pulse propagating in an optical medium (Adapted from Chin et al., 2005. *Can. J. Phys.* **83**, 863-905). The pulse is demonstrated by the ellipse at the left. The central slice of the pulse self-focuses to a small area where the resulting high intensity ionizes the air molecules (yellow star). The front part keeps on self-focusing becoming thinner and thinner. At the end of the propagation, the pulse degenerates into a colourful white-light laser pulse, as called conical emission.

The distortion is similar to that imposed on the beam by a positive lens. Since the optical ray propagation is in the direction perpendicular to the wavefront, the beam appears to focus by itself. This degenerative process is stabilized in the femtosecond regime, by generation of electrons forming a filament (Chin et al., 2005; Chin, 2006; Couairon and Mysyrowicz, 2007). The phenomenon is called light bullet (Silberberg, 1990), supercontinuum generation (Chin and Lagacé, 1996; Couairon and Mysyrowicz, 2007), or filamentation (Weyl, 1989; Chin and Lagacé, 1996; Chin, 2006; Couairon and Mysyrowicz, 2007) which is believed to be mainly the result of self-phase modulation as shown in Figures 7 and 8. Electrons produced by multiphoton or tunnel ionization are further accelerated by the electric field of the pulse in an inverse Bremstrahlung effect (Vogel et al., 2005). If they acquire enough kinetic energy, they give rise to a second generation of electrons by impact ionization of

other molecules in an avalanche-like process ionization cascade (Vogel, 1997). Free electrons form via an interplay between multiphoton and avalanche processes, as shown schematically in Figure 9.

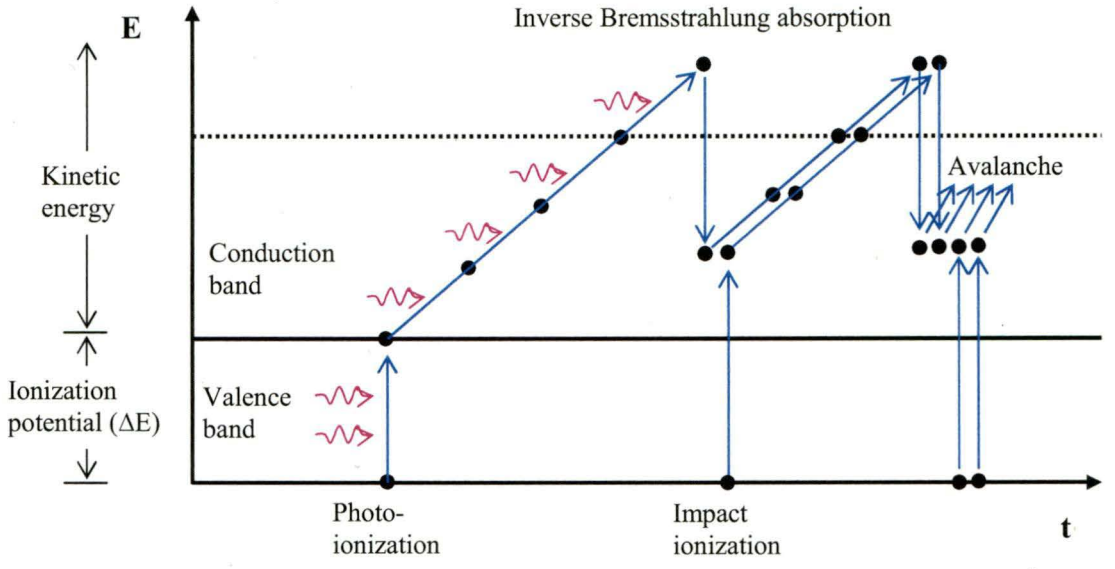

Figure 9. Interplay of multiphoton ionization, inverse Bremsstrahlung absorption, and impact ionization in the process of plasma formation (Adapted from Vogel et al., 2005. *Appl. Phys. B.*, **81**, 1015-1047). Free electrons result from inverse Bremsstrahlung absorption events and impact ionization.

It is important to note that the electronic excitation threshold of liquid water is ~ 6.5 eV (Johannin-Gilles and Vodar, 1954; Goulet et al., 1990.) while the ionization potential of a single water molecule is 12.6 eV (Table 1). The promotion of an electron from the ground state to the valence band requires the energy of, for example, five, three and two photons for UV wavelengths of 800 (1.56 eV), 532 (2.34 eV) and 355 (3.51 eV) nm, respectively in order to overcome the band-gap energy of water (Δ = 6.5 eV) (Vogel et al. 2005). In pure water, this energy can be provided only when several photons interact simultaneously with a bound electron. The multiphoton ionization rate is proportional to I^k, where I is the laser irradiance (intensity) and k the number of photons required for ionization (Vogel 1997; Vogel and Venugopalan, 2003). In case of inverse Bremsstrahlung absorption, the effect of

the photon increases the kinetic energy of the free electron. After the absorption events, the kinetic energy of the electron exceeds the band gap energy (ΔE), and the electron can generate another free electron via impact ionization. Thus, two free electrons with low energies are available which can again gain energy through the inverse Bremsstrahlung effect. The recurring results of the absorption events and impact ionization bring about an avalanche of LEEs (Vogel and Venugopalan, 2003). Obviously, two sources of free electrons when a femtosecond laser pulse propagations and self-focuses through liquid or solid media are direct excitation of the electrons from the valence to the conduction bands by multiphoton absorption and cascade or avalanche process (inverse Bremsstrahlung effect) (Chin et al., 2005). The free-electron density is estimated in the range 10^{17}-10^{19} cm^{-3} (Brodeur and Chin, 1998; Chin et al., 2005) in the liquid phase. This linear distribution of electrons transfer their excess energy to the surrounding water molecules, generating in the self-focusing region chemically reactive species such as e^-_{aq} (Brastaviceanu, 2004), $H^\bullet$, $^\bullet O^\bullet$ (Meesungnoen and Jay-Gerin 2005; Meesungnoen and Jay-Gerin 2009) and $^\bullet OH$. In addition H_2, O_2, H_2O_2 (Chin and Lagacé, 1996) and $O_2^{\bullet-}$ (or $HO_2^\bullet$, pK_a = 4.8) (Meesungnoen and Jay-Gerin 2005; Meesungnoen and Jay-Gerin 2009) are also produced due to recombination of the radicals. The production of molecular species such as, H_2, O_2 and H_2O_2, using intense femtosecond laser pulses have already been reported (Chin and Lagacé, 1996). The absorption of e^-_{aq} along the filament and the corresponding intensity dependence of the spatial distribution of e^-_{aq} have been observed (Brastaviceanu, 2004). In this project, the femtosecond filamentation is studied in view of its possible medical and biological applications. We specifically investigated the deposited dose and the morphology of the ultra-short pulse laser filamentation. A combination of Fricke, ceric-cerous and polyacylamide gel dosimetry was used to investigate these aspects. In addition, the molecular damage of thymidine and DNA damage was used to study the effect of the laser irradiation. We uncovered several striking features of laser-based irradiation.

I.9. Objectives of the research project

As seen earlier, the radiation sensitizers and protectors play a significant role in clinical radiation therapy. The overall aims of this research project are 1) to quantitatively

assess the efficiency of potential radiation sensitizers and protectors, 2) to understand their underlying mechanisms of action using radiation chemical dosimetry, and 3) to assess and characterize the potential utility of filamentation from femtosecond infra-red laser pulses in radiotherapy . The findings are described in three manuscripts:

- to evaluate the dose enhancement of iodinated compounds by polyacrylamide gel dosimetry (**article I**).
- to evaluate the radioprotective potential of cystamine using the Fricke and polyacrylamide gel dosimetry. In this case we carried out an experimental and Monte-Carlo simulation study (**article II**).
- to characterize a new and unique approach to radiation therapy using femtosecond laser pulse filamentation (**acticle III**).

II. Article No. 1

In this chapter, we investigate the sensitizing effect of iodinated compounds using the polyacylamide gel (PAG) dosimeter. The sensitizing potential is quantified by a dose enhancement ratio determined by an increased R_2-dose sensitivity of the PAG dosimeter incorporating an iodinated-sensitizing compound as compared to the sensitivity recorded without this compound. In addition, this technique can be used not only to evaluate dose enhancement of radiosensitizers, but also to assess radioprotectors via a decreased R_2-dose sensitivity.

This work is presented in the following article, entitled: "**Evaluation of dose-enhancement of iodinated compounds by polyacrylamide gel dosimetry**", By Ridthee Meesat, Jean-Paul Jay-Gerin, Abdelouahed Khalil, and Martin Lepage. *Physics in Medicine and Biology*, Vol **54**, pages 5909-5917 (17 September 2009). (Reprinted with permission)

Co-authorship: Ridthee Meesat designed and performed research, analyzed data and wrote manuscript. Martin Lepage supervised the project advised on data interpretation and edited the manuscript. Jean-Paul Jay-Gerin was co-supervisor of the project and edited the manuscript. Abdelouahed Khalil was the co-supervisor of the project and edited the final manuscript.

Résumé

Dans cette étude, nous avons déterminé de façon quantitative l'efficacité de certains radiosensibilisateurs à l'aide de la dosimétrie avec gel de polyacrylamide (PAG). L'augmentation de dose locale causée par l'absorption-K de certains atomes tels le brome et l'iode peut augmenter le dommage aux molécules et cellules voisines. Des essais clonogéniques peuvent évaluer l'efficacité des radiosensibilisateurs à diminuer la survie cellulaire. Toutefois, cette technique nécessite une croissance cellulaire en culture fiable et demande un fort investissement en temps. Notre objectif est d'utiliser la dosimétrie PAG pour déterminer le potentiel radiosensibilisant de composés iodés. L'incorporation de radiosensibilisateurs iodés tels le NaI et un agent de contraste iodé a mené à une augmentation quantifiable de la dose déposée. Suite à une irradiation de faible énergie (~ 40 keV), le rapport d'augmentation de dose attribué à l'agent de contraste iodé était de 1,16 ± 0,02, 1,39 ± 0,03 et 1,82 ± 0,04 pour des concentrations respectives de 0,01 (3,5 mg ml^{-1}), 0,05 (6 mg ml^{-1}) et 0,1 (12 mg ml^{-1}) M. Aucune augmentation n'a été observée lorsque les échantillons étaient irradiés avec des photons gamma de 1,25 MeV.

Abstract

In this study, polyacrylamide gel (PAG) dosimetry is used to quantitatively assess the efficiency of radiation sensitizers. The local dose enhancement caused by the K-edge absorption of certain atoms such as bromine and iodine can be employed to increase the damage to neighboring molecules and cells. Clonogenic assays can assess the radiation survival of cells to evaluate the efficiency of radiation sensitizers, but this technique requires reliable cell growth in culture media and is time-consuming. Our purpose is to use PAG dosimetry to investigate the sensitizing potential of radiation sensitizers such as iodinated compounds. Incorporation of iodinated radiation sensitizers such as NaI and an iodinated contrast agent, leads to a quantifiable sensitizer enhancement ratio. When irradiated at low energy (~40 keV), the dose enhancement ratio of the iodinated contrast agent at concentrations of 0.01 (3.5 mg ml^{-1}), 0.05 (6 mg ml^{-1}) and 0.1 (12 mg ml^{-1}) M are 1.16 ± 0.02, 1.39 ± 0.03 and 1.82 ± 0.04, respectively. No dose enhancement was observed when the samples were irradiated with 1.25 MeV gamma photons.

Keywords: radiation sensitizer – dose enhancement – iodinated contrast agent – polyacrylamide gel dosimeter – alkaline halide

1. Introduction

Radiation sensitizers play an important role in clinical radiotherapy in order to enhance tumor cell killing (Wardman 2007). It is therefore important to understand the mechanisms of the action of such compounds at the chemical level in order to help better control and perhaps optimize their biological effects. In the interaction of ionizing radiation with a medium one distinguishes between the *direct* and *indirect* effects. The direct mode of action (often termed the *target theory*) exerts its effect directly on target molecules in form of ionization and excitation. By contrast, the indirect action involves transfer of energy to water molecules, which prompts the formation of highly reactive species (through the *radiolysis of water*) and, in turn, induces damage to the target molecules (Anderson 1984).

Radiation sensitizers are intended to enhance tumor cell killing while having much less effect on normal tissues. Enhancement of the radiation damage by radiosensitizers (also called "dose enhancers") originates from the direct action of radiation on the sensitizing compounds. This mechanism of radiosensitization can generate a variety of effects such as the production of secondary electrons and Auger electron cascades (Ertl *et al* 1970), X-ray fluorescence (Ertl *et al* 1970), high-LET α-particles and charged fragments (Barth *et al* 2005) as well as free-radical species (Wardman 1987). These products can damage critical cellular targets such as DNA, RNA, proteins or lipids, increasing the extent of initial radiation injury and thus improving tumor killing.

From radiobiological experiments, several studies have reported radiosensitization properties of iodine compounds such as KI (Quintiliani 1987, Joubert *et al* 2005), NaI (Joubert *et al* 2005) and iodinated contrast agents (Matsudaira *et al* 1980, Quintiliani 1987, Dawson *et al* 1987, Adam *et al* 2003, Joubert *et al* 2005). At energies above the K-edge

absorption of the iodine atom, photoelectric absorption leads to additional photoelectric effect, this ultimately results in the production of a photoelectron, characteristic X-ray photons, and Auger electrons. These radiations result in locally-enhanced cell killing (Matsudaira *et al* 1980, Quintiliani 1987, Dawson *et al* 1987, Corde *et al* 2004, Joubert *et al* 2005), frequency of micronuclei (Matsudaira *et al* 1980) and other types of chromosomal damage (Matsudaira *et al* 1980, Matsubara *et al* 1997). Clonogenic assays, referred to as "biological dosimetry" (Prasad 1995), measure the radiation survival of cells but this technique requires reliable cell growth in culture media (Tubiana *et al* 1990, Slavotinek *et al* 1994) and can overestimate the radiation injuries (Prasad 1995). Moreover, this technique is time-consuming (Tubiana *et al* 1990, Slavotinek *et al* 1994, Prasad 1995). In this study, we propose to develop a chemical radiation dosimetry method based on polymer gel dosimetry to assess the efficiency of radiation sensitizers.

The polyacrylamide gel (PAG) dosimeter is a three-dimensional radiation dosimeter (Maryanski *et al* 1993, Baldock *et al* 1998) and a radiological tissue equivalence dosimeter (Venning et al 2005) that is composed of monomers such as acrylamide (AA) and *N,N'*-methylene-bis-acrylamide (BIS) dissolved in an aqueous gelatin matrix. The principle of the dosimeter is based on the polymerization of the monomers initiated by radical species produced by the radiolysis of water (Lepage *et al* 2001a). On average, every polymer chain contains on the order of 10^4 monomer units (Lepage *et al* 2000).

Several techniques can be used to evaluate the radiation-induced chemical changes in the dosimeter gels, such as optical techniques, X-ray computed tomography, ultrasound and magnetic resonance imaging (MRI) (Lepage *et al* 2001b). Generally, in the evaluation of polymer gel dosimeters by MRI, the spin-spin relaxation time (T_2) of protons in the gel following irradiation is determined in two or three dimensions In general, the quasi-linear

relationship between the inverse of T_2 (R_2) and the absorbed dose is called the "R_2-dose response"(Lepage *et al* 2001b). The sensitivity of a polymer gel dosimeter is defined as the slope of the linear part of the dosimeter response to dose at low doses which is called the "R_2-dose sensitivity" (De Deene 2006). When a radiosensitizer (or "dose enhancer") is added to the gel dosimeter, the effect of radiation on the sensitizing compound is expected to result in more radical species and in a larger extent of polymerization for a given dose (Boudou *et al* 2007). Under these conditions, the R_2-dose sensitivity will be higher than without the sensitizer. Recently, Boudou *et al* (2007) have used this method to measure the dose enhancement in polymer gels doped with sodium iodide and irradiated with synchrotron radiation. In the present study, we confirm these results with an iodinated contrast agent and with more conventional irradiation sources. In addition, we report on similar experiments where halide ions (iodine and bromine) are present in an ionic form for which the observation of sensitization is ambiguous.

2. Experiment

2.1. Sample preparation

The dosimeter gels were prepared under a controlled N_2 atmosphere inside a glove box with AA and BIS (99+%, electrophoresis grade, Aldrich), gelatin (300 bloom, Aldrich), and de-ionized water. The two monomers, AA (3% w/w, 0.475 *M*) and BIS (3% w/w, 0.219 *M*), were dissolved in an aqueous gelatin (5% w/w) matrix. In the manufacture process, gelatin was added to water at room temperature and left to soak for 10 min. The solution was then

heated and maintained at a temperature of 45°C. AA and BIS were successively added and magnetically stirred for typically 15 min until complete dissolution. The solution was divided in separate containers where different concentrations of NaI (99.999%, Aldrich), NaBr (99.9%, Aldrich), thiourea (99%, Aldrich) or of an iodinated contrast agent (ICA, Conray®30, Tyco healthcare) were added. A stock solution of ICA with a concentration of iodine of 141 mg/ml was prepared. The gel solutions were poured into 2 ml cylindrical glass vials having a Teflon-lined screw-top cap (Lepage *et al* 2001a). The samples were kept inside the glove box and were irradiated 24 hours after manufacture.

2.2. Irradiation of the gel

The samples were irradiated up to 9 Gy at 25°C in a ^{60}Co Gammacell 220 (Atomic Energy of Canada Limited) or with photons from an X-ray therapy system (Therapax HF150T). For the gamma irradiation, the sample vials were placed in the center of a polystyrene holder which was positioned at middle of the chamber of the irradiator and the dose rate was 3.44 Gy/min. The dose rate was determined by a Fricke dosimeter. In the x-ray irradiation, the X-ray system was operated at 10.4 mA and 100 kV. The beam was filtered with 1.8 mm of aluminum and 0.1 mm of copper to yield photons with a most probable energy of ~40 keV. The dose was delivered via a cone applicator with a 10 cm diameter at the base and a source to skin distance of 25 cm. The vials were placed perpendicularly to the beam at the end of the applicator. Each vial was marked to indicate the direction of the incident radiation. The absorbed dose was derived from relative dose measurement and absolute calibration in a known controlled geometry. The uniformity of the irradiation field was verified by placing vials filled with a Fricke solution at various locations within the

field (~79 cm^2) enabled irradiation of 4 vials simultaneously. The precision was found to be ~ 3 % in the middle. The dose rate for X-ray photons was 0.86 Gy/min.

2.3. Determination of T_2 relaxation times

The T_2 relaxation times of water protons in the gel samples were determined 24 hours after irradiation using a head coil in a Siemens Sonata 1.5 T MRI scanner. The vials were imaged upright in a single slice in the coronal plane at 21°C using a 32-echo spin-echo sequence. A repetition time of 4 s and repeated echoes with an echo spacing of 50 ms were used in order to the lowest uncertainty (Baldock et al 2001). The field of view was 256 × 256 mm^2, the slice thickness 4 mm and the pixel size 1.0 × 1.0 mm^2. ROIs were drawn on the vials and the mean values along with the standard deviation on the mean are reported. Hemispheric ROIs (area ~20 mm^2) were placed on the side of the vials where the x-rays were incident. A circular ROI with the same area was placed in the center of the gamma-irradiated vials. The uncertainty in the measurement is related to many factors, including the echo spacing. We report relative R_2 values which are the R_2 values for each gel with the respective value of R_2 at 0 Gy ($R_2(0)$) subtracted.

2.4. Mesurment of the dose enhancement ratio

The dose enhancement ratio (DER) was defined as the ratio between the R_2-dose sensitivity of the gels with an iodine compound and the sensitivity of the gels without iodine compound (Boudou *et al* 2007):

$$\mathrm{DER} = \frac{R_2 \text{ - dose sensitivity with iodine compound}}{R_2 \text{ - dose sensitivity without iodine compound}} \quad (1)$$

3. Results and Discussion

The PAG dosimeter can be used to measure 3D radiation absorbed doses since the amount of polymer formed in the dosimeter is related to the absorbed dose within a given dose range. As mentioned above, the polymerization is initiated by radical species produced by the radiolysis of water. Various species are generated during water radiolysis, such as the radical species e^-_{aq}, $HO^\bullet$, $H^\bullet$ and $HO_2^\bullet/O_2^{\bullet-}$ ($pK_a = 4.8$), and the molecular products H_2O_2 and H_2 (Ferradini and Jay-Gerin 2000). Among these radiolytic species, only e^-_{aq}, $HO^\bullet$ and $H^\bullet$ can react efficiently with the monomers (Wojnárovits *et al* 2001, Kozicki *et al* 2003), the latter being inert to hydrogen gas, water or hydrogen peroxide (Armstrong *et al* 1958, Collinson *et al* 1957).

The results shown in Figs. 1 and 2 indicate R_2 as a function of dose for PAG dosimeters irradiated either with gamma or X-ray photons, as expected. When sodium chloride (NaCl), sodium bromide (NaBr), sodium iodide (NaI), thiourea or an ICA are added to the PAG dosimeter and irradiated by ^{60}Co γ-rays, a decrease of R_2-dose sensitivity is observed (see Fig. 1), which reveals a lower extent of polymerization. This decrease is more pronounced for larger concentrations of the compounds. In fact, there appears to be an absence of response at the lowest doses in each case, an observation that is similar to cases where oxygen is present in the dosimeter (Maryanski *et al* 1993). Our control dosimeters without sensitizers clearly show that O_2 contamination can be ruled out. An absence of

sensitization was expected since the gamma photon energy (~1.25 MeV) is well beyond the K-edge absorption of iodine (~33 keV) (Humm and Charlton 1988). In water, sodium halides (NaX where X = Cl, Br or I) are present in the ionic form (halide ion X^- and sodium ion). For example, in neutral water, NaI is dissociated into Na^+ and I^- such that I^- can rapidly scavenge (via electron-transfer-type reactions) the radiolytically formed $HO^\bullet$ radicals (Ertl *et al* 1970), thus preventing the initiation of the polymerization reaction. The reaction of halide ions with $HO^\bullet$ takes place through the following steps (Spinks and Woods 1990, von Sonntag 2006):

$$X^- + HO^\bullet \rightarrow HOX^{\bullet-} \quad (2)$$

$$HOX^{\bullet-} \rightarrow X^\bullet + HO^- \quad (3)$$

$$X^\bullet + X^- \leftrightarrow X_2^{\bullet-} \quad (4)$$

The reaction rate constants of $HO^\bullet$ with Cl^-, Br^- and I^- are ~1×10^3, 1.2×10^9 and 1.1×10^{10} $M^{-1}s^{-1}$ at pH 7, respectively (Anbar and Neta 1967), while AA and BIS can react with $HO^\bullet$ with a rate constant of 5.9×10^9 (Wojnárovits *et al* 2001) and 1.37×10^{10} (Kozicki *et al* 2003) $M^{-1}s^{-1}$, respectively. Thus, there is a competition between the monomers and the halide ions to react with $HO^\bullet$ resulting in less initiation of polymerization. The process leads to a decreased R_2-dose response as seen in Fig. 1.

The decrease in R_2-dose response may represent the efficiency of the halide ions to scavenge hydroxyl radicals. Figure 1a-c shows that the decrease in response is more pronounced in the order $I^- < Br^- < Cl^-$, which is consistent with the reaction rates of these

ions with $HO^{\bullet}$ (Huie and Neta 1999, von Sonntag 2006). Thiourea is a powerful scavenger of $HO^{\bullet}$ and e^{-}_{aq} radicals. When thiourea was added to the PAG dosimeter, a decrease in R_2-dose response was also observed (Fig. 1d). Note that the concentrations of thiourea added were ten times smaller than for the halide ions. These results are consistent with the rate constants between thiourea and hydroxyl radicals and hydrated electrons, which are $4.7 \times 10^9\ M^{-1}s^{-1}$ (Wasil *et al* 1987) and $3 \times 10^9\ M^{-1}s^{-1}$ (Anbar and Neta 1967), respectively.

Given the AA and BIS molecules are present in larger concentrations (i.e., 0.475 and 0.219 *M*, respectively) compared with sodium halides (0.01–0.1 *M*), it is not surprising to observe an increase in R_2 even at the highest NaX concentration. As can also be observed from Fig. 1a-c, the slope becomes larger at higher doses for the samples containing sodium halides, although this slope remains smaller than for the control samples. This suggests that these halide ions (i.e., X = Cl^-, Br^- and I^-) get neutralized after reaction with $HO^{\bullet}$ such that I^- ions are progressively removed from the solution, until they are all neutralized, at which point the R_2-dose response is restored.

The results were different when the samples were irradiated with X-ray photons whose most probable energy (~40 keV) is close to the K-edge absorption of iodine (~33 keV). Typically, at an absorbed dose of 5 Gy, the results shown in Fig. 2a indicate that the R_2-dose response decreases (taking the control line in the absence of NaI as a reference) at the lowest NaI concentration considered (0.01 *M*) and then increases at the highest concentrations (0.05 and 0.1 *M*). This peculiar behaviour can be explained as follows. At low enough concentrations, NaI exhibits protective properties. We have already discussed how halide ions can react with the water free radicals in competition with the monomers. However, as the NaI concentration increases, the direct action of the radiation on iodine

becomes progressively dominant and radiosensitizing effects can be observed. PAG dosimeters containing NaBr were irradiated under the same conditions as for NaI. Even if the K-edge energy of bromine (~13.6 keV) is lower than that of iodine, we still see sensitization at high dose and high NaBr concentration.

The same experiment was repeated with a PAG dosimeter containing an ICA where the iodine atoms are covalently bound to the molecule and are therefore not present as I^- in the dosimeter gel. Figure 2c shows a clear increase of the R_2-dose response. The R_2- dose sensitivity increases from 0.199 $s^{-1}Gy^{-1}$ in the absence of ICA to 0.362 $s^{-1}Gy^{-1}$ at an ICA concentration of 0.1 *M*. This sensitizing property of ICA increases as the concentration increases, as expected. This confirms that iodine atoms covalently linked to a molecule cannot react with water free radicals, such that only the sensitizing effect is observed. We can calculate the dose enhancement ratio of the ICA at 3.5, 6, and 12 mg/ml as shown in Table 1. A clinical investigation compared irradiation of a brain tumor with diagnostic x-rays in the presence or absence of an iodiated contrast agent at concentrations reaching 5 mg of iodine per gram of tumor (Rose *et al* 1999). The authors concluded that this approach could be highly useful for the treatment of brain and other contrast-enhanced tumors.

4. Conclusion

Our results strongly suggest that the polyacrylamide gel dosimeter can be used to evaluate the efficiency of an iodinated contrast agent when photon the photon energy is carefully selected. For accurate results, experiments should be performed at several doses such that

competition processes between ions and monomers can be observed. We suggest the role of this type of approach consists in determining the physical and chemical efficiency of radiation sensitizers as a prerequisite before undertaking biological experiments. The overall efficiency of radiation sensitizers must still be assessed from *in vivo* experiments.

Acknowledgments

This work was funded by the Natural Sciences and Engineering Research Council of Canada. RM acknowledges a scholarship from the Ministry of Science and Technology of the Royal Thai Government. ML is the Canada Research Chair in Magnetic Resonance Imaging, J-P J-G and ML are members of the FRSQ-funded Centre de recherche clinique Étienne-Le Bel.

Table 1. Radiosensitization by an iodinated contrast agent (ICA) in a PAG dosimeter. The samples were irradiated by ~40 keV X-ray photons. The standard deviations of the dose enhancement ratios (DER) are derived from the uncertainties in the linear fits.

Concentration of iodine in the PAG	R_2-Dose sensitivity ($s^{-1}Gy^{-1}$)	Correlation coefficient (r^2)	DER[a]
0 (control)	0.199 ± 0.003	0.9968	1.00 ± 0.02
0.01 M (3.5 mg/ml)	0.232 ± 0.003	0.9979	1.16 ± 0.02
0.05 M (6.0 mg/ml)	0.276 ± 0.004	0.9987	1.39 ± 0.03
0.10 M (12.0 mg/ml)	0.362 ± 0.006	0.9991	1.82 ± 0.04

[a]DER = R_2-dose sensitivity of ICA in PAG /R_2-dose sensitivity of control PAG

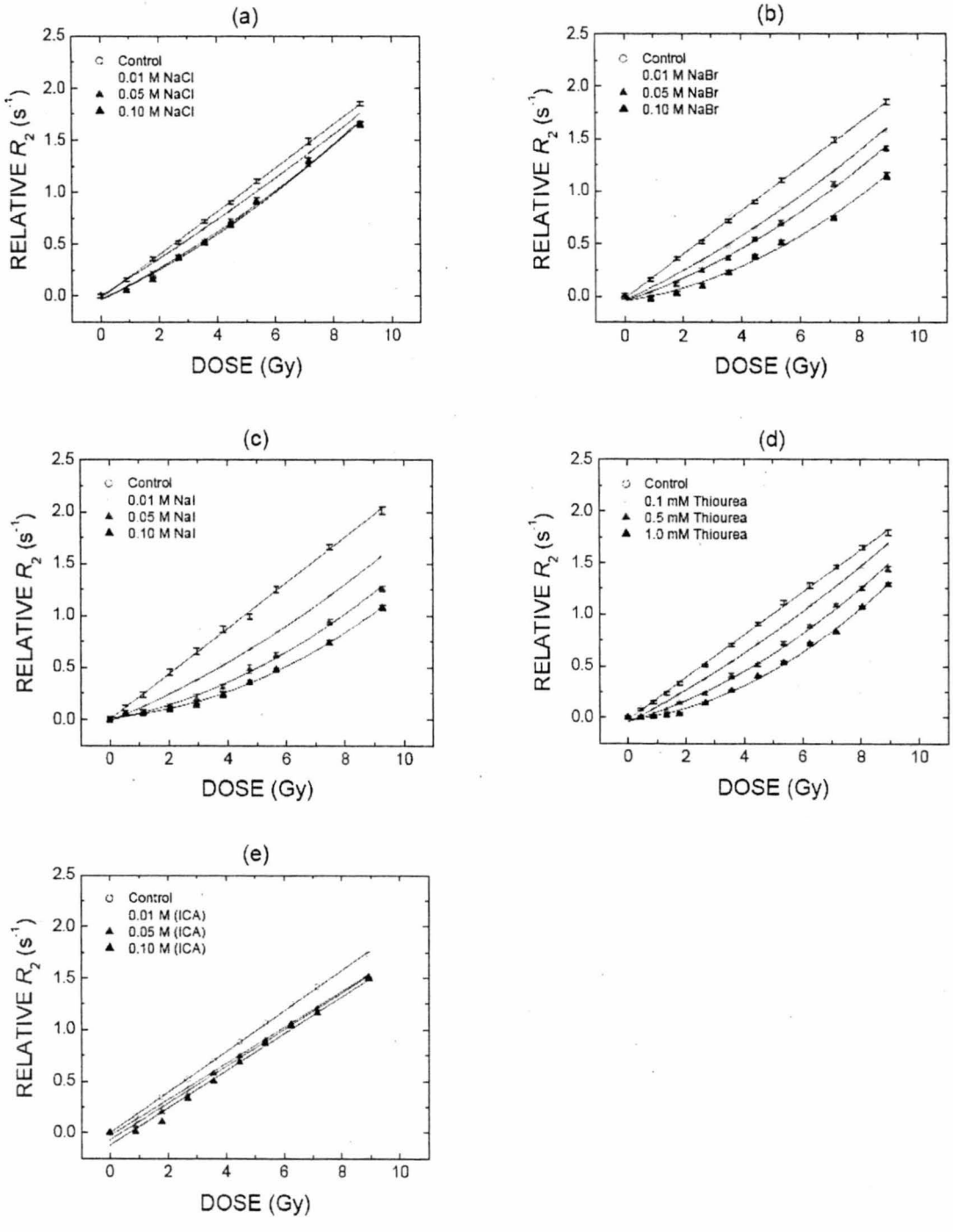

Figure 1. Plot of relative R_2 against absorbed dose for PAG dosimeters containing different concentrations of (a) NaCl, (b) NaBr, (c) NaI, (d) thiourea and (e) ICA (the concentrations of iodine atoms are shown, there are three iodine atoms per ICA molecule) irradiated with 1.25 MeV gamma photons. A lower extent of polymerization is noted for every compound added to the PAG dosimeter at this irradiation energy.

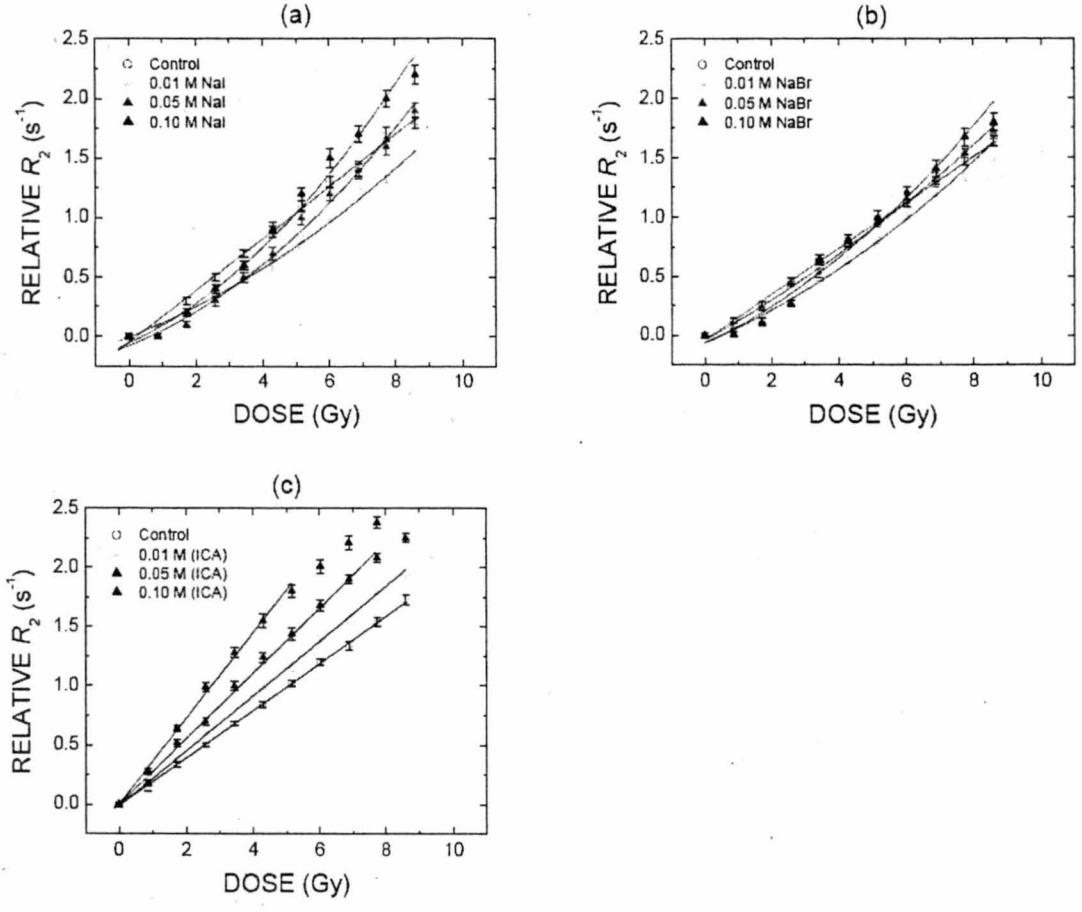

Figure 2. Plot of relative R_2 against absorbed dose for PAG dosimeters containing different concentrations of (a) NaI, (b) NaBr and (c) ICA (the concentrations of iodine atoms are shown) irradiated with 40 kVp X-ray photons. At this energy, a competition between the scavenging of free radicals by the halide ions and a sensitization is observed for NaI (panel a) and NaBr (panel b), which are in an ionic form in the solution. When the iodine atoms are covalently bound to a molecule such as an ICA, only the sensitization is observed (panel c).

References

Adam J-F, Elleaume H, Joubert A, Biston M-C, Charvet A-M, Balosso J, Le Bas J-F and Estève F 2003 Synchrotron radiation therapy of malignant brain glioma loaded with an iodinated contrast agent: First trial on rats bearing F98 gliomas *Int. J. Radiat. Oncol. Biol. Phys.* **57,** 1413-26

Armstrong D, Collinson E and Dainton F S 1958 Radical and molecular yields in solutions of acrylamide in light and heavy water irradiated with Co^{60} γ rays *Proceedings of the Second United Nations International Conference on the Peaceful Uses of Atomic Energy* **29,** 85-8

Anbar M and Neta P 1967 A compilation of specific bimolecular rate constants for the reactions of hydrated electrons, hydrogen atoms and hydroxyl radicals with inorganic and organic compounds in aqueous solution *Int. J. Appl. Radiat. Isotopes* **18,** 493-523

Anderson D W 1984 *Absorption of Ionizing Radiation* (Baltimore: University Park Press)

Baldock C, Burford R P, Billingham N, Wagner G S, Patval S Badawi R D and Keevil S F 1998 Experimental procedure for the manufacture and calibration pf polyacrylamide gel (PAG) for magnetic resonance imaging (MRI) radiation dosimetry *Phys. Med. Biol.* **43,** 695-702

Baldock C, Lepage M , Bäck S Å J, Murry P J Jayasekera P M Porter D and Kron T 2001 Dose resolution in radiotherapy polymer gel dosimetry: effect of echo spacing in MRI pulse sequence *Phys. Med. Biol.* **46,** 449-60

Barth R F, Coderre J A, Vicente M G H and Blue T E 2005 Boron neutron capture therapy of cancer: Current status and future prospects *Clin. Cancer Res.* **11,** 3987-4002

Boudou C, Troprès I, Rousseau J, Lamalle L, Adam J F, Estève F and Elleaume H 2007 Polymer gel dosimetry for synchrotron stereotactic radiotherapy and iodine dose-enhancement measurements *Phys. Med. Biol.* **52,** 4881-92

Collinson E, Dainton F S and McNaughton G S 1957 The effect of acrylamide on the X- and γ-ray yields of hydrogen peroxide from de-aerated water *Trans. Faraday. Soc.* **53,** 357-62

Corde S, Joubert A, Adam J-F, Charvet A-M, Le Bas J-F, Estève F, Elleaume H and Balosso J 2004 Synchrotron radiation-based experimental determination of the optimal energy for cell radiotoxicity enhancement following photoelectric effect on stable iodinated compounds *Br. J. Cancer* **91,** 544-51

De Deena Y, Vergote K, Claeys C and De Wagter C 2006 The fundamental radiation properties of normoxic polymer gel dosimeters: a comparison between a methacrylic acid based gel and acrylamide based gels *Phys. Med. Biol.* **50,** 653-73.

Dawson P, Penhaligon M, Smith E and Saunders J 1987 Iodinated contrast agents as "radiosensitisers" *Br. J. Radiol.* **60,** 201-3

Ertl H H, Feinendegen L E and Heiniger H J 1970 Iodine-125, a tracer in cell biology: Physical properties and biological aspects *Phys. Med. Biol.* **15,** 447-56

Ferradini C and Jay-Gerin J-P 2000 The effect of pH on water radiolysis: A still open question - A minireview *Res. Chem. Intermed.* **26,** 549-65

Huie R E and Neta P 1999 Chemistry of reactive oxygen species *Reactive Oxygen Species in Biological systems: An Interdisciplinary Approach* ed D L Gilbert and C A Colton (New York: Kluwer Academic/Plenum Publishers) pp 33-73

Humm J L and Charlton D E 1988 Double strand breakage in DNA produced by the photoelectric interaction with incorporated 'cold' bromine *DNA Damage by Auger Emitters* ed K F Baverstock and D E Charlton (London: Taylor & Francis) pp 111-22

Joubert A, Biston M-C, Boudou C, Ravanat J-L, Brochard T, Charvet A-M, Estève F, Balosso J and Foray N 2005 Irradiation in presence of iodinated contrast agent results in radiosensitization of endothelial cells: Consequences for computed tomography therapy *Int. J. Radiat. Oncol. Biol. Phys.* **62,** 1486-96

Kozicki M, Filipczak K and Rosiak J M 2003 Reactions of hydroxyl radicals, H atoms and hydrated electrons with *N, N'*-methylenebisacrylamide in aqueous solution. A pulse radiolysis study *Radiat. Phys. Chem.* **68,** 827-35

Lepage M, Whittaker A K, Rintoul L and Baldock C 2000 ^{13}C-NMR, ^{1}H-NMR, and FT-Raman study of radiation-induced modifications in radiation dosimetry polymer gels *J. Appl. Polym. Sci.* **79,** 1572-81

Lepage M, Whittaker A K, Rintoul L, Bäck S Å J and Baldock C 2001a The relationship between radiation-induced chemical processes and transverse relaxation times in polymer gel dosimeters. *Phys. Med. Biol.* **46,** 1061-74

Lepage M, Jayasakera P M, Bäck S Å J and Baldock C 2001b Dose resolution optimization of polymer gel dosimeters using different monomers *Phys. Med. Biol.* **46,** 2665-80

Maryanski M J, Gore J C, Kennan R P and Schulz R J 1993 NMR relaxation enhancement in gels polymerized and cross-linked by ionizing radiation: A new approach to 3D dosimetry by MRI *Magn. Reson. Imaging* **11,** 253-8

Matsubara S, Kong Z S, Omura M, Kurihara H, Torigoe S, Iwasawa T, Yoshida T and Kubota N 1997 The effect of iodine-based contrast agents on the levels of radiation-induced chromosomal aberrations *Radiat. Res.* **147,** 263-8

Matsudaira H, Ueno A M and Furuno I 1980 Iodine contrast medium sensitizes cultured mammalian cells to X rays but not to γ rays *Radiat. Res.* **84,** 144-8

Prasad K N 1995 *Handbook of Radiobiology* 2nd ed (Boca Raton: CRC Press)

Quintiliani M 1987 Physico-chemical basis of radiosensitization by iodine compounds *Radiat. Phys. Chem.* **30,** 409-22

Rose J H, Norman A, Ingram M, Aoki C Solberg T and Mesa A 1999 First radiotherapy of human metastatic brain tumours delivered by a computerized tomography scanner *Int. J. Radiat. Oncol. Biol.* **45,** 1127-32

Slavotinek A, McMillan T J and Steel C M 1994 Measurement of radiation survival using the MTT assay. *Eur. J. Cancer* **30A,** 1376-82

Spinks J W T and Woods R J 1990 *An Introduction to Radiation Chemistry,* 3r ed. (New York: Wiley)

Tubiana M, Dutreix J and Wambersie A 1990 *Introduction to Radiobiology* (London: Taylor & Francis).

Venning A J, Nitschke K N, Keall P J and Baldock C 2005 Radiological properties of normoxic polymer gel dosimeters *Med. Phys.* **32,** 1047-53

von Sonntag C 2006 *Free-Radical-Induced DNA Damage and Its Repair: A Chemical perspective* (Berlin: Springer-Verlag)

Wardman P 1987 The mechanism of radiosensitization by electron-affinic compounds *Radiat. Phys. Chem.* **30,** 423-32

Wardman P 2007 Chemical radiosensitizers for use in radiotherapy *Clin. Oncol.* **19,** 397-417

Wasil M, Halliwell B, Grootveld M, Moorhouse C P, Hutchison D C S and Baum H 1987 The specificity of thiourea, dimethylthiourea and dimethyl sulphoxide as scavengers of hydroxyl radicals *Biochem. J.* **243,** 867-70

Wojnárovits L, Takács E, Dajka K, D'Angelantonio M and Emmi S S 2001 Pulse radiolysis of acrylamide derivatives in dilute aqueous solution *Radiat. Phys. Chem.* **60,** 337-43

III. Article No. 2

In this chapter, we report using Fricke dosimeter to measure protecting effect of cystamine. The protecting capacity of the disulfide compound is shown in term of decreasing of the yield of Fe^{3+}. In this study, we have used both experimental and simulation study to evaluate the radioprotective potential of this compound.

This work is presented in the following article, entitled: "**Utilization of the Ferrous Sulfate (Fricke) Dosimeter for Evaluating the Radioprotective Potential of Cystamine: Experiment and Monte-Carlo Simulation**", By Ridthee Meesat, Sunuchakan Sanguanmith, Jintana Meesungnoen, Martin Lepage, Abdelouahed Khalil and Jean-Paul Jay-Gerin.

This article has been accepted for publication in *Radiation Research*.

Co-authorship: Ridthee Meesat designed and performed research, analyzed data and wrote manuscript. Jean-Paul Jay-Gerin supervised the project, advised on data interpretation, wrote and edited the manuscript. Sunuchakan Sangusnmith performed computer simulation and wrote the manuscript. Jintana Meesungnoen advised on computer simulation program. Abdelouahed Khalil was co-supervisor of this project and edited the final manuscript. Martin Lepage was co-supervisor of this project and edited the final manuscript.

Résumé

La cystamine est un compose organique disulfide qui compte parmi les meilleurs radioprotecteurs pour protéger les tissus sains en radiothérapie. Récemment, ce composé s'est aussi avéré bénéfique dans le traitement de désordre du système nerveux central en modèle animal. Toutefois, le mécanisme d'action de ce composé au niveau chimique moléculaire n'est pas encore bien compris. Cette étude vise à évaluer de façon quantitative le potentiel radioprotecteur de ce composé en utilisant la dosimètre de sulfate ferreux (Fricke) tant en situation expérimentale qu'en modélisation théorique. Notre méthode se base sur la réaction d'espèces oxydantes issues de la radiolyse de l'eau, tel que $^{\bullet}OH$, $HO_2^{\bullet}$, et H_2O_2 pour la conversion des ions ferreux en ions ferriques dans le dosimètre de Fricke. La présence de la cystamine dans la solution du dosimètre de Fricke empêche l'oxydation du Fe^{2+} et contribue donc à diminuer le rendement en ions ferriques Fe^{3+} (c.-à-d. le rendement G). La diminution observée de la valeur $G(Fe^{3+})$ s'accentue avec une augmentation de la concentration du composé disulfide sur la plage 0-0.1 M, que ce soit en condition aérée ou désaérée. Un code Monte-Carlo complet a été mis au point pour simuler en détail la chimie radio-induite dans ce sysème. En se basant sur les connaissances disponibles à propos de la chimie sous rayonnement de la cystamine, les simulations Monte Carlo nous ont permis de proposer des mécanismes de réaction et d'incorporer des réactions spécifiques décrivant la radiolyse de la cystamine dans une solution aérée ou désaérée de Fricke. De plus, les rendements chimiques calculés sont en accord avec les données expérimentales. Les résultats indiquent clairement que l'effet protecteur de la cystamine provient de sa capacité à capturer des radicaux libres, ce qui cause une compétition avec les ions ferreux pour la réaction avec plusieurs espèces radicalaires, tout spécialement les radicaux $^{\bullet}OH$ et $H^{\bullet}$ formés pendant la radiolyse de l'eau. Nous concluons que les simulations Monte-Carlo sont une méthode efficace pour comprendre les mécanismes de dommages indirects à l'échelle moléculaire sous rayonnement.

Utilization of the Ferrous Sulfate (Fricke) Dosimeter for Evaluating the Radioprotective Potential of Cystamine: Experiment and Monte-Carlo Simulation

by

Ridthee Meesat,[a] Sunuchakan Sanguanmith,[a] Jintana Meesungnoen,[a] Martin Lepage,[a] Abdelouahed Khalil[a,b] and Jean-Paul Jay-Gerin[a,2]

[a] *Département de Médecine Nucléaire et de Radiobiologie and* [b] *Département de Médecine (Service de Gériatrie), Faculté de Médecine et des Sciences de la Santé, Université de Sherbrooke, Sherbrooke (Québec) J1H 5N4, Canada*

Number of pages: **51** (including text, references, tables, listing of footnotes, figure captions, and figures)
Number of tables: **2**
Number of figures: **7**
Number of references: **89**
Number of footnotes: **14**
Running title: **Fricke dosimeter and radioprotection evaluation of cystamine**

Radiation Research
Manuscript No. RR2829 - Revised version

November 2011

Meesat, R., Sanguanmith, S., Meesungnoen, J., Lepage, M., Khalil, A. and Jay-Gerin, J.-P. Utilization of the Ferrous Sulfate (Fricke) Dosimeter for Evaluating the Radioprotective Potential of Cystamine: Experiment and Monte-Carlo Simulation. *Radiat. Res.*

[2] Address for correspondence: Département de Médecine Nucléaire et de Radiobiologie, Faculté de Médecine et des Sciences de la Santé, Université de Sherbrooke, 3001, 12ème Avenue Nord, Sherbrooke (Québec) J1H 5N4, Canada. Tel. +1-819-346-1110, ext. 14682 or 14773; fax: +1-819-564-5442; e-mail: jean-paul.jay-gerin@USherbrooke.ca

ABSTRACT

Cystamine, an organic disulfide (RSSR), is among the best of the known radiation-protective compounds and has been used to protect normal tissues in clinical radiation therapy. Recently, it has also proved to be beneficial in the treatment of disorders of the central nervous system in animal models. However, the underlying mechanism of its action at the chemical level is not well understood yet. The present study aims at using the ferrous sulfate (Fricke) dosimeter to quantitatively evaluate, both experimentally and theoretically, the radioprotective potential of this compound. The well-known radiolysis of the Fricke dosimeter by ^{60}Co γ-rays or fast electrons, based on the oxidation of ferrous ions to ferric ions by the oxidizing species $^{\bullet}OH$, $HO_2^{\bullet}$, and H_2O_2 produced in the radiolytic decomposition of water, forms the basis for our method. The presence of cystamine in Fricke dosimeter solutions during irradiation prevents the radiolytic oxidation of Fe^{2+} and leads to decreased ferric yields (or *G*-values). The observed decrease in $G(Fe^{3+})$ increases upon increasing the concentration of the disulfide compound over the range 0-0.1 *M* under both aerated and deaerated conditions. To help assess the basic radiation-protective mechanism of this compound, a full Monte-Carlo computer code is developed to simulate in complete detail the radiation-induced chemistry of the studied Fricke/cystamine solutions. Benefiting from the fact that cystamine is reasonably well characterized in terms of radiation chemistry, this computer model proposes reaction mechanisms and incorporates specific reactions describing the radiolysis of cystamine in aerated and deaerated Fricke solutions that lead to the observable quantitative chemical yields. Results clearly indicate that the protective effect of cystamine originates from its radical-capturing ability, which allows this compound to act by competing with the ferrous ions for the various free radicals – especially $^{\bullet}OH$ radicals and $H^{\bullet}$ atoms – formed during irradiation of the surrounding water. Most interestingly, our simulation modeling also shows that the predominant pathway in the oxidation of cystamine by $^{\bullet}OH$ radicals involves an electron-

transfer mechanism, yielding $RSSR^{\bullet+}$ and OH^-. A very good agreement is found between calculated $G(Fe^{3+})$ values and experiment. This study concludes that Monte-Carlo simulations represent a very efficient method for understanding indirect radiation damage at the molecular level.

Keywords: cystamine, radioprotector, antioxidant, ferrous sulfate (Fricke) dosimeter, linear energy transfer (LET), Monte-Carlo simulation, reaction scheme, aerated and deaerated solutions, free radicals, competition kinetics, scavenging capacity, radiation chemical yields (*G*-values).

INTRODUCTION

Radiotherapy is the most common modality for treating human cancers. In order to obtain improved local tumor control with higher doses of radiation, a possible way is to selectively protect the surrounding normal critical tissues against radiation damage. This can be achieved by administration of a radioprotector. Hence radiation-protective compounds are important in clinical radiotherapy to modulate tissue and tumor responses to radiation and, thus, to enhance the therapeutic benefit for cancer patients (*1*). It should also be recalled here that the potential application of radioprotectors to protect a large population in the event of nuclear accidents or possible nuclear/radiological terrorism, or yet astronauts and cosmonauts in case of exposure to high doses of space radiation still remains a reason not only for pursuing research on currently available radioprotective agents but also for developing new, more effective, and nontoxic ones (*2, 3*).

In such a context, understanding the mechanisms of the action of cytoprotective compounds at the *chemical* level is certainly highly desirable to help better control their biological effects. This is especially true when we recognize that short-lived free radicals are obligate intermediates in the complex pathways leading ultimately to cell kill or pathological change after radiation (*4*).

Because living cells and tissues consist mainly of water (~70-85% by weight), the main action of radiation on biological systems is with water (*5*). As a result of water radiolysis, highly reactive species with well-known cytotoxic potential are generated. For low linear energy transfer (LET) radiation such as ^{60}Co γ-rays, fast electrons or high-energy protons, the major species resulting from the radiolytic decomposition of water are the free radicals e^-_{aq}, $^{\bullet}OH$, $H^{\bullet}$, $HO_2^{\bullet}/O_2^{\bullet-}$ (depending on pH, pK_a = 4.8), and the molecular products H_2O_2 and H_2 (*6, 7*). Under ordinary irradiation conditions, these species are produced nonhomogeneously on subpicosecond time scales in small, spatially isolated regions of dense ionization and excitation events (referred to as "spurs") along the path of

the radiation. Owing to diffusion from their initial positions, the radiolytic products either react within the spurs as they expand or escape into the bulk solution. The "primary" (or "escape") radical and molecular yields $g(e_{aq}^-)$, $g(H^\bullet)$, $g(H_2)$, $g(^\bullet OH)$, $g(H_2O_2)$, etc., are defined as the number of species of each kind formed or destroyed per 100 eV of absorbed energy that remain after spur expansion (~10^{-6}-10^{-7} s at room temperature) and become available to react with added solutes at moderate concentrations (case of dilute aqueous solutions) (*6-8*) or with potentially critical target molecules within a cell, such as DNA ("indirect effect" of ionizing radiation) (*9, 10*).[3]

In cellular systems, chemical radioprotectors are usually thought to exert their protective effects by a combination of different mechanisms, including free radical scavenging and hydrogen atom donation. If the radiolysis water-produced reactive intermediates are scavenged (or intercepted) by the protector compound before they can interact with vital cellular components (especially DNA) (*9, 10*), the damaging effect of radiation is reduced. Cytoprotection by radioprotective compounds containing sulfhydryl – SH groups (i.e., with labile hydrogen atoms) is also formulated in terms of $H^\bullet$-atom donation to chemically repair (or restore) DNA damage (where C-H bonds have been broken) which would otherwise be "fixed" by oxygen (*9, 10, 12*). In this latter case, sulfhydryl compounds exert their protective activity by efficiently competing with oxygen in reactions with key DNA free radicals (*13*), thereby reducing DNA damage and increasing cell survival.

---

[3] Throughout this paper, radiation chemical yields are quoted in units of molecules per 100 eV (abbreviated as "molec./100 eV"), as $g(X)$ for primary yields and $G(X)$ for experimentally measured yields. For conversion into SI units (mol/J), 1 molec./100 eV ≈ 0.10364 μmol/J (*7, 11*).

Cystamine is an organic diamino-disulfide compound (RSSR). Below pH 8, it is predominantly in the form of the doubly protonated molecule $^{+}NH_3$-CH_2-CH_2-S-S-CH_2-CH_2-NH_3^{+} (pK_a ~ 9 for both of the amino-groups) (*14, 15*). The mutual Coulombic repulsion of the two positive charges at opposite ends of the molecule favors an open conformation with a high collision-accessibility of the –S-S– group to approaching radicals. This factor is an important determinant of the vulnerability of this compound to attack by water free radicals (such as $^{\bullet}OH$) (*14*). Besides its radical-scavenging role in protection against cellular oxidative stress, cystamine further holds anti-apoptotic properties, which may potentially prevent or delay progression of neuronal degeneration that leads to central nervous system (CNS) disorders (such as Huntington, Alzheimer, and Parkinson diseases) in animal models (*16, 17*). Cystamine has also been shown to reduce brain edema, cell death and neurological deficits following intracerebral hemorrhage in rats (*18*). However, the precise molecular mechanisms by which it operates are still unclear (*19*).

In this study, we use the aqueous ferrous sulfate, or Fricke, chemical dosimeter to quantitatively assess the radical scavenging properties of cystamine and thereby evaluate the radiation-protective potential of this compound. The Fricke dosimeter system, which is the radiolytic oxidation of ferrous ions in acid solution, was developed originally as a dose measuring device (*20*). It is, however, a most valuable tool to examine the kinetics and chemistry of the interaction of reactive water species with any scavenger (*21-24*). By inference, if scavenger molecules other than Fe^{2+} are present in Fricke solutions during irradiation, they will competitively react with the products of the radiolysis of water, and the yield of Fe^{3+} will be reduced, i.e., there will be protection of Fe^{2+}. The evaluation of the radiation-protective efficiency of cystamine using the Fricke dosimeter solution as the "indicator" solution was first reported by Jayson and Wilbraham (*25*) and later by Lalitha and Mittal (*26*). These authors demonstrated that, on irradiation, the addition of cystamine produced a marked inhibition of ferrous oxidation. Here, we have ourselves performed *G*-

value determinations to investigate, over a wide concentration range, the effect of cystamine on the Fe^{3+} yield of the Fricke dosimeter in the presence as well as in the absence of oxygen. Furthermore, based on our current knowledge of the radiation chemistry of cystamine, we have developed in parallel with experiments, a full Monte-Carlo code to simulate the radiation-induced chemistry of the studied Fricke/cystamine solutions. This computer code proposes reaction mechanisms and incorporates specific reactions describing the radiolysis of cystamine in both aerated and deaerated Fricke solutions that are obtained from various literature sources and that lead to the observed quantitative chemical yields. It is, to our knowledge, the first time that the radiolysis of a sulfur-containing molecular system is studied by means of Monte-Carlo simulation techniques.[4]

THE FRICKE DOSIMETER

Of all aqueous systems studied, the ferrous sulfate dosimeter, referred to as the "Fricke dosimeter" after Hugo Fricke who first published accounts of its properties in 1927-1929 (*27, 28*), is certainly the best understood, and the most commonly used, liquid chemical dosimeter (*6, 8, 20, 23, 29*). It is widely accepted in radiation-chemical work because of the accuracy, reproducibility, and linearity of its response as a function of dose (*6, 30, 31*). The response of the dosimeter is linear over a wide range of doses (*6, 30*), the maximum absorbed dose that can be measured accurately amounting to ~400 Gy with low-LET radiation.

The standard Fricke solution consists of 1 m*M* $FeSO_4$ (or ferrous ammonium sulfate) in 0.4 *M* H_2SO_4 (pH 0.46) and is saturated with air (the concentration of oxygen is ~0.25

[4] A preliminary report of this work was presented at the *3rd Asia Pacific Symposium on Radiation Chemistry, Treasure Island Resorts, Lonavala, India*, September 14-17, 2010; see Proceedings, Vol. I-Invited Talks, Paper ITRC-13, p. 50-55 (ISBN: 81-88513-37-7).

m*M*). The mechanism for the radiolytic oxidation of Fe^{2+} ions to Fe^{3+} is well-understood (*6, 8, 20, 23, 29, 32, 33*) and the rate constants at 25 °C of the individual reactions taking place are known (*33-38*). The major reactions for ferric ion production in a Fricke dosimeter solution are:

$$e^-_{aq} + H^+ \rightarrow H^\bullet \qquad k_1 = 2.3 \times 10^{10}\ M^{-1}\ s^{-1}\ ^5 \qquad (1)$$

$$H^\bullet + O_2 \rightarrow HO_2^\bullet \qquad k_2 = 2.1 \times 10^{10}\ M^{-1}\ s^{-1} \qquad (2)$$

$$^\bullet OH + Fe^{2+} \rightarrow Fe^{3+} + OH^- \qquad k_3 = 3.4 \times 10^{8}\ M^{-1}\ s^{-1} \qquad (3)$$

$$HO_2^\bullet + Fe^{2+} \rightarrow Fe^{3+} + HO_2^- \qquad k_4 = 7.9 \times 10^{5}\ M^{-1}\ s^{-1} \qquad (4)$$

$$HO_2^- + H^+ \rightarrow H_2O_2 \qquad k_5 = 5.0 \times 10^{10}\ M^{-1}\ s^{-1}\ ^4 \qquad (5)$$

$$H_2O_2 + Fe^{2+} \rightarrow Fe^{3+} + {}^\bullet OH + OH^- \qquad k_6 = 52\ M^{-1}\ s^{-1} \qquad (6)$$

$$H^\bullet + Fe^{2+} \xrightarrow{H^+} Fe^{3+} + H_2 \qquad k_7 = 1.3 \times 10^{7}\ M^{-1}\ s^{-1}\ . \qquad (7)$$

At the acid concentration of 0.4 *M* H_2SO_4, the H^+ ions very rapidly scavenge most, if not all, of the e^-_{aq} radicals in spurs to form $H^\bullet$ atoms (*11*). In the presence of oxygen, each $H^\bullet$ atom reacts with O_2 to give a hydroperoxyl radical, and each of these radicals oxidizes three Fe^{2+} ions.[6] Each $^\bullet OH$ radical oxidizes one Fe^{2+} ion, and each molecule of H_2O_2 oxidizes two Fe^{2+} ions. Summing all sources of Fe^{3+} ions, the yield of ferric ions in *aerated* solution can be expressed in terms of the "escape" yields of the free radicals and molecular species of the radiolysis of the solution by the following stoichiometric equation (*6, 29, 32, 33, 39*):

---

[5] Rate constant in the limit of infinite dilution, i.e., *not* corrected for the effects due to the ionic strength of the solutions.

[6] Some $H^\bullet$ atoms may also directly react with Fe^{2+} [reaction (7)]. However, at 25 °C and a ferrous ion concentration of 1 m*M*, the contribution of this reaction to the formation of Fe^{3+} can be neglected.

$$G(Fe^{3+})_{aerated} = 3\,g(e^-_{aq} + H^\bullet) + g(^\bullet OH) + 2\,g(H_2O_2) + 3\,g(HO_2^\bullet)\,, \qquad (8)$$

where $g(e^-_{aq} + H^\bullet)$ represents the sum of the primary yields of the reducing radicals e^-_{aq} and $H^\bullet$.[7] In air-free ^{60}Co γ-irradiated 0.4 *M* H_2SO_4 aqueous solutions (LET ~ 0.3 keV/μm), the escape yields of free radicals and molecular products are well determined. Most representative values at room temperature are *(11)*:

$$g(e^-_{aq} + H^\bullet) = 3.70 \qquad g(HO_2^\bullet) = 0.02 \qquad g(H_2) = 0.40$$

$$g(^\bullet OH) = 2.90 \qquad g(H_2O_2) = 0.80 \qquad g(-H_2O) = 4.50\,. \qquad (11)$$

Using these primary radiolytic yield values in Eq. (8) leads to a value for the yield of Fe^{3+} which is well within the range of 1-2% of the recommended yield of 15.5 ± 0.2 ions/100 eV reported in the literature for ^{60}Co γ-rays (*20, 32, 43*).

In the absence of oxygen, reaction (7) replaces reaction (2) cutting down the number of ferric ions oxidized by $H^\bullet$ to one instead of three in aerated solutions:

$$G(Fe^{3+})_{deaerated} = g(e^-_{aq} + H^\bullet) + g(^\bullet OH) + 2\,g(H_2O_2) + 3\,g(HO_2^\bullet)\,, \qquad (12)$$

where the experimentally observed Fe^{3+} ion yield for ^{60}Co γ radiation is 8.2 ± 0.3 molecules/100 eV (*20, 32, 44*).

Experimentally, under both aerated and deaerated conditions, the presence of cystamine in the Fricke dosimeter solution during irradiation is found to significantly affect

---

[7] Note that, for solutions of 0.4 *M* in H_2SO_4, there is a small amount of $^\bullet OH$ radicals that react with HSO_4^- to form the sulfate radical $SO_4^{\bullet-}$ according to (*40, 41*)

$$^\bullet OH + HSO_4^- \rightarrow H_2O + SO_4^{\bullet-} \qquad k_9 = 1.5 \times 10^5\ M^{-1}\ s^{-1}. \qquad (9)$$

However, the overall ferric ion yield remains the same as given by Eq. (8) since the sulfate radical reacts with Fe^{2+} in the same way as $^\bullet OH$ (*42*):

$$SO_4^{\bullet-} + Fe^{2+} \rightarrow Fe^{3+} + SO_4^{2-} \qquad (10)$$

with $k_{10} = 9.9 \times 10^8\ M^{-1}\ s^{-1}$ (in the limit of zero ionic strength).

the rate of radiolytic oxidation of Fe^{2+}, producing markedly decreased ferric ion yields (*25*, *26*, this work). According to Eqs. (8) and (12), it clearly indicates that the protective effect of cystamine at the molecular level originates from its radical-capturing ability, which allows this compound to act by competing with the ferrous ions for the various free radicals produced in the radiolysis of the surrounding water.

EXPERIMENTAL

The Fricke dosimeter solutions were prepared using ammonium ferrous sulfate hexahydrate $(NH_4)_2Fe(SO_4)_2.6H_2O$ (99.99%, Sigma Aldrich), sulfuric acid (98%, Sigma Aldrich), and doubly distilled water. These chemicals were used as received. Special attention based on standard procedures of radiation chemistry (*6*) was given to the cleaning of glassware that came into contact with the solutions to be irradiated. The solutions, either air-saturated or deaerated, consisted of 1 m*M* Fe^{2+} ions in 0.4 *M* H_2SO_4. No chloride was added.[8] The density of the solutions was 1.024 g/cm^3. In the case of deaerated solutions, the samples were prepared under a nitrogen atmosphere in a glove box and purged with nitrogen. The prepared stock solution was divided into separate containers in which different concentrations of cystamine sulfate hydrate (98%, Aldrich), over the range 5×10^{-7}-0.1 *M*, were added.[9] The samples, consisting of 2-ml glass vials, were irradiated up to 80 Gy at 25 °C by ^{60}Co γ-rays in a Gammacell 220 (Atomic Energy of Canada Limited) at a

[8] Note that sodium chloride is often added to the Fricke solution in order to protect it from the detrimental effects of organic impurities, so lower quality water may be suitable (*20*).

[9] The UV-absorption spectrum of cystamine, which exhibits a broad maximum centered at ~245 nm in neutral pH (*45*), was found to be unchanged in aqueous 0.4 *M* H_2SO_4 solution, indicating that this compound did not degrade at low pH under the acidic conditions of the Fricke dosimeter.

dose rate of 3.44 Gy/min.[10] Measurements of the optical density (OD) of the Fricke solutions were carried out using a U3300 spectrophotometer (Hitachi) and the concentration of ferric ions was calculated from the increase in the OD at 304 nm using a value of 2205 M^{-1} cm^{-1} (*6*, *46*) for the molar extinction coefficient of Fe^{3+}. The radiation yield of Fe^{3+}, $G(Fe^{3+})$, was obtained from the slope of the linear plot of the Fe^{3+} concentration against the absorbed dose. All *G*-values were reported as means ± SEM (standard error of mean) calculated from triplicate experiments.

MONTE-CARLO SIMULATIONS

To help assess the basic molecular processes that are involved in the mechanism of radioprotective action of cystamine, a full Monte-Carlo computer code, called IONLYS-IRT (*47*), has been used to simulate in complete detail the radiolysis of the studied Fricke/cystamine solutions. Monte-Carlo simulation methods are indeed well adapted to take into account the stochastic nature of the complex sequence of events that are generated in these solutions following absorption of ionization radiation. More specifically, the code we use here is an extension of the one we previously developed in our group to simulate the radiolysis of air-free aqueous 0.4 *M* H_2SO_4 (pH ~ 0.46) solutions (*33*, *41*, *48*) and the radiation-induced oxidation of ferrous sulfate solutions in the (aerated) Fricke dosimeter at both ambient (*8*, *33*) and elevated temperatures (*8*, *48*). In brief, the IONLYS simulation program covers the early "physical" and "physicochemical" stages of radiation action up to ~10^{-12} s. It models, event by event, all the basic physical interactions (energy deposition) and the subsequent establishment of thermal equilibrium in the system (conversion of the physical products created locally after completion of the physical stage into the various

[10] The dose rate was determined by Fricke dosimetry, taking $G(Fe^{3+})$ to be 15.6 molec./100 eV (*20*).

initial radical and molecular products of the radiolysis (distributed in a highly nonhomogeneous track structure). The complex spatial distribution of reactants at the end of the physicochemical stage, which is provided as an output of the IONLYS program, is then used directly as the starting point for the subsequent "nonhomogeneous chemical" stage (from ~10^{-12} to ~10^{-7}-10^{-6} s at 25 °C). This third stage, during which the individual reactive species diffuse randomly at rates determined by their diffusion coefficients and react with one another or, competitively, with any added solutes present at the time of irradiation until all spur processes are complete, is covered by our IRT program. This IRT program can obviously also be used efficiently to describe the "homogeneous" chemical stage that takes place at longer times, as is precisely the case here for the simulation of the Fricke dosimeter in which ferric ions are produced at a wide variety of times (*8*, *33*, *37*, *48*). This program employs the "independent reaction times" (IRT) method, a computer-efficient stochastic simulation technique that is used to simulate reaction times without following the trajectories of the diffusing species (*49*, *50*). Its implementation has been described in detail (*51*). The ability of this program to give accurate time-dependent chemical yields under different irradiation conditions has been well validated by comparison with full random flights (or "step-by-step") Monte-Carlo simulations, which do follow the reactant trajectories in detail (*52*, *53*).

The model assumptions and procedures employed to carry out the Monte-Carlo simulations of the radiolysis of 0.4 *M* H_2SO_4 aqueous solutions with IONLYS-IRT have already been given. To summarize briefly, the effects of the background concentration of H^+ in solutions were added to the IRT program as pseudo first-order reactions. We also supplemented the reaction scheme for the radiolysis of pure deaerated liquid water (*8*, *47*, *51*) to include the reactions listed in Table 1, which account for the species (HSO_4^-, SO_4^{2-}, $SO_4^{\bullet-}$, and $S_2O_8^{2-}$) present in irradiated sulfuric acid solutions (*33*, *40*). To stochastically model the chemistry of the Fricke dosimeter, we added to the IRT program the reactions

(3), (4), and (6) of Fe^{2+} ions with the oxidizing species $^{\bullet}OH$, $HO_2^{\bullet}$, and H_2O_2 that are formed in the water of the irradiated solutions under aerated conditions, respectively. As seen above, in the absence of oxygen, the difference in the Fe^{3+} yield comes from reaction (7) replacing reaction (2). Under normal irradiation conditions, the concentrations of radiolytic products are low compared with the background concentrations of Fe^{2+} ions and O_2 (~2.5×10^{-4} *M*) in solution, and their reactions could also be modeled in the IRT program as pseudo first-order. Finally, to simulate the radiolysis of the aerated or deaerated Fricke dosimeter in the presence of cystamine, we supplemented the ferrous-sulfate Fricke dosimeter reaction scheme to include the twenty seven chemical reactions listed in Table 2. This set of reactions is proposed here to account for the experimental values of the ferric ion yield as a function of the concentration of added cystamine, in the presence or absence of oxygen.

In addition, we have introduced in the IRT program the effect of ionic strength of the solutions on all reactions between ions. The correction to the reaction rate constants was made using the following equation (*48*, *85*, *86*):

$$\log\left(\frac{k}{k_0}\right) = 1.02\ Z_a Z_b \left(\frac{I^{1/2}}{1 + I^{1/2}}\right), \qquad (13)$$

where k is the rate constant at ionic strength I, k_0 is the rate constant in the limit of zero ionic strength (i.e., at infinite dilution of ions), Z_a and Z_b are the algebraic numbers of charges on the reactants (positive for cations and negative for anions), and I (in *M*) is defined as (*87*)

$$I = \frac{1}{2} \sum_i Z_i^2 C_i , \qquad (14)$$

where Z_i is the charge number of the i_{th} ion and C_i is its molar concentration (the sum extends over all ionic species present in the solution). According to Eq. (13), the rate constants will increase, decrease, or remain the same with increasing ionic strength,

depending on whether the ions have the same sign, opposite signs, or whether one species is uncharged. Finally, in our simulations the "direct" action of ionizing radiation on the various solutes (sulfuric acid anions, ferrous ions, oxygen, and cystamine) present in the solution was neglected, which is a reasonably good approximation over the range of H_2SO_4 (0.4 *M*)/$FeSO_4$ (1-5 × 10^{-3} *M*)/O_2 (2.5 × 10^{-4} *M*)/RSSR (5 × 10^{-7}-0.1 *M*) concentrations studied (*48*).

To reproduce the effects of ^{60}Co γ-radiolysis, we used short (typically, ~150 μm) segments of 300-MeV proton tracks, over which the average LET value obtained in the simulations was nearly constant and equal to ~0.3 keV/μm at 25 °C. Such model calculations thus gave "track segment" yields at a well-defined LET (*88*).[11] The number of proton histories (usually ~150) was chosen so as to ensure only small statistical fluctuations in the computed averages of chemical yields, while keeping acceptable computer time limits. In the simulations reported here, the time evolution of $G(Fe^{3+})$ has been followed until ~200 s.

RESULTS AND DISCUSSION

Figures 1a and 2a show the time evolution of $G(Fe^{3+})$ formation as obtained from our simulations of the radiolysis of the Fricke dosimeter in aerated and deaerated conditions, respectively, for 300-MeV irradiating protons (LET ~ 0.3 keV/μm) at ambient temperature. As can be seen from these figures, $G(Fe^{3+})$ is time dependent, a result of the differences in the lifetimes of the reactions that make up the radiolysis mechanisms in the presence or

[11] We should note that the use of high-energy protons as primary particles was more appropriate here than that of fast electrons since we wanted to study track segments over which the LET is essentially constant. In fact, a proton that has the *same* LET as an electron must also have an energy ~2000 times larger, and consequently its LET is much less affected by a given series of energy depositions (*41*, *51*).

absence of oxygen (*6*, *8*, *33*, *37*, *48*, *89*). This is clearly indicated in Figs. 1b and 2b where we show the time profiles of the extents $\Delta G(Fe^{3+})$ of each of the reactions (2-4), (6), (7), and (10) that contribute to the formation of Fe^{3+}, calculated from our simulations. While the kinetics of formation of Fe^{3+} in the radiolysis of aerated Fricke solutions has already been discussed in detail previously, the time evolution of $G(Fe^{3+})$ in the absence of oxygen has received only little attention. Similar to what is observed for aerated solutions, Fig. 2a shows the existence of three main stages, well separated in time, corresponding here to the reactions of Fe^{2+} ions with the species $^{\bullet}OH$, $H^{\bullet}$ (instead of $HO_2^{\bullet}$ in aerated solutions), and H_2O_2. As can be seen from Fig. 2b, the most rapid reaction of Fe^{2+} ions is with $^{\bullet}OH$ radicals. It is completed by about 20 μs. The oxidation of Fe^{2+} by $H^{\bullet}$ atoms [reaction (7)] is slower and requires about 0.5 ms for completion. The slowest component in the formation of Fe^{3+} is due to hydrogen peroxide oxidation. This latter reaction takes place at times longer than ~0.5 s and is completed by about 100 s.[12] Under the present low-LET conditions, our computed ferric ion yields in aerated and deaerated solutions at ~200 s are equal to ~15.45 and 8.0 molec./100 eV, respectively (see Figs. 1a and 2a), in very good agreement with the standard experimental values (*20*, *32*, *43*, *44*).

In Fig. 3a and b, we compare the kinetics of Fe^{3+} formation as obtained from our simulations of the radiolysis of the Fricke dosimeter, under both aerated and deaerated conditions, in the presence of various concentrations of added cystamine. As we can see immediately from this figure, $G(Fe^{3+})$ at ~200 s decreases markedly with increasing cystamine concentration. For example, in the presence of oxygen, $G(Fe^{3+})$ decreases from ~15.45 to about 4.65 molec./100 eV when going from the Fricke solution without added

[12] Note that the reaction of the sulfate radical with Fe^{2+} [reaction (10)], whose contribution to the formation of Fe^{3+} is close to that found for reaction (6) (see Fig. 2b), is completed at about the same time as reaction (3).

cystamine to a solution containing 0.1 *M* of the disulfide (Fig. 3a). Such markedly decreased ferric ion yields in the presence of cystamine are also observed in deaerated solutions (Fig. 3b). These reduced yields of Fe^{3+} when cystamine is present in Fricke solutions during irradiation are obviously a clear signature that this molecule can readily scavenge the different primary products of acid water radiolysis (predominantly, $^{\bullet}OH$ radicals and $H^{\bullet}$ atoms; see below) that contribute to the radiolytic oxidation of ferrous ions. This influence of the concentration of cystamine on the Fricke yield is further illustrated in Fig. 4, where our calculated $G(Fe^{3+})$ values are compared with experimental data (*25*, *26*, this work), in the presence and absence of oxygen, for cystamine concentrations varying from 5×10^{-7} to 0.1 *M*.

Before looking more closely at these comparisons, it should be noted first that, throughout the range of cystamine concentrations studied, our measured Fe^{3+} ion yields are in very good agreement with other values of $G(Fe^{3+})$ previously reported in the literature (*25*, *26*). This is clearly shown in Fig. 4 where the ferric ion yields are plotted as a function of the logarithm of the concentration of added cystamine. As we can see from this figure, for air-saturated solutions, $G(Fe^{3+})$ is fairly constant for low cystamine concentrations ($< 10^{-6}$ *M*), falls sharply between $\sim 10^{-6}$ and 10^{-2} *M* cystamine, and then decreases slowly as the concentration of cystamine increases above 10^{-2} *M*. Deaerated solutions show a relatively similar variation of $G(Fe^{3+})$ with cystamine concentration, with the difference however that the drop in the Fe^{3+} yields, between $\sim 10^{-6}$ and 10^{-3} *M* cystamine, is much smaller. Moreover, unlike solutions containing oxygen, the slight decrease of $G(Fe^{3+})$ observed above 10^{-3} *M* is followed by a more pronounced decline around 0.1 *M* cystamine.

Having at our disposal a larger amount of experimental data (from the data available so far), covering the widest possible range of cystamine concentrations, was in fact a primary objective of this work. This is obviously a great advantage when one considers that our ultimate goal is to compare, as effectively as possible, the results of our simulations

with experiment. As we will see below, the quality of these comparisons will allow us to support not only the Monte-Carlo simulation approach developed here, but also its usefulness in investigating with many details the mechanism of the action of ionizing radiations upon the studied system.

Figure 4 shows a very good agreement between the results of the simulations and the experimental yields of Fe^{3+} in both aerated and deaerated solutions. This agreement, however, could be obtained *only* after adjusting the fraction of $^{\bullet}OH$ radicals that react with cystamine to form either transient $RSSR^{\bullet+}$ radical ions [reaction (R3a)] or the non-ionic intermediates RSH and $RSO^{\bullet}$ [reaction (R3b)] (*9*, *57*, *58*). This is demonstrated in the figure where our simulations clearly show the marked effect of changing the branching ratio for reactions (R3a) and (R3b) on the radiolytic yields of Fe^{3+}. As can be seen, this effect is especially pronounced in the absence of oxygen. For example, at 0.1 *M* cystamine under deaerated conditions, a decrease in our calculated Fe^{3+} yields of ~37.5% from ~5.65 to 3.53 molec./100 eV is predicted when the branching ratio for the two oxidation pathways is varied from 50% to 100% in favor of reaction (R3a). These results are obviously interesting in view of their predictive nature. In fact, little information exists in the literature as to the *exact* value of this branching ratio. In this regard, Bonifačić et al. (*57*) suggested that the interaction of $^{\bullet}OH$ radicals with simple aliphatic disulfides leads to the generation of disulfide radical cations or to the formation of thiols, in acid solution, with about equal probability. However, in dithiodipropionic acid and cystine, Elliot et al. (*58*) reported that the thiol is indeed a major product, but formed only in a proportion of 30-40% (*9*). No data are available for cystamine, even if the processes that occur with this compound are believed to be fairly similar to those observed for cystine (*58*). Given these uncertainties, we have treated in our simulation code the branching ratio for reactions (R3a) and (R3b) as an adjustable parameter whose value is chosen to give the best possible agreement between the simulated yields of Fe^{3+} and the experimental data. As shown in

Fig. 4, the electron-transfer reaction (R3a) appears clearly to be the predominant pathway in the oxidation of cystamine by •OH radicals, *under both aerated and deaerated conditions*. Indeed, a branching ratio close to ~100% in favor of this reaction pathway is required to give the best *simultaneous* agreement between calculated and measured Fe^{3+} yields as a function of cystamine concentration. Remarkably, this conclusion agrees very well with the hypothesis of an initial electron transfer mechanism between cystamine and •OH radicals and the postulation of the $RSSR^{\bullet+}$ species, suggested earlier by Jayson and coworkers (*14*, *25*), and later by Lalitha and Mittal (*26*) to explain their observations under gamma irradiation of the oxidation of Fe^{2+} ions in Fricke dosimeter solutions containing cystamine. Based on these results, we have thus assumed in all simulations reported in this work, either in the presence or absence of oxygen, a negligibly small intervention of reaction (R3b).

Returning now to the detailed analysis of Fig. 3a and b, we have chosen here, as an example, to focus our attention more specifically on the kinetics of Fe^{3+} formation in aerated and deaerated 10^{-3} *M* cystamine solutions (Figs. 5a and 6a, respectively). In *aerated* solution, Fig. 5a and b shows that the oxidation of Fe^{2+} ions to Fe^{3+} involves reactions mainly with $HO_2^{\bullet}$, H_2O_2, and the cystamine-radical species $RSSR^{\bullet+}$ and $RS^{\bullet}$. The observed time dependence of $G(Fe^{3+})$ is a direct result of the differences that exist in the lifetimes of these different reactions. It is noteworthy that in solutions containing 1 m*M* Fe^{2+} ions and 1 m*M* cystamine (case under consideration), virtually all the •OH radicals are scavenged by cystamine prior they can react with Fe^{2+}. Such a result, already established earlier (*14*, *25*, *26*), was readily confirmed from our simulations by a systematic study of the time profiles of the extents $\Delta G(^{\bullet}OH)$ of the reactions (3) and (R3a) as a function of the concentration of cystamine (data not shown here). At equal concentration, the competition between RSSR and Fe^{2+} for the scavenging of •OH is indeed quite to the advantage of cystamine, as the rate constant for reaction (R3a) (1.7×10^{10} M^{-1} s^{-1}; see Table 2) is 500

times larger than that for reaction (3).[13] The fact that the •OH radicals are preferably taken by the cystamine not only eliminates the contribution of reaction (3) to the formation of Fe^{3+}[14] but also that of reaction (10) which no longer occurs given the non-occurrence of reaction (9) and the absence of production of sulfate radicals $SO_4^{\bullet-}$ that follows. From Fig. 5a and b it is seen that the fastest reaction of Fe^{2+} ions is with the thiyl radicals RS•. This reaction (R6) is completed by about 4 μs. Interestingly, these thiyl radicals mainly come from the RSSR + H• reaction (R2) which takes place on a time scale of tenths of a microsecond (see Fig. 7a). The oxidation of Fe^{2+} by $HO_2^{\bullet}$ is slower, requiring a few milliseconds for completion. Finally, at times longer than ~1 s, there are two additional components to the formation of Fe^{3+}, nearly superimposed, one being due to the Fe^{2+} + H_2O_2 reaction (6) and the other to the Fe^{2+} + $RSSR^{\bullet+}$ reaction (R24). As can be seen from Fig. 5b, these two reactions are completed by about 200 s. In fact, the latter two components are closely interrelated since the yield of H_2O_2 [both the escape molecular product yield and that formed by reactions (4) and (5)] that contributes to the ferric ion yield in reaction (6) also contributes to the formation of a stoichiometrically equivalent

---

[13] From the reciprocal of the "scavenging power" (*6*), defined as the product k_{R3a} [RSSR] (in units of s^{-1}), we can estimate the time scale over which the scavenging of •OH by RSSR is occurring. At 1 m*M* cystamine, this reaction with cystamine takes place at about 5.9×10^{-8} s, that is, well before that with ferrous ions ($1/k_3$ [Fe^{2+}] ~ 2.9×10^{-6} s). This is well illustrated in Fig. 7a where we show the time profiles of the extents ΔG(RSSR) of each reaction that contributes to the formation and removal of cystamine, calculated from our Monte-Carlo simulations. In fact, as we can see from this figure, ΔG(RSSR) due to reaction (R3a) actually corresponds to the escape yield g(•OH) as soon as one reaches ~3×10^{-7} s.

[14] As can be seen from Fig. 5b, this elimination is not total; in fact, a small contribution to $G(Fe^{3+})$ due to reaction (3) (~0.11 molec./100 eV) is still observed at ~200 s.

yield of •OH. The •OH radicals so formed subsequently react almost entirely with cystamine (only very few react with Fe^{2+}; see Fig. 5b), which explains the marked decrease (about 2.1 *G*-units) of the extent ΔG(RSSR) due to reaction (R3a) observed in Fig. 7a in the time interval ~1-200 s. Concomitantly, it also quantitatively explains the corresponding increase in ΔG(RSSR) due to reaction (R24), since virtually all of the $RSSR^{\bullet+}$ radical ions created directly by reaction (R3a) in this same time interval are found to eventually oxidize Fe^{2+} ions to Fe^{3+} (rather than reacting with themselves) (see Fig. 7a).

In *deaerated* 10^{-3} *M* cystamine solution, Fig. 6a and b shows that the oxidation of Fe^{2+} ions to Fe^{3+} involves reactions mainly with H_2O_2, $RSSR^{\bullet+}$, and RS•. The most noticeable difference with the mechanism prevailing in aerated solution is that the $H^\bullet + O_2$ reaction (2) no longer occurs. Under these conditions of irradiation and contrary to what is observed in the Fricke dosimeter in the absence of cystamine (where, in particular, the reaction $Fe^{2+} + H^\bullet$ plays a predominant role; see Fig. 2), the introduction of 10^{-3}-*M* cystamine is sufficient to scavenge all H• atoms [those created directly by radiolysis and those formed via reaction (1) by protonation of e^-_{aq}] thus generating the thiyl free radicals RS• [reaction (R2)].[15] This is shown clearly in Fig. 7b where we see that the decrease in ΔG(RSSR) caused by reaction (R2) actually corresponds to the escape yield $g(e^-_{aq} + H^\bullet)$. Figure 7b also shows that, as in aerated 1 m*M* ferrous solutions at 1 m*M* cystamine, scavenging of the •OH radicals by the disulfide is nearly complete within about 3×10^{-7} s,[12] that is, long before •OH can react with Fe^{2+}. Therefore, in the absence of oxygen, the oxidation of Fe^{2+} to Fe^{3+} primarily occurs via the $Fe^{2+} + RS^\bullet$ reaction (R6) only. From Fig.

---

[15] In the absence of oxygen, cystamine molecules compete with Fe^{2+} ions for H•. Consideration of the scavenging powers k_{R2}[RSSR] and $k_7[Fe^{2+}]$ readily shows that, in 1-m*M*-ferrous solution, half of the H• atoms react with cystamine and half react with ferrous ions at a cystamine concentration of about 2×10^{-6} *M*.

6b, it is seen that these reactions are completed by about 4 μs. Finally, as in aerated solutions, there are two additional components of Fe^{3+} formation due to the oxidation of Fe^{2+} by H_2O_2 [reaction (6)] and by $RSSR^{\bullet+}$ [reaction (R24)]. These latter two interrelated reactions become significant at times longer than ~1 s and are completed around 200 s. Here, however, the yield of H_2O_2 is limited to the sole escape molecular product yield $g(H_2O_2)$ ~ 0.8 molec./100 eV since reactions (4) and (5) do not occur under deaerated conditions. The $^{\bullet}OH$ radicals formed subsequently via reaction (R6) react mostly with cystamine (only a few react with Fe^{2+}; see Fig. 6b), which explains the 0.8-*G* units decrease of the extent ΔG(RSSR) due to reaction (R3a) observed in Fig. 7b in the time interval ~1-200 s. It also readily explains the corresponding increase in ΔG(RSSR) due to the Fe^{2+} + $RSSR^{\bullet+}$ reaction (R24), since as in aerated solutions, virtually all of the $RSSR^{\bullet+}$ radical ions created directly by reaction (R3a) in this same time interval eventually oxidize Fe^{2+} ions to Fe^{3+} (rather than reacting with themselves) (see Fig. 7b).

CONCLUSION

In this work, we have evaluated quantitatively the radioprotective ability of cystamine by studying at the chemical level, the behavior of this compound towards the primary species produced in the radiolysis of water, which is the main constituent of living cells and tissues. The well-known oxidation of Fe^{2+} ions to Fe^{3+} in irradiated Fricke dosimeter solutions containing cystamine was used as an "indicator" and formed the basis of our method.

This study was conducted both experimentally and theoretically, in the presence as well as in the absence of oxygen. Experimentally, a number of Fe^{3+} ion yield measurements were performed over a wide range of cystamine concentrations (5×10^{-7}-0.1 *M*). On irradiation, the addition of cystamine markedly reduced the yields of Fe^{3+} under both aerated and deaerated conditions. A very good agreement of our measured ferric

yields was found with other values of $G(Fe^{3+})$ previously reported in the literature. On the theoretical side, a detailed analysis of the radiation-induced chemistry of the studied Fricke/cystamine solutions using Monte-Carlo computer simulations allowed a better understanding of the basic molecular processes that are involved in the mechanism of radioprotective action of cystamine. Benefiting from the fact that the radiation chemistry of this molecule is reasonably well characterized, we have been able to successfully reproduce the experimental yields of Fe^{3+} over the entire cystamine concentration range studied in both the presence and absence of oxygen.

The results obtained in this study showed unambiguously that the protecting effect of cystamine towards the Fricke dosimeter solution comes from its *radical-capturing ability*, which allows this compound to act by competing with the Fe^{2+} ions for the various free radicals resulting from the irradiation of the surrounding water. In fact, corroborating earlier results very well, our simulated experiments indicated that, among the primary products of water radiolysis, the species capable of attacking *predominantly* the cystamine molecule were $^{\bullet}OH$ radicals and $H^{\bullet}$ atoms. The marked decrease in $G(Fe^{3+})$ as a function of the concentration of added cystamine is a clear signature of the scavenging of these radicals by cystamine.

Another most interesting result of our simulations modeling the radiolysis of cystamine in both aerated and deaerated Fricke dosimeter solutions, was to show that the predominant pathway in the oxidation of cystamine by $^{\bullet}OH$ radicals does involve an *electron-transfer mechanism* – at the expense of nonionic pathways as generally suggested, at least partly, by various authors for the reaction of $^{\bullet}OH$ radicals with disulfides – yielding $RSSR^{\bullet+}$ and OH^{-}.

Finally, in light of all results obtained in this work, the good overall agreement between calculated and measured yield values supports the calculational approach and its usefulness for understanding, at the molecular level, indirect radiation damage to complex

molecules, such as cystamine – a sulfur-containing molecular system whose radiolysis had never previously been studied by means of Monte-Carlo simulation techniques. It also gives, in turn, good support to the validity and consistency of the mechanism of action employed in this study to describe the radiolysis of this molecule in both aerated and deaerated Fricke solutions.

ACKNOWLEDGMENTS

This work has benefited greatly from many stimulating discussions and correspondence with Professor P. Wardman, Professor K.-D. Asmus, Professor C. von Sonntag, Dr. N.V. Klassen, Dr. A.J. Elliot, as well as with our colleague the late Professor D.A. Armstrong. R.M. is the recipient of a Royal Thai Government scholarship from the Ministry of Science and Technology of Thailand. We are grateful to the Natural Sciences and Engineering Research Council of Canada for its financial support.

REFERENCES

1. Nair CKK, Parida DK, Nomura T. Radioprotectors in radiotherapy. J Radiat Res 2001; 42:21-37.
2. Maisin JR. Chemical radioprotection: past, present and future prospects. Int J Radiat Biol 1998; 73:443-450.
3. Dziegielewski J, Goetz W, Baulch JE. Heavy ions, radioprotectors and genomic instability: implications for human space exploration. Radiat Environ Biophys 2010; 49:303-316.
4. Wardman P. Chemical radiosensitizers for use in radiotherapy. Clin Oncol 2007; 19:397-417.
5. Bensąsson RV, Land EJ, Truscott TG. Excited states and free radicals in biology and medicine: contributions from flash photolysis and pulse radiolysis. Oxford: Oxford University Press; 1993.
6. Spinks JWT, Woods RJ. An introduction to radiation chemistry. 3rd ed. New York: Wiley; 1990.
7. Ferradini C, Jay-Gerin J-P. La radiolyse de l'eau et des solutions aqueuses: historique et actualité. Can J Chem 1999; 77:1542-1575.
8. Tippayamontri T, Sunuchakan S, Meesungnoen J, Sunaryo GR, Jay-Gerin J-P. Fast neutron radiolysis of the ferrous sulfate (Fricke) dosimeter: Monte-Carlo simulations. Recent Res Devel Physical Chem 2009; 10:143-211.
9. von Sonntag C. Free-radical-induced DNA damage and its repair. A chemical perspective. Berlin: Springer-Verlag; 2006.
10. Hall EJ, Giaccia AJ. Radiobiology for the radiologist. Philadelphia: Lippincott Williams & Wilkins; 2006.

11. Ferradini C, Jay-Gerin J-P. The effect of pH on water radiolysis: a still open question – A minireview. Res Chem Intermed 2000; 26:549-565.

12. Wardman P. The importance of radiation chemistry to radiation and free radical biology (The 2008 Silvanus Thompson Memorial Lecture). Br J Radiol 2009; 82:89-104.

13. Ward JF. Chemical aspects of DNA radioprotection. In: Nygaard OF, Simic MG, editors. Radioprotectors and Anticarcinogens. New York: Academic Press; 1983. p. 73-85.

14. Jayson GG, Owen TC, Wilbraham AC. The radiation chemistry of cystamine sulphate. J Chem Soc (B) 1967; 944-949.

15. Bidzilya VA, Golovkova LP, Beregovskaya NN, Basyuk VV, Korol' ÉN, Chuiko AA, Znamenskii VV, Barkaya VS. Radioprotective effect of immobilized cystamine. Pharm Chem J 1991; 25:782-786.

16. Dedeoglu A, Kubilus JK, Jeitner TM, Matson SA, Bogdanov M, Kowall NW, Matson WR, Cooper AJL, Ratan RR, Beal MF, Hersch SM, Ferrante RJ. Therapeutic effects of cystamine in a murine model of Huntington's disease. J Neurosci 2002; 22:8942-8950.

17. Tremblay M-È, Saint-Pierre M, Bourhis E, Lévesque D, Rouillard C, Cicchetti F. Neuroprotective effects of cystamine in aged parkinsonian mice. Neurobiol Aging 2006; 27:862-870.

18. Okauchi M, Xi G, Keep RF, Hua Y. Tissue-type transglutaminase and the effects of cystamine on intracerebral hemorrhage-induced brain edema and neurological deficits. Brain Res 2009; 1249:229-236.

19. Borrell-Pagès M, Canals JM, Cordelières FP, Parker JA, Pineda JR, Grange G, Bryson EA, Guillermier M, Hirsch E, Hantraye P, Cheetham ME, Néri C, Alberch J, Brouillet E, Saudou F, Humbert S. Cystamine and cysteamine increase brain levels of

BDNF in Huntington disease via HSJ1b and transglutaminase. J Clin Invest 2006; 116:1410-1424.

20. Fricke H, Hart EJ. Chemical dosimetry. In: Attix FH, Roesch WC, editors. Radiation dosimetry. 2nd ed. Vol. II. New York: Academic Press; 1966. p. 167-239.

21. Dewhurst HA. Effect of organic substances on the γ-ray oxidation of ferrous sulphate. J Chem Phys 1951; 19:1329.

22. Guczi L. Étude de l'effet d'addition de diverses substances sur l'oxydation des ions ferreux en solution aqueuse. J Chim Phys 1962; 59:795-796.

23. Das RC. Radiation chemistry of aqueous aerated ferrous sulphate solution. Radiat Res Rev 1971; 3:121-139.

24. Alpen EL. Radiation biophysics. 2nd ed. San Diego: Academic Press; 1998.

25. Jayson GG, Wilbraham AC. The utilization of the Fricke dosimeter for evaluating the biological radiation-protective potential of water-soluble organic compounds. Chem Commun (London) 1968; 641-642.

26. Lalitha B, Mittal JP. Electron transfer reaction in the radiation chemistry of some biologically important disulphide compounds. Radiat Eff 1971; 7:159-162.

27. Fricke H, Morse S. The chemical action of roentgen rays on dilute ferrosulphate solutions as a measure of dose. Am J Roentgenol Radium Ther 1927; 18:430-432.

28. Fricke H, Morse S. The action of X-rays on ferrous sulphate solutions. Philos Mag 1929;7th Ser. 7:129-141.

29. Matthews RW. Aqueous chemical dosimetry. Int J Appl Radiat Isot 1982; 33:1159-1170.

30. Klassen NV, Shortt KR, Seuntjens J, Ross CK. Fricke dosimetry: the difference between $G(Fe^{3+})$ for ^{60}Co γ-rays and high-energy x-rays. Phys Med Biol 1999; 44:1609-1624.

31. The dosimetry of pulsed radiation. ICRU Report No. 34. Bethesda: International Commission on Radiation Units and Measurements; 1982.

32. Allen AO. The radiation chemistry of water and aqueous solutions. Princeton: D. Van Nostrand Co.; 1961.

33. Autsavapromporn N, Meesungnoen J, Plante I, Jay-Gerin J-P. Monte Carlo simulation study of the effects of acidity and LET on the primary free-radical and molecular yields of water radiolysis – Application to the Fricke dosimeter. Can J Chem 2007; 85:214-229.

34. Lundström T, Christensen H, Sehested K. Reactions of the HO_2 radical with OH, H, Fe^{2+} and Cu^{2+} at elevated temperatures. Radiat Phys Chem 2004; 69:211-216.

35. Buxton GV, Greenstock CL, Helman WP, Ross AB. Critical review of rate constants for reactions of hydrated electrons, hydrogen atoms and hydroxyl radicals ($^{\bullet}OH/^{\bullet}O^{-}$) in aqueous solution. J Phys Chem Ref Data 1988; 17:513-886.

36. Ilan Y, Rabani J. On some fundamental reactions in radiation chemistry: Nanosecond pulse radiolysis. Int J Radiat Phys Chem 1976; 8:609-611.

37. Běgusová M, Pimblott SM. Stochastic simulation of γ radiolysis of acidic ferrous sulfate solution at elevated temperatures. Radiat Prot Dosim 2002; 99:73-76.

38. Elliot AJ, Bartels DM. The reaction set, rate constants and *g*-values for the simulation of the radiolysis of light water over the range 20° to 350°C based on information available in 2008. Report AECL No. 153-127160-450-001. Chalk River, Ontario: Atomic Energy of Canada Ltd.; 2009.

39. Klassen NV, Marchington D, McGowan HCE. H_2O_2 determination by the I_3^- method and by $KMnO_4$ titration. Anal Chem 1994; 66:2921-2925.

40. Jiang P-Y, Katsumura Y, Nagaishi R, Domae M, Ishikawa K, Ishigure K, Yoshida Y. Pulse radiolysis study of concentrated sulphuric acid solutions: formation mechanism,

yield and reactivity of sulfate radicals. J Chem Soc Faraday Trans 1992; 88:1653-1658.

41. Meesungnoen J, Benrahmoune M, Filali-Mouhim A, Mankhetkorn S, Jay-Gerin J-P. Monte Carlo calculation of the primary radical and molecular yields of liquid water radiolysis in the linear energy transfer range 0.3-6.5 keV/μm: application to ^{137}Cs gamma rays. Radiat Res 2001; 155:269-278.

42. Neta P, Huie RE, Ross AB. Rate constants for reactions of inorganic radicals in aqueous solution. J Phys Chem Ref Data 1988; 17:1027-1284.

43. Radiation dosimetry: X rays and gamma rays with maximum photon energies between 0.6 and 50 MeV. ICRU Report No. 14. Washington: International Commission on Radiation Units and Measurements; 1969.

44. Katsumura Y, Takeuchi Y, Ishigure K. Radiation chemistry of high temperature water – I. Degradation products in acid by gamma radiolysis. Radiat Phys Chem 1988; 32:259-263.

45. Svensson BE, Lindvall S. Myeloperoxidase-oxidase oxidation of cysteamine. Biochem J 1988; 249:521-530.

46. Broszkiewicz RK, Bulhak Z. Errors in ferrous sulphate dosimetry. Phys Med Biol 1970; 15:549-556.

47. Meesungnoen J, Jay-Gerin J-P. Radiation chemistry of liquid water with heavy ions: Monte Carlo simulation studies. In: Hatano Y, Katsumura Y, Mozumder A, editors. Charged particle and photon interactions with matter: recent advances, applications, and interfaces. Boca Raton: Taylor & Francis; 2011. p. 355-400.

48. Sanguanmith S, Muroya Y, Tippayamontri T, Meesungnoen J, Lin M, Katsumura Y, Jay-Gerin J-P. Temperature dependence of the Fricke dosimeter and spur expansion time in the low-LET high-temperature radiolysis of water up to 350 °C: a Monte-Carlo simulation study. Phys Chem Chem Phys 2011; 13:10690-10698.

49. Pimblott SM, Pilling MJ, Green NJB. Stochastic models of spur kinetics in water. Radiat Phys Chem 1991; 37:377-388.

50. Pimblott SM, Green NJB. Recent advances in the kinetics of radiolytic processes. Res Chem Kinet 1995; 3:117-174.

51. Frongillo Y, Goulet T, Fraser M-J, Cobut V, Patau JP, Jay-Gerin J-P. Monte-Carlo simulation of fast electron and proton tracks in liquid water – II. Nonhomogeneous chemistry. Radiat Phys Chem 1998; 51:245-254.

52. Goulet T, Fraser M-J, Frongillo Y, Jay-Gerin J-P. On the validity of the independent reaction times approximation for the description of the nonhomogeneous kinetics of liquid water radiolysis. Radiat Phys Chem 1998; 51:85-91.

53. Plante I. Développement de codes de simulation Monte-Carlo de la radiolyse de l'eau et de solutions aqueuses par des électrons, ions lourds, photons et neutrons : application à divers sujets d'intérêt expérimental. Ph.D. Thesis, Université de Sherbrooke; 2009.

54. Neta P, Schuler RH. Rate constants for reaction of hydrogen atoms with compounds of biochemical interest. Radiat Res 1971; 47:612-627.

55. Hoffman MZ, Hayon E. One-electron reduction of the disulfide linkage in aqueous solution. Formation, protonation, and decay kinetics of the $RSSR^-$ radical. J Am Chem Soc 1972; 94:7950-7957.

56. Asmus K-D. Heteroatom-centered free radicals. Some selected contributions by radiation chemistry. In: Jonah CD, Rao BSM, editors. Radiation chemistry: present status and future trends. Amsterdam: Elsevier; 2001. p. 341-393.

57. Bonifačić M, Schäfer K, Möckel H, Asmus K-D. Primary steps in the reactions of organic disulfides with hydroxyl radicals in aqueous solution. J Phys Chem 1975; 79:1496-1502.

58. Elliot AJ, McEachern RJ, Armstrong DA. Oxidation of amino-containing disulfides by $Br_2^{\bullet-}$ and $^{\bullet}OH$. A pulse-radiolysis study. J Phys Chem 1981; 85:68-75.

59. Asmus K-D, Bonifačić M. Sulfur-centered reactive intermediates as studied by radiation chemical and complementary techniques. In: Alfassi ZB, editor. S-centered radicals. Chichester: Wiley; 1999. p. 141-191.

60. Mezyk SP. Direct rate constant measurement of radical disulphide anion formation for cysteine and cysteamine in aqueous solution. Chem Phys Lett 1995; 235:89-93.

61. Hoffman MZ, Hayon E. Pulse radiolysis study of sulfhydryl compounds in aqueous solution. J Phys Chem 1973; 77:990-996.

62. Abedinzadeh Z, Gardès-Albert M, Ferradini C. Reactions of $^{\bullet}OH$ and $Br_2^{\bullet-}$ radicals with glutathione. A radiolysis study. Radiat Phys Chem 1992; 40:551-558.

63. Armstrong DA. Redox systems with sulphur-centered species. In: Chatgilialoglu C, Asmus K-D, editors. Sulfur-centered reactive intermediates in chemistry and biology. New York: Plenum Press; 1990. p. 341-351.

64. Wardman P. Thiyl radicals in biology: their role as a 'molecular switch' central to cellular oxidative stress. In: Alfassi ZB, editor. S-centered radicals. Chichester: Wiley; 1999. p. 289-309.

65. Adams GE, McNaughton GS, Michael BD. The pulse radiolysis of sulphur compounds. Part I. Cysteamine and cystamine. In: Johnson GRA, Scholes G, editors. The chemistry of ionization and excitation. London: Taylor & Francis; 1967. p. 281-293.

66. Wardman P, von Sonntag C. Kinetic factors that control the fate of thiyl radicals in cells. Methods Enzymol 1995; 251:31-45.

67. Halliwell B, Gutteridge JMC. Free radicals in biology and medicine. 4th ed. Oxford: Oxford University Press; 2007.

68. Schöneich C. Kinetics of thiol reactions. Methods Enzymol 1995; 251:45-55.

69. Mišík V, Miyoshi N, Riesz P. Effects of cysteamine and cystamine on the sonochemical accumulation of hydrogen peroxide – Implications for their mechanisms of action in ultrasound-exposed cells. Free Radic Biol Med 1999; 26:961-967.

70. Bonifačić M, Asmus K-D. Adduct formation and absolute rate constants in the displacement reaction of thiyl radicals with disulfides. J Phys Chem 1984; 88:6286-6290.

71. Prütz WA, Butler J, Land EJ. The glutathione free radical equilibrium, $GS^{\bullet} + GS^{-} \leftrightarrow GSS^{\bullet-}G$, mediating electron transfer to Fe(III)-cytochrome *c*. Biophys Chem 1994; 49:101-111.

72. Armstrong DA. Applications of pulse radiolysis for the study of short-lived sulphur species. In: Chatgilialoglu C, Asmus K-D, editors. Sulfur-centered reactive intermediates in chemistry and biology. New York: Plenum Press; 1990. p. 121-134.

73. Neta P, Huie RE, Ross AB. Rate constants for reactions of peroxyl radicals in fluid solutions. J Phys Chem Ref Data 1990; 19:413-513.

74. Khaikin GI, Alfassi ZB, Huie RE, Neta P. Oxidation of ferrous and ferrocyanide ions by peroxyl radicals. J Phys Chem 1996; 100:7072-7077.

75. Tamba M, Simone G, Quintiliani M. Interactions of thiyl free radicals with oxygen: a pulse radiolysis study. Int J Radiat Biol 1986; 50:595-600.

76. Zhang X, Zhang N, Schuchmann H-P, von Sonntag C, Pulse radiolysis of 2-mercaptoethanol in oxygenated aqueous solution. Generation and reactions of the thiylperoxyl radical. J Phys Chem 1994; 98:6541-6547.

77. Barton JP, Packer JE. The radiolysis of oxygenated cysteine solutions at neutral pH. The role of $RSSR^{-}$ and O_2^{-}. Int J Radiat Phys Chem 1970; 2:159-166.

78. Wardman P. Thiol reactivity towards drugs and radicals: some implications in the radiotherapy and chemotherapy of cancer. In: Chatgilialoglu C, Asmus K-D, editors.

Sulfur-centered reactive intermediates in chemistry and biology. New York: Plenum Press; 1990. p. 415-427.

79. Wardman P. Reactions of thiyl radicals. In: Packer L, Cadenas E, editors. Biothiols in health and disease. New York: Marcel Dekker; 1995. p. 1-19.

80. Willson RL. Pulse radiolysis studies of electron transfer in aqueous disulphide solutions. J Chem Soc, Chem Commun 1070; 1425.

81. Abedinzadeh Z. Sulfur-centered reactive intermediates derived from the oxidation of sulfur compounds of biological interest. Can J Physiol Pharmacol 2001; 79:166-170.

82. Purdie JW, Gillis HA, Klassen NV. The pulse radiolysis of penicillamine and penicillamine disulfide in aqueous solution. Can J Chem 1973; 51:3132-3142.

83. Bonifačić M, Asmus K-D. Free radical oxidation of organic disulfides. J Phys Chem 1976; 80:2426-2430.

84. Lal M. Radiation induced oxidation of sulphydryl molecules in aqueous solutions. A comprehensive review. Radiat Phys Chem 1994; 43:595-611.

85. Weston Jr. RE, Schwarz HA. Chemical kinetics. Englewood Cliffs: Prentice-Hall; 1972.

86. Elliot AJ, McCracken DR, Buxton GV, Wood ND. Estimation of rate constants for near-diffusion-controlled reactions in water at high temperatures. J Chem Soc Faraday Trans 1990; 86:1539-1547.

87. Solomon T. The definition and unit of ionic strength. J Chem Educ 2001; 78:1691-1692.

88. LaVerne JA., Radiation chemical effects of heavy ions. In: Mozumder A, Hatano Y, editors. Charged particle and photon interactions with matter: chemical, physicochemical, and biological consequences with applications. New York: Marcel Dekker; 2004. p. 403-429.

89. Keene JP. Pulse radiolysis of ferrous sulfate solution. Radiat Res 1964; 22:14-20.

TABLE 1

Reactions Added to the Pure Water Reaction Scheme to Simulate the Radiolysis of De-aerated Aqueous H_2SO_4 Solutions, at 25 °C [a]

Reaction	k (M^{-1} s^{-1})
$H^{\bullet} + SO_4^{\bullet-} \rightarrow HSO_4^-$	1.0×10^{10}
$H^{\bullet} + S_2O_8^{2-} \rightarrow SO_4^{\bullet-} + HSO_4^-$	2.5×10^{7}
$^{\bullet}OH + HSO_4^- \rightarrow H_2O + SO_4^{\bullet-}$ [b]	1.5×10^{5}
$e_{aq}^- + S_2O_8^{2-} \rightarrow SO_4^{\bullet-} + SO_4^{2-}$	1.2×10^{10}
$H_2O_2 + SO_4^{\bullet-} \rightarrow HO_2^{\bullet} + HSO_4^-$	1.2×10^{7}
$OH^- + SO_4^{\bullet-} \rightarrow {}^{\bullet}OH + SO_4^{2-}$	8.3×10^{7}
$SO_4^{\bullet-} + SO_4^{\bullet-} \rightarrow S_2O_8^{2-}$	4.4×10^{8}

Note. The rate constants given here for the reactions between ions are in the limit of zero ionic strength (i.e., at infinite dilution of ions).

[a] From ref. (*33*).

[b] Reaction (9).

TABLE 2

Chemical Reactions and Rate Constants Used in Simulations of the Radiolysis of Cystamine (RSSR) in the Fricke Dosimeter in the Presence or in the Absence of Oxygen, at 25 °C

Symbol	Reaction	k^a
R1	$RSSR + e^-_{aq} \rightarrow (RSSR)^{\bullet -}$ [b]	4.1×10^{10} (*35*)
R2	$RSSR + H^\bullet \rightarrow RS^\bullet + RSH$	8×10^9 [c, d]
R3	$RSSR + {}^\bullet OH \rightarrow$ $(RSSR)^{\bullet +} + OH^-$ (a); $RSO^\bullet + RSH$ (b)	1.7×10^{10} (*9, 35*) [e]
R4	$RS^\bullet + RSH \rightarrow (RSSR)^{\bullet -} + H^+$	3.5×10^8 (*60-62*)
R5	$RS^\bullet + RS^\bullet \rightarrow RSSR$	1.5×10^9 (*61*)
R6	$Fe^{2+} + RS^\bullet \rightarrow Fe^{3+} + RS^-$	2.5×10^8 [f]
R7	$RS^- + H^+ \rightarrow RSH$	10^{10} [g]
R8	$RS^\bullet + RS^- \rightarrow (RSSR)^{\bullet -}$	8×10^8 (*56, 60, 61, 64-67*)
R9	$RSH + {}^\bullet OH \rightarrow RS^\bullet + H_2O$	1.7×10^{10} (*35*)
R10	$RSH + H^\bullet \rightarrow RS^\bullet + H_2$	1.8×10^9 [h]
R11	$RSH + H_2O_2 \rightarrow RSOH + H_2O$	1 [i]
R12	$RS^\bullet + RSSR \rightarrow RSSSR + R^\bullet$	10^6 (*6, 70*)
R13	$Fe^{3+} + (RSSR)^{\bullet -} \rightarrow Fe^{2+} + RSSR$	10^8 (*64, 71*)
R14	$(RSSR)^{\bullet -} + H^+ \rightarrow RS^\bullet + RSH$ [d]	4.2×10^9 (*55, 59, 65, 72*)
R15	$R^\bullet + O_2 \rightarrow ROO^\bullet$	2×10^9 (*9, 73*)
R16	$Fe^{2+} + ROO^\bullet (+ H^+) \rightarrow Fe^{3+} + ROOH$	7.9×10^5 (*74*)

R17	$RS^{\bullet} + O_2 \rightarrow RSOO^{\bullet}$	2×10^{9} [j]
R18	$RSOO^{\bullet} \rightarrow RS^{\bullet} + O_2$	6.2×10^{5} s^{-1} (*64*, *66*, *75*, *76*)
R19	$Fe^{2+} + RSOO^{\bullet} (+ H^{+}) \rightarrow Fe^{3+} + RSOOH$	10^{7} [k]
R20	$RSSR^{\bullet-} + O_2 (+ H^{+}) \rightarrow RSSR + HO_2^{\bullet}$	5.1×10^{8} [l]
R21	$RSOO^{\bullet} + RSH \rightarrow RSO^{\bullet} + RSOH$	2×10^{6} (*64*, *76*)
R22	$Fe^{2+} + RSO^{\bullet} (+ H^{+}) \rightarrow Fe^{3+} + RSOH$	5×10^{5} [m]
R23	$R^{\bullet} + RSH \rightarrow RH + RS^{\bullet}$	1.1×10^{8} (*9*, *68*, *81*, *82*)
R24	$Fe^{2+} + RSSR^{\bullet+} \rightarrow Fe^{3+} + RSSR$	2×10^{6} (*57*)
R25	$RSSR^{\bullet+} + RSSR^{\bullet+} \rightarrow RSSR^{2+} + RSSR$	2.5×10^{9} (*57*, *72*, *83*)
R26	$RSSR^{\bullet+} + OH^{-} \rightarrow$ products	9×10^{8} (*57*, *72*)
R27	$RSH + HO_2^{\bullet} \rightarrow RS^{\bullet} + H_2O_2$	6×10^{2} (*64*, *84*)

Notes. The rate constants quoted here for the reactions between ions are in the limit of zero ionic strength (i.e., at infinite dilution of ions). In cases where rate constants were unavailable, estimates were made from analogous reactions and optimized (using trial-and-error procedures) so that our simulations could globally best reproduce the present experimental yield data.

[a] Units M^{-1} s^{-1} unless stated.

[b] At the acid concentration of 0.4 M H_2SO_4 (pH ~ 0.46), e_{aq}^{-} is mostly scavenged by H^{+} rather than cystamine.

[c] Assuming that the rate constant of this reaction is comparable to the rate at which $H^{\bullet}$ reacts with cystine [CysSSCys, with Cys = COOH-CH(NH_2)-CH_2] in aqueous solution (k ~ 1.3-8 × 10^{9} M^{-1} s^{-1}) (*6*, *35*, *54*).

[d] Little information exists on the sulfenium radical "intermediate" $RSSRH^{\bullet}$ produced in an acidic environment (either from the reaction of $H^{\bullet}$ atoms with disulfide or from the protonation of $RSSR^{\bullet-}$) other than the statement of Hoffman and Hayon (*55*)

that it is short-lived with, presumably, "a lifetime << 10^{-7} s", and that of Asmus (*56*) that it is "basically hypothetical and immediately dissociates into its thiyl and thiol components".

[e] It has been found (*9*, *57*, *58*) that in the reaction of disulfides with hydroxyl radicals a certain proportion of the •OH radicals leads to $RSSR^{\bullet+}$ radical ions (via electron transfer) while the remainder, in acid solution, leads to the production of sulfinyl radicals ($RSO^{\bullet}$) and thiols (via non-ionic pathways). Note that in the latter case, the possible formation of a very short-lived (much shorter than 1 μs; K.-D. Asmus, private communication) •OH adduct of RSSR as an intermediate (whose dissociative chemical fate is a pronounced function of the pH of the solution) has been proposed. Such a complex mechanistic scheme, however, still remains an open question (*59*). With $RSSR(OH)^{\bullet}$ assumed to have a very short mean life, it did not need to be modeled explicitly in the simulations.

[f] At low pH, thiyl free radicals $RS^{\bullet}$ are expected to oxidize Fe^{2+} ions to Fe^{3+} rather rapidly, with rate constants estimated in the range ~1-5 × 10^8 M^{-1} s^{-1} (P. Wardman, private communication). For RSH = β-mercaptoethanol ($OH\text{-}CH_2\text{-}CH_2\text{-}SH$), a value of 10^8 M^{-1} s^{-1} was also quoted by Armstrong (*63*) for the rate of the reaction of $RS^{\bullet}$ with ferrocyanide $[Fe(CN)_6]^{4-}$.

[g] Representative value for glutathione (GSH) (*64*).

[h] Assuming that the rate constant for this reaction is comparable to the rate at which $H^{\bullet}$ reacts with cysteine (CysSH) in aqueous solution (k ~ 1-4 × 10^9 M^{-1} s^{-1}) (*6*, *35*, *54*, *68*).

[i] Based on the reaction between H_2O_2 and sulfhydryl molecules such as cysteamine ($NH_2\text{-}CH_2\text{-}CH_2\text{-}SH$) ($k \leq 1$ M^{-1} s^{-1}) (*63*, *69*).

[j] Representative value for glutathione (*64*, *66*, *75*) and for β-mercaptoethanol (*76*). Barton and Packer (*77*) also reported a rate constant of 8 × 10^9 M^{-1} s^{-1} for the reaction of the cysteine thiyl radical ($CysS^{\bullet}$) with O_2.

[k] In strong acid, thiyl peroxyl free radicals $RSOO^{\bullet}$ are expected to oxidize Fe^{2+} ions much slower than thiyl radicals $RS^{\bullet}$ (P. Wardman, private communication). For example, for glutathione, the reactivity of $GSOO^{\bullet}$ towards chlorpromazine (CPZ), an

oxidizable substrate, was found to be at least an order of magnitude lower than that of $GS^{\bullet}$ (*78*, *79*).

[l] Estimate for RSH = GSH (*66*, *67*, *71*). Values of 9×10^8 and 4.3×10^8 M^{-1} s^{-1} were also reported by Willson (*80*) for the rate of the reaction of the reducing disulfide lipoic acid radical anion with O_2 and by Barton and Packer (*77*) for that of the reaction $CysSSCys^{\bullet-} + O_2$, respectively.

[m] Assuming the oxidizing sulfinyl radical $RSO^{\bullet}$ to be as reactive towards Fe^{2+} ions as commonly studied peroxyl radicals (73, 74, 81).

LISTING OF FOOTNOTES

1. Address for correspondence: Département de Médecine Nucléaire et de Radiobiologie, Faculté de Médecine et des Sciences de la Santé, Université de Sherbrooke, 3001, 12ème Avenue Nord, Sherbrooke (Québec) J1H 5N4, Canada. Tel. +1-819-346-1110, ext. 14682 or 14773; fax: +1-819-564-5442; e-mail: jean-paul.jay-gerin@USherbrooke.ca

2. Throughout this paper, radiation chemical yields are quoted in units of molecules per 100 eV (abbreviated as "molec./100 eV"), as g(X) for primary yields and G(X) for experimentally measured yields. For conversion into SI units (mol/J), 1 molec./100 eV ≈ 0.10364 μmol/J (*7*, *11*).

3. A preliminary report of this work was presented at the *3rd Asia Pacific Symposium on Radiation Chemistry, Treasure Island Resorts, Lonavala, India*, September 14-17, 2010; see Proceedings, Vol. I-Invited Talks, Paper ITRC-13, p. 50-55 (ISBN: 81-88513-37-7).

4. Rate constant in the limit of infinite dilution, i.e., *not* corrected for the effects due to the ionic strength of the solutions.

5. Some $H^{\bullet}$ atoms may also directly react with Fe^{2+} [reaction (7)]. However, at 25 °C and a ferrous ion concentration of 1 m*M*, the contribution of this reaction to the formation of Fe^{3+} can be neglected.

6. Note that, for solutions of 0.4 *M* in H_2SO_4, there is a small amount of $^{\bullet}OH$ radicals that react with HSO_4^- to form the sulfate radical $SO_4^{\bullet-}$ according to (*40*, *41*)

$$^{\bullet}OH + HSO_4^- \rightarrow H_2O + SO_4^{\bullet-} \qquad k_9 = 1.5 \times 10^5\ M^{-1}\ s^{-1}. \qquad (9)$$

However, the overall ferric ion yield remains the same as given by Eq. (8) since the sulfate radical reacts with Fe^{2+} in the same way as $^{\bullet}OH$ (*42*):

$$SO_4^{\bullet-} + Fe^{2+} \rightarrow Fe^{3+} + SO_4^{2-} \qquad (10)$$

with $k_{10} = 9.9 \times 10^8\ M^{-1}\ s^{-1}$ (in the limit of zero ionic strength).

7. Note that sodium chloride is often added to the Fricke solution in order to protect it from the detrimental effects of organic impurities, so lower quality water may be suitable (*20*).

8. The UV-absorption spectrum of cystamine, which exhibits a broad maximum centered at about 245 nm in neutral pH (*45*), was found to be unchanged in aqueous 0.4 *M* H_2SO_4 solution, indicating that this compound did not degrade at low pH under the acidic conditions of the Fricke dosimeter.

9. The dose rate was determined by Fricke dosimetry, taking $G(Fe^{3+})$ to be 15.6 molec./100 eV (*20*).

10. We should note that the use of high-energy protons as primary particles was more appropriate here than that of fast electrons since we wanted to study track segments over which the LET is essentially constant. In fact, a proton that has the *same* LET as an electron must also have an energy ~2000 times larger, and consequently its LET is much less affected by a given series of energy depositions (*41*, *51*).

11. Note that the reaction of the sulfate radical with Fe^{2+} [reaction (10)], whose contribution to the formation of Fe^{3+} is close to that found for reaction (6) (see Fig. 2b), is completed at about the same time as reaction (3).

12. From the reciprocal of the "scavenging power" (*6*), defined as the product k_{R3a}[RSSR] (in units of s^{-1}), we can estimate the time scale over which the scavenging of $^{\bullet}OH$ by RSSR is occurring. At 1 m*M* cystamine, this reaction with cystamine takes place at about 5.9×10^{-8} s, that is, well before that with ferrous ions ($1/k_3\,[Fe^{2+}] \sim 2.9 \times 10^{-6}$ s). This is well

illustrated in Fig. 7a where we show the time profiles of the extents ΔG(RSSR) of each reaction that contributes to the formation and removal of cystamine, calculated from our Monte-Carlo simulations. In fact, as we can see from this figure, ΔG(RSSR) due to reaction (R3a) actually corresponds to the escape yield $g(^{\bullet}OH)$ as soon as one reaches ~3 × 10^{-7} s.

13. As can be seen from Fig. 5b, this elimination is not total; in fact, a small contribution to $G(Fe^{3+})$ due to reaction (3) (~0.11 molec./100 eV) is still observed at ~200 s.

14. In the absence of oxygen, cystamine molecules compete with Fe^{2+} ions for $H^{\bullet}$. Consideration of the scavenging powers k_{R2}[RSSR] and $k_7[Fe^{2+}]$ readily shows that, in 1-m*M*-ferrous solution, half of the $H^{\bullet}$ atoms react with cystamine and half react with ferrous ions at a cystamine concentration of about 2 × 10^{-6} *M*.

FIGURE CAPTIONS

Figure 1:

(Panel a) Time evolution of $G(Fe^{3+})$ (in molec./100 eV) for 300-MeV incident protons (LET ~ 0.3 keV/μm) in the radiolysis of *aerated* solution of 1 m*M* $FeSO_4$ in aqueous 0.4 *M* H_2SO_4 (Fricke solution) at 25 °C. The concentration of dissolved oxygen used in the calculations is 2.5×10^{-4} *M*. The solid line shows our simulated kinetics of Fe^{3+} ion formation. The arrow on the right of the figure shows the accepted value (15.5 ± 0.2 molec./100 eV) of the yield of the Fricke dosimeter for ^{60}Co γ-rays and fast electrons.

(Panel b) Time dependence of the extents $\Delta G(Fe^{3+})$ (in molec./100 eV) of the different reactions that contribute to the formation of Fe^{3+} ions, calculated from our Monte-Carlo simulations in the interval 10^{-12}-200 s (see text).

Figure 2:

(Panel a) Time evolution of $G(Fe^{3+})$ (in molec./100 eV) for 300-MeV incident protons (LET ~ 0.3 keV/μm) in the radiolysis of *deaerated* solution of 1 m*M* $FeSO_4$ in aqueous 0.4 *M* H_2SO_4 at 25 °C. The solid line shows our simulated kinetics of Fe^{3+} ion formation. The arrow on the right of the figure shows the accepted value (8.2 ± 0.3 molec./100 eV) of the yield of the Fricke dosimeter in the absence of oxygen for ^{60}Co γ-rays and fast electrons.

(Panel b) Time dependence of the extents $\Delta G(Fe^{3+})$ (in molec./100 eV) of the different reactions that contribute to the formation of Fe^{3+} ions, calculated from our Monte-Carlo simulations in the interval 10^{-12}-200 s (see text).

Figure 3:

Time evolution of $G(Fe^{3+})$ (in molec./100 eV) as obtained from our Monte-Carlo simulations of the radiolysis of Fricke dosimeter solutions (1 m*M* $FeSO_4$ in aqueous 0.4 *M* H_2SO_4) containing various concentrations of cystamine, under both *aerated* (a) and

deaerated (b) conditions, using 300-MeV incident protons (LET ~ 0.3 keV/μm) at 25 °C. The different lines correspond to three different concentrations of cystamine added (indicated to the right of the figure): 10^{-4} *M* (dash-dot line), 10^{-3} *M* (dotted line), and 0.1 *M* (dashed line). The solid line shows our simulated kinetics of Fe^{3+} ion formation for the Fricke dosimeter without added cystamine (for reference).

Figure 4:

Dependence of ferric ion production from irradiated Fricke solutions (1 m*M* $FeSO_4$ in aqueous 0.4 *M* H_2SO_4) upon the concentration of added cystamine in the range 5×10^{-7}-0.1 *M*, under both aerated (panel a) and deaerated (panel b) conditions. The different lines show the Fe^{3+} ion yields obtained from our Monte-Carlo simulations (at ~200 s following ionization) using different values of the fraction of $^{\bullet}OH$ radicals that react with cystamine to form either transient $RSSR^{\bullet+}$ radical ions [reaction (R3a)] or the non-ionic intermediates RSH and $RSO^{\bullet}$ [reaction (R3b)]. The dotted and dashed lines correspond to a branching ratio of 50% and 70% in favor of the oxidation pathway (R3a), respectively. The solid line is obtained by assuming a negligibly small intervention of reaction (R3b). As clearly seen, a branching ratio of ~100% in favor of reaction (R3a) is required to achieve the best *simultaneous* agreement between calculated and measured Fe^{3+} yields as a function of cystamine concentration in the presence and absence of oxygen (see text). Experiment: (●) ref. (*25*), (▲) ref. (*26*), and (□) this work.

Figure 5:

(Panel a) Time evolution of $G(Fe^{3+})$ (in molec./100 eV) for 300-MeV incident protons (LET ~ 0.3 keV/μm) in the radiolysis of aerated Fricke dosimeter solutions containing 1 mM $FeSO_4$ and 1 mM cystamine in aqueous 0.4 M H_2SO_4 at 25 °C. The concentration of dissolved oxygen used in the calculations is 2.5×10^{-4} M. The solid line shows our simulated kinetics of Fe^{3+} ion formation.

(Panel b) Time dependence of the extents $\Delta G(Fe^{3+})$ (in molec./100 eV) of the different reactions that contribute to the formation of Fe^{3+} ions, calculated from our Monte-Carlo simulations in the interval 10^{-12}-200 s. The oxidation of Fe^{2+} ions to Fe^{3+} involves reactions mainly with $HO_2^{\bullet}$, H_2O_2, and the cystamine-radical species $RS^{\bullet}$ and $RSSR^{\bullet+}$ (see text).

Figure 6:

(Panel a) Time evolution of $G(Fe^{3+})$ (in molec./100 eV) for 300-MeV incident protons (LET ~ 0.3 keV/μm) in the radiolysis of *deaerated* Fricke solutions containing 1 m*M* $FeSO_4$ and 1 m*M* cystamine in aqueous 0.4 *M* H_2SO_4 at 25 °C. The solid line shows our simulated kinetics of Fe^{3+} ion formation.

(Panel b) Time dependence of the extents $\Delta G(Fe^{3+})$ (in molec./100 eV) of the different reactions that contribute to the formation of Fe^{3+} ions, calculated from our Monte-Carlo simulations in the interval 10^{-12}-200 s. The oxidation of Fe^{2+} ions to Fe^{3+} involves reactions mainly with H_2O_2 and the cystamine-radical species $RS^{\bullet}$ and $RSSR^{\bullet+}$ (see text).

Figure 7:

Time dependence of the extents $\Delta G(Fe^{3+})$ (in molec./100 eV) of the different reactions that contribute to the formation and decay of cystamine (RSSR) (see text and Table 2), calculated from our Monte-Carlo simulations of the radiolysis of Fricke solutions containing 1 m*M* $FeSO_4$ and 1 m*M* cystamine in aqueous 0.4 *M* H_2SO_4 by 300-MeV incident protons (LET ~ 0.3 keV/μm) at 25 °C and in the interval ~10^{-12}-200 s, when oxygen is present (panel a) or absent (panel b).

Figure 1

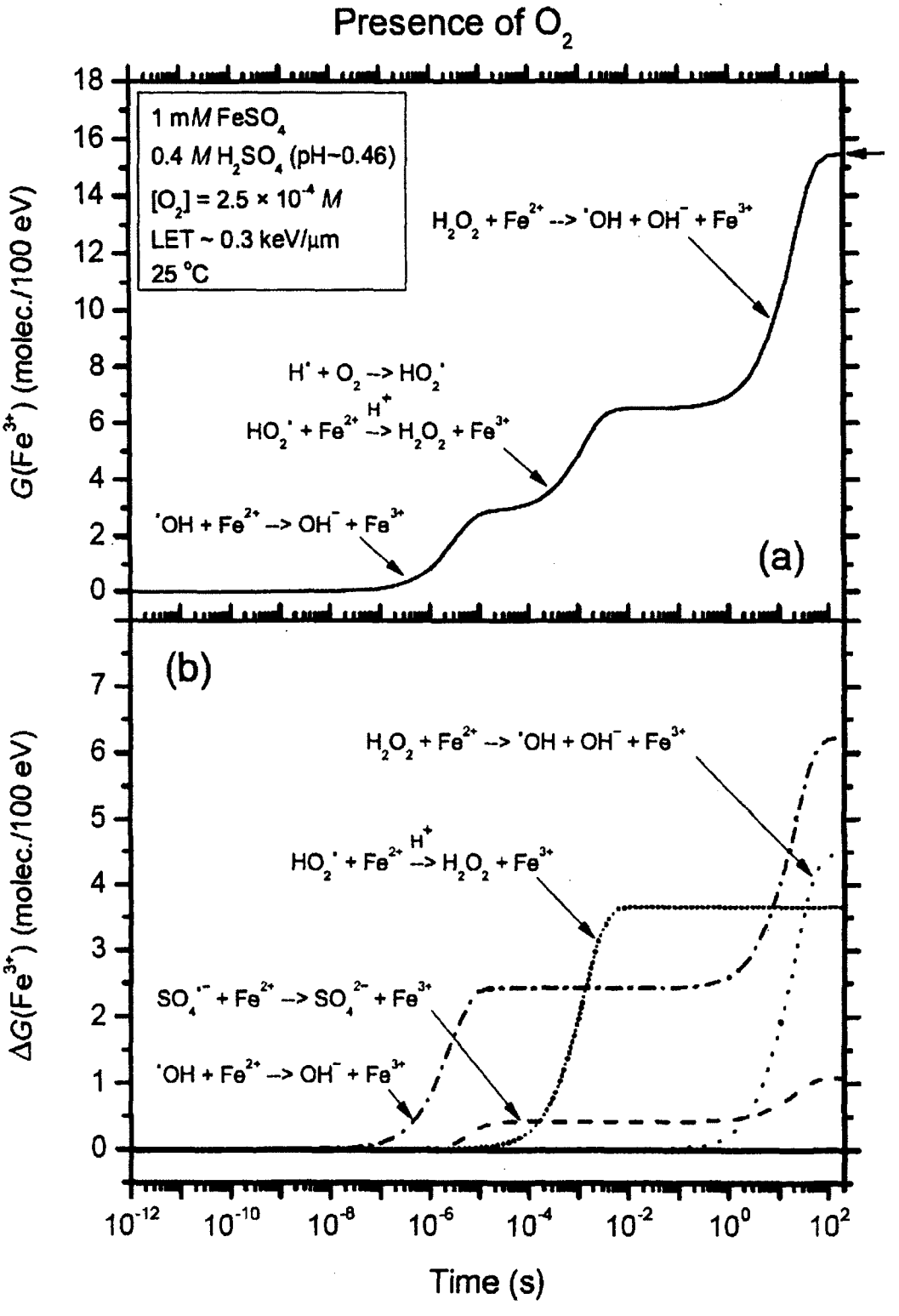
Presence of O_2
1 m*M* $FeSO_4$
0.4 *M* H_2SO_4 (pH~0.46)
$[O_2] = 2.5 \times 10^{-4}$ *M*
LET ~ 0.3 keV/µm
25 °C
$H_2O_2 + Fe^{2+} \rightarrow {}^{\bullet}OH + OH^- + Fe^{3+}$
$H^{\bullet} + O_2 \rightarrow HO_2^{\bullet}$
$HO_2^{\bullet} + Fe^{2+} \xrightarrow{H^+} H_2O_2 + Fe^{3+}$
$^{\bullet}OH + Fe^{2+} \rightarrow OH^- + Fe^{3+}$
(a)
(b)
$SO_4^{\bullet-} + Fe^{2+} \rightarrow SO_4^{2-} + Fe^{3+}$
$G(Fe^{3+})$ (molec./100 eV)
$\Delta G(Fe^{3+})$ (molec./100 eV)
Time (s)

Figure 2

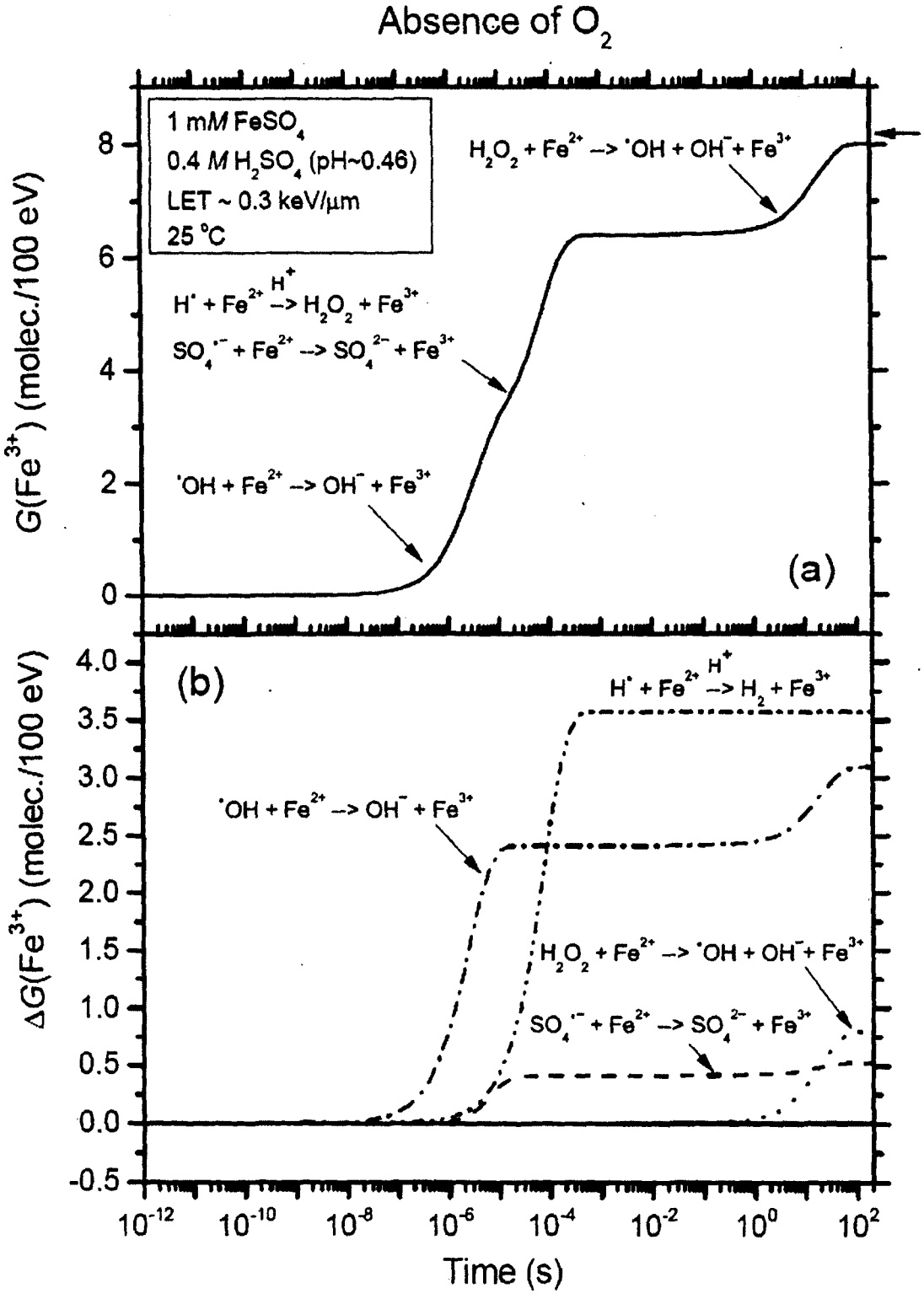
Absence of O_2
1 m*M* $FeSO_4$
0.4 *M* H_2SO_4 (pH~0.46)
LET ~ 0.3 keV/µm
25 °C
$H_2O_2 + Fe^{2+} \rightarrow {}^{\bullet}OH + OH^- + Fe^{3+}$
$H^{\bullet} + Fe^{2+} \xrightarrow{H^+} H_2O_2 + Fe^{3+}$
$SO_4^{\bullet-} + Fe^{2+} \rightarrow SO_4^{2-} + Fe^{3+}$
${}^{\bullet}OH + Fe^{2+} \rightarrow OH^- + Fe^{3+}$
(a)
(b)
$H^{\bullet} + Fe^{2+} \xrightarrow{H^+} H_2 + Fe^{3+}$
$G(Fe^{3+})$ (molec./100 eV)
$\Delta G(Fe^{3+})$ (molec./100 eV)
Time (s)

Figure 3

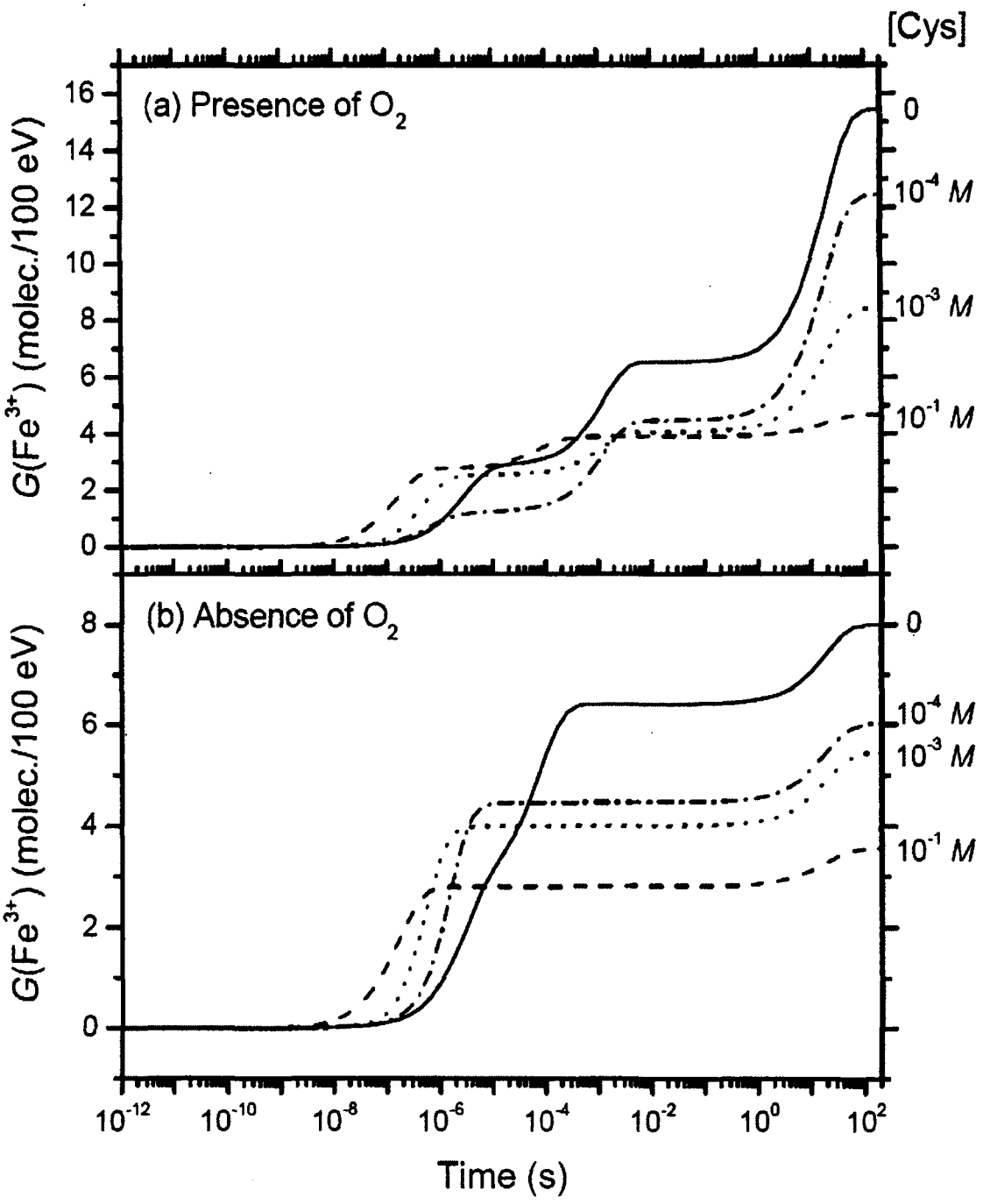
[Cys]
(a) Presence of O_2
$G(Fe^{3+})$ (molec./100 eV)
16
14
12
10
8
6
4
2
0
0
10^{-4} M
10^{-3} M
10^{-1} M
(b) Absence of O_2
$G(Fe^{3+})$ (molec./100 eV)
8
6
4
2
0
0
10^{-4} M
10^{-3} M
10^{-1} M
10^{-12}
10^{-10}
10^{-8}
10^{-6}
10^{-4}
10^{-2}
10^{0}
10^{2}
Time (s)

Figure 4

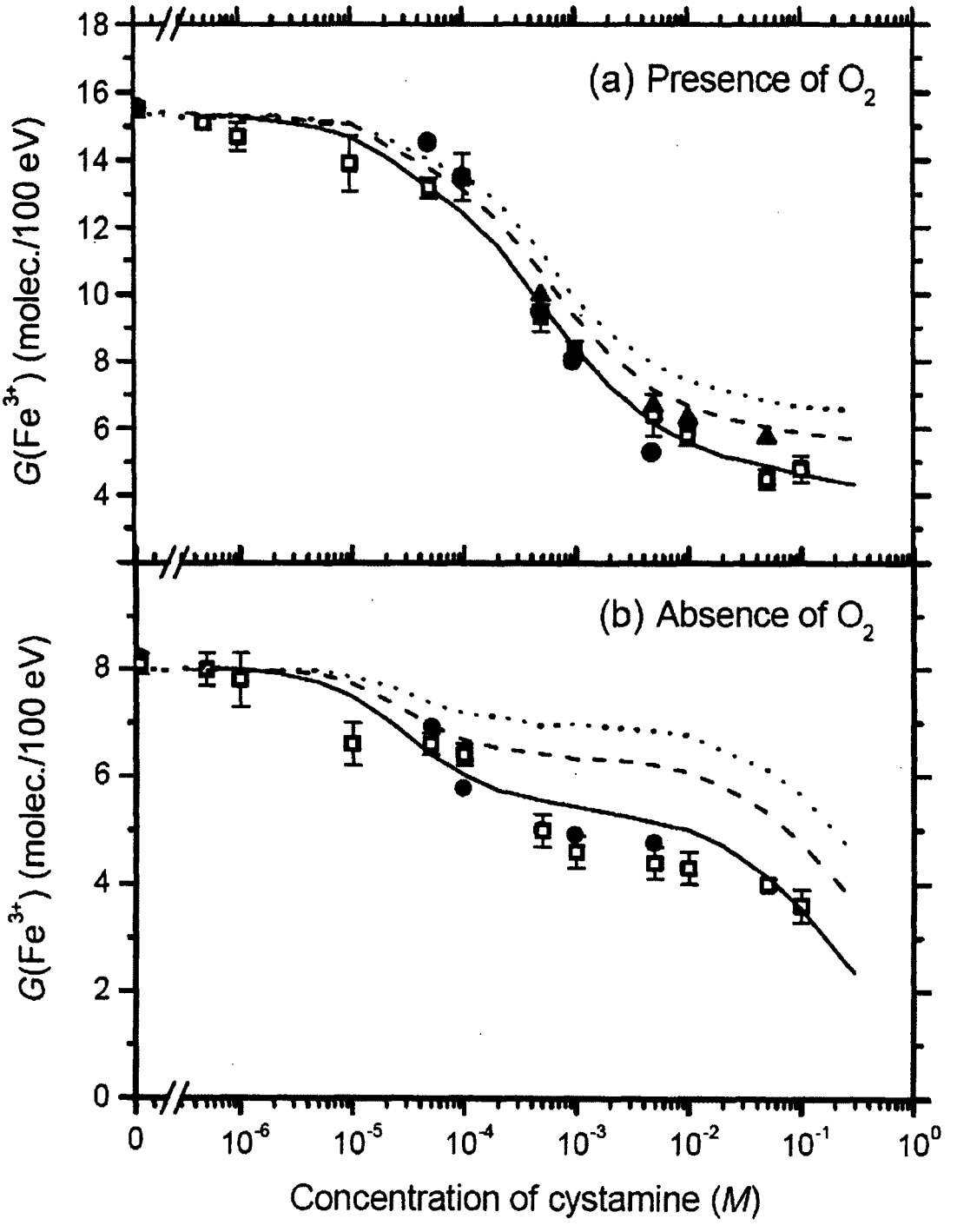
(a) Presence of O_2
(b) Absence of O_2
$G(Fe^{3+})$ (molec./100 eV)
Concentration of cystamine (*M*)
0
10^{-6}
10^{-5}
10^{-4}
10^{-3}
10^{-2}
10^{-1}
10^{0}

Figure 5

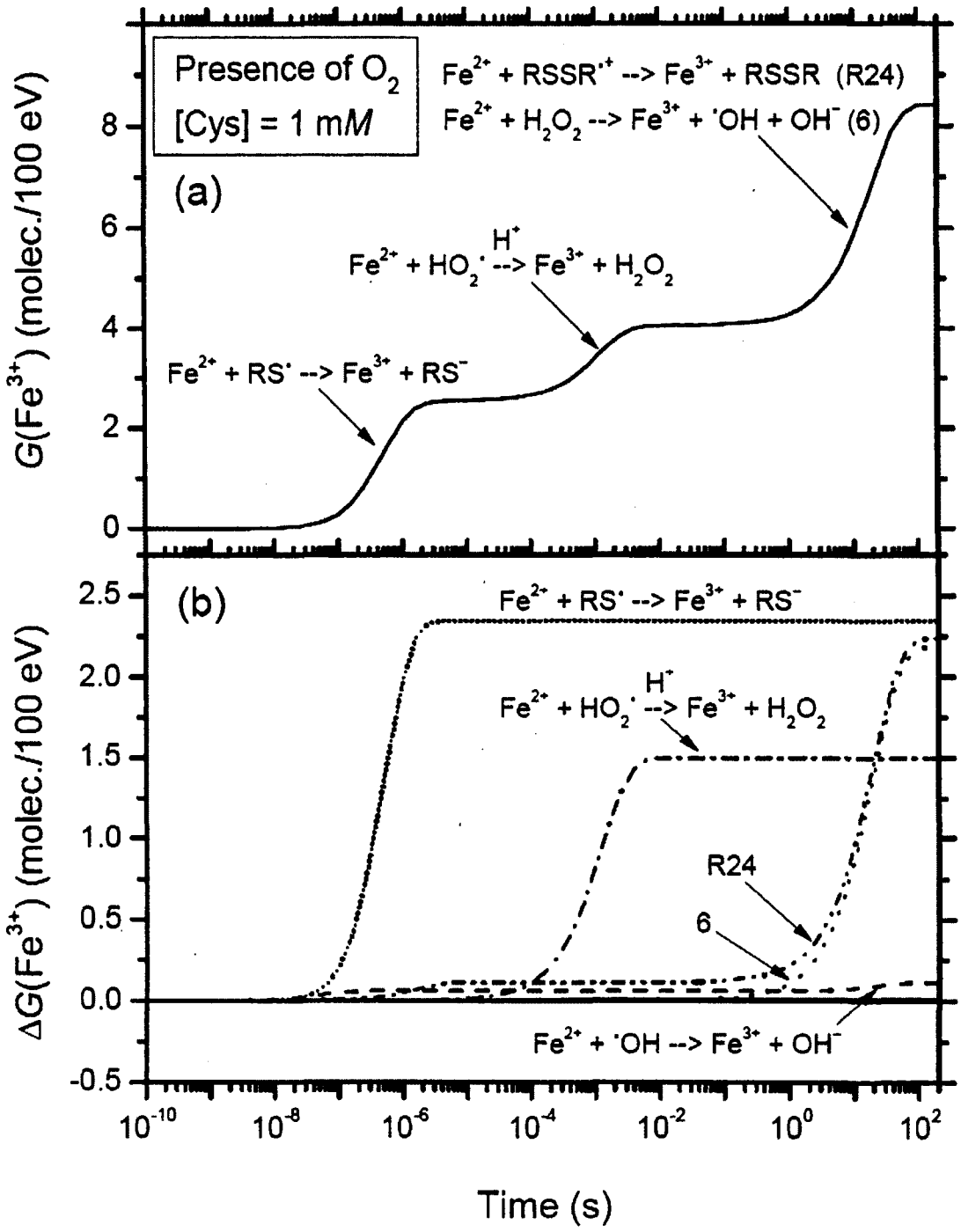
Presence of O_2
[Cys] = 1 m*M*
$Fe^{2+} + RSSR^{\cdot+} \rightarrow Fe^{3+} + RSSR$ (R24)
$Fe^{2+} + H_2O_2 \rightarrow Fe^{3+} + {}^{\cdot}OH + OH^-$ (6)
(a)
$Fe^{2+} + HO_2^{\cdot} \xrightarrow{H^+} Fe^{3+} + H_2O_2$
$Fe^{2+} + RS^{\cdot} \rightarrow Fe^{3+} + RS^-$
$G(Fe^{3+})$ (molec./100 eV)
(b)
$Fe^{2+} + RS^{\cdot} \rightarrow Fe^{3+} + RS^-$
$Fe^{2+} + HO_2^{\cdot} \xrightarrow{H^+} Fe^{3+} + H_2O_2$
R24
6
$Fe^{2+} + {}^{\cdot}OH \rightarrow Fe^{3+} + OH^-$
$\Delta G(Fe^{3+})$ (molec./100 eV)
Time (s)

Figure 6

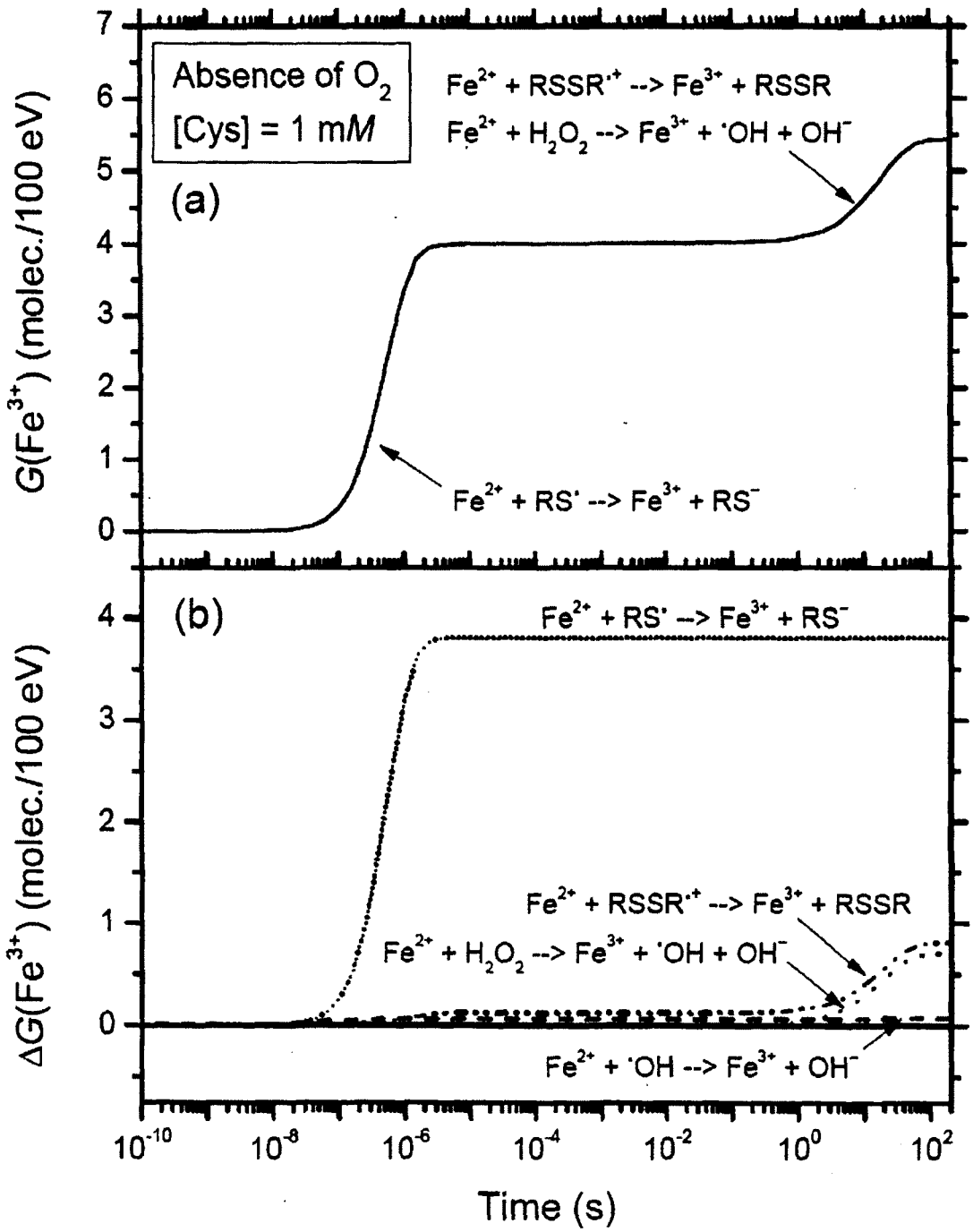
Absence of O_2
[Cys] = 1 m*M*
(a)
$Fe^{2+} + RSSR^{\cdot+} \rightarrow Fe^{3+} + RSSR$
$Fe^{2+} + H_2O_2 \rightarrow Fe^{3+} + {}^{\cdot}OH + OH^-$
$Fe^{2+} + RS^{\cdot} \rightarrow Fe^{3+} + RS^-$
(b)
$Fe^{2+} + RS^{\cdot} \rightarrow Fe^{3+} + RS^-$
$Fe^{2+} + RSSR^{\cdot+} \rightarrow Fe^{3+} + RSSR$
$Fe^{2+} + H_2O_2 \rightarrow Fe^{3+} + {}^{\cdot}OH + OH^-$
$Fe^{2+} + {}^{\cdot}OH \rightarrow Fe^{3+} + OH^-$
$G(Fe^{3+})$ (molec./100 eV)
$\Delta G(Fe^{3+})$ (molec./100 eV)
Time (s)

Figure 7

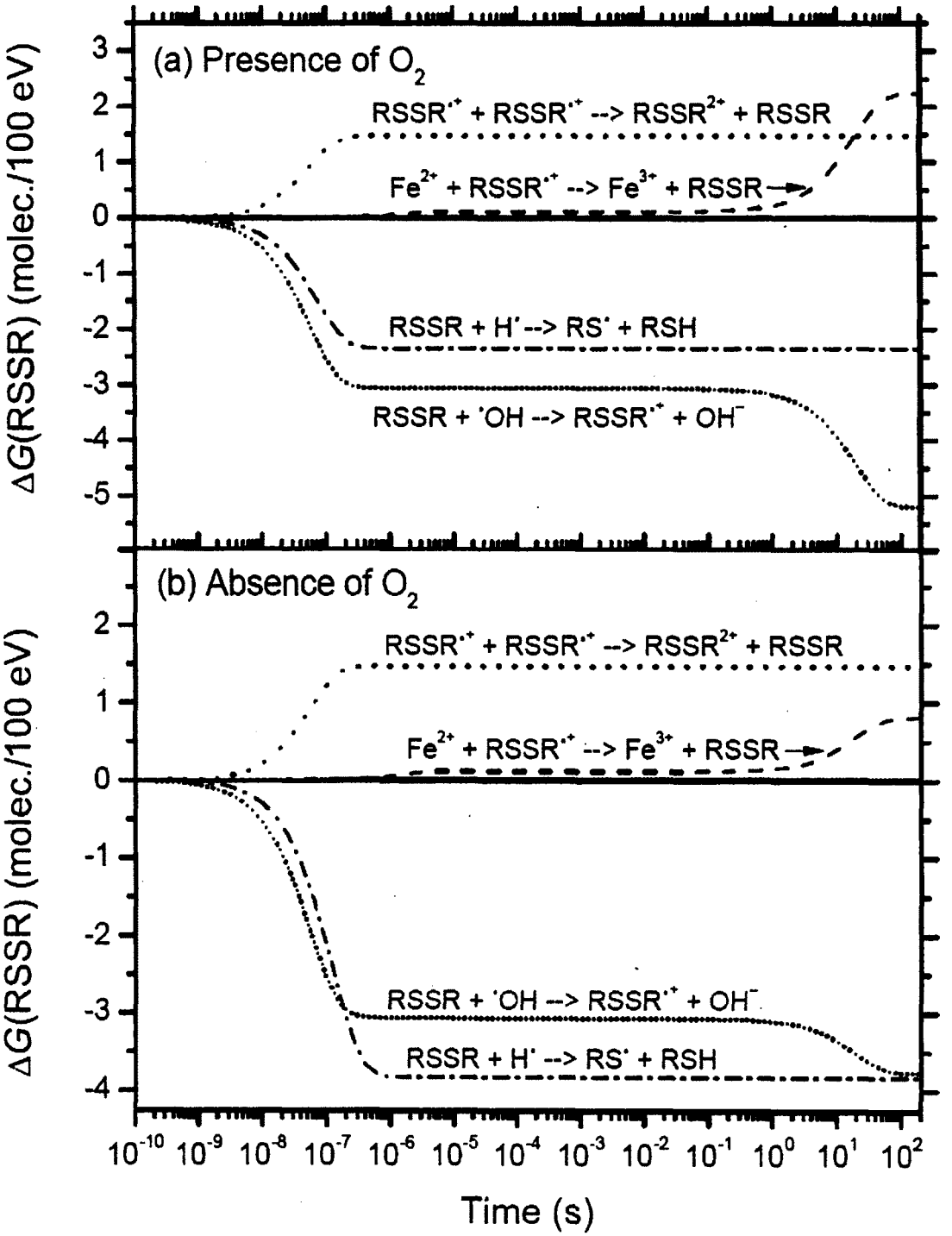
(a) Presence of O_2
$RSSR^{\bullet+} + RSSR^{\bullet+} \rightarrow RSSR^{2+} + RSSR$
$Fe^{2+} + RSSR^{\bullet+} \rightarrow Fe^{3+} + RSSR$
$RSSR + H^{\bullet} \rightarrow RS^{\bullet} + RSH$
$RSSR + {}^{\bullet}OH \rightarrow RSSR^{\bullet+} + OH^{-}$
(b) Absence of O_2
$RSSR^{\bullet+} + RSSR^{\bullet+} \rightarrow RSSR^{2+} + RSSR$
$Fe^{2+} + RSSR^{\bullet+} \rightarrow Fe^{3+} + RSSR$
$RSSR + {}^{\bullet}OH \rightarrow RSSR^{\bullet+} + OH^{-}$
$RSSR + H^{\bullet} \rightarrow RS^{\bullet} + RSH$
ΔG(RSSR) (molec./100 eV)
Time (s)

IV. Article No. 3

In this chapter, we report using intense ultra-short infrared laser pulse we are able to deposit a large dose with a very high dose rate inside a well-controlled macroscopic volume without deposition of energy in front or behind the target volume.

This work is presented in the following article, entitled: "**A beam for cancer radiotherapy based on femtosecond IR laser-filamentation yielding ultra-high dose rates and zero entrance dose**", By Ridthee Meesat, Jean-François Allard, Hakim Belmouaddine, Catherine Tanguay-Renaud, Rosalie Lemay, Tiberius Brastaviceanu, Luc Tremblay, Benoit Paquette, J. Richard Wagner, Jean-Paul Jay-Gerin, Martin Lepage, Michael A. Huels, and Daniel Houde.

This article is currently under consideration for publication in *The Proceedings of the National Academy of Sciences USA (PNAS)*, (3 October 2011).

Co-authorship: Ridthee Meesat designed research, performed dosimetry, thymidine decomposition, DNA damage, gamma and laser irradiation, analysed data and wrote the manuscript. Jean-François Allard and Hakim Belmouaddine performed dosimetry, animal experiments and laser irradiation. Catherine Tanguay-Renaud, Rosalie Lemay and Benoit Paquette performed animal experiments. Tiberius Brastaviceanu provided information about a measurement of solvated electrons. Luc Tremblay performed MRI. J. Richard Wagner performed thymidine decomposition, analysed data and edited the manuscript. Martin Lepage supervised the project on data interpretation, performed MRI analysis, analysed data and edited the manuscript. Jean-Paul Jay-Gerin, Michael A. Huels and Daniel Houde designed research, analysed data and edited the manuscript.

Résumé

Le but principal de la radiothérapie du cancer est de maximiser l'effet létal des radiations dans le volume tumoral tout en épargnant les tissus sains environnants. Malheureusement, les sources conventionnelles de radiation (rayons γ ou X, électrons) utilisés depuis des décennies, incluant les faisceaux multiples ou avec intensité modulée, déposent inévitablement la majorité de leur dose devant ou derrière la tumeur, causant ainsi des dommages aux tissus sains et pouvant causer des cancers secondaires survenant des années après le traitement. Même les plus récentes avancées dans les thérapies coûteuses avec des protons et des ions carbone ne peuvent complètement éviter la déposition de dose devant le volume tumoral. Dans cette étude, nous démontrons que le but ultime de la radiothérapie pourrait être finalement atteint. Des impulsions laser infrarouge (IR) intenses et ultra-courtes peuvent déposer de très grandes doses avec un débit de dose inégalé (jusqu'à 10^{11} Gy/s) en profondeur à l'intérieur d'un volume contrôlable, sans aucune dose devant et derrière le volume cible. Nos impulsions laser IR produisent des avalanches d'électrons de basse énergie avec une haute densité via un processus de filamentation laser, ce qui produit une distribution spatiale d'énergie de densité et de débit de dose qui dépasse par des ordres de grandeur les valeurs rapportées pour les systèmes de radiothérapie clinique les plus puissants. De plus, nous démontrons que (a) le type de dommage final et les mécanismes dans un milieu aqueux, aux niveaux moléculaire et biomoléculaire, sont comparables à ceux des radiations ionisantes conventionnelles, et (b) la méthode d'irradiation laser produit des effets thérapeutiques bénéfiques au niveau des tissus tumoraux en modèle animal.

Classification: Biological Science, Biophysics, Medical Science

Title: **A beam for cancer radiotherapy based on femtosecond IR laser-filamentation yielding ultra-high dose rates and zero entrance dose**

Author affiliation: Ridthee Meesat, Jean-François Allard, Hakim Belmouaddine, Catherine Tanguay-Renaud, Rosalie Lemay, Tiberius Brastaviceanu, Luc Tremblay, Benoit Paquette, J. Richard Wagner, Jean-Paul Jay-Gerin, Martin Lepage, Michael A. Huels, and Daniel Houde

Département de médecine nucléaire et de radiobiologie, Faculté de médecine et des sciences de la santé, Université de Sherbrooke, Sherbrooke (Québec) J1H 5N4, Canada

Corresponding author: Prof. Daniel Houde

Département de médecine nucléaire et de radiobiologie, Faculté de médecine et des sciences de la santé, Université de Sherbrooke, Sherbrooke

3001 12th Avenue North, Sherbrooke (Québec) J1H 5N4, Canada

Tel. +1 819-346-1110 ext 14502

Fax: +1 819-564-5442

E-mail: daniel.houde@usherbrooke.ca

Abstract

Since the invention of cancer radiotherapy, its primary goal has been to maximize lethal radiation doses to the tumor volume while keeping the dose to surrounding healthy tissues at zero. Sadly, conventional radiation sources (γ or X rays, electrons) used for decades, including multiple or modulated beams, inevitably deposit the majority of their dose in front or behind the tumor, thus damaging healthy tissue, and causing secondary cancers years after treatment. Even the most recent pioneering advances in costly proton or carbon ion therapies can not completely avoid dose buildup in front of the tumor volume. Here we show that this ultimate goal of radiotherapy is yet within our reach: using intense ultra-short infrared (IR) laser pulses we can now deposit a very large energy dose at unprecedented microscopic dose rates (up to 10^{11} Gy/s) deep inside an adjustable, well-controlled macroscopic volume, without any dose deposit in front or behind the target volume. Our IR laser pulses produce high density avalanches of low energy electrons via laser filamentation, a phenomenon which results in a spatial energy density and temporal dose rate that both exceed by orders of magnitude any values previously reported even for the most intense clinical radiotherapy systems. Moreover, we show that (a) the type of final damage and its mechanisms in aqueous media, at the molecular and biomolecular level, is comparable to that of conventional ionizing radiation, and (b) at the tumor tissue level in an animal cancer model, the laser irradiation method shows clear therapeutic benefits.

Introduction

Radiation therapy is the most widely used modern cancer treatment and continues to play an irreplaceable role in the management of a vast array of potentially curable malignancies (1). Many of the most recent advances in conventional radiation therapy have derived from innovations, and technology and engineering developments, of three dimensional computer imaging techniques (2). These advances have lead to sophisticated radiation therapy methods such as intensity-modulated radiation therapy (IMRT) (3), and many others. As with all advances in radiation therapy, the final goal of these technology improvements is to deliver the highest possible energy dose to the tumor volume while sparing surrounding normal tissues. This is the most important challenge to modern radiotherapy since all high-energy photons or electrons used in the clinic result in a dominant entrance dose in front of the tumor and a non-negligible exit dose behind it (Fig. 1d) (4). Proton and heavy ion beams (mainly carbon beams) have a much more desirable dose deposition patterns for the individual particle trajectories (5). However, even here the entrance dose in healthy tissue of the actual therapeutic many-particle beams used on patients is about 20-70 % of the dose in the "spread out Bragg peak" placed in the tumor volume (Fig.1d) (5). While such results are certainly an improvement on radiation therapy using X or γ rays, the very high costs of proton or carbon ion beam irradiation facilities however drastically limits their widespread clinical availability (6). The unwanted irradiation of healthy tissue surrounding tumors may not only lead to secondary cancers in young patients (3), but it more importantly constrains clinicians to optimize radiation doses according to the overall tolerance of the healthy tissue, rather than giving a therapeutic high dose allowing the elimination of eventually all cancer cells. Moreover, irradiating healthy

tissue near tumors promotes invasion and migration of cancer cells, leading to metastasis. Thus, it is the utmost challenge to develop a novel irradiation method, or source, with much more advantageous dose distribution properties that allow us to avoid damage to healthy tissue surrounding the malignant tumors. Such improvement to radiation therapy has, as its ultimate goal, to deposit the highest possible dose of spatially concentrated energy density (so far only from ionizing radiation), at the highest possible temporal dose rate (mainly to overload the tumor's cellular repair mechanisms), exclusively to the tumor volume, while leaving the surrounding healthy tissue in a pristine and undamaged state as the so called "dream beam" (Fig. 1d). Moreover, the dose delivered to a specific volume inside the medium, or organism, must be controllable in both space and time to cover the entire range of tumor extent or response to such energy depositions.

While numerous biomedical applications of ultra fast lasers have been established (7), they are not used for radiotherapy of tumors that reside macroscopic distances inside human tissue. This is of interest, since, e.g., many of the modern, long wavelength high power lasers can deliver high energy density pulses, i.e. doses and dose rates, which in principle surpass any clinical radiation sources. Thus, some of the fundamental questions that arise naturally from this fact are (*i*) *Can lasers, non-linear optics, and near visible photons (IR, visible) be used to somehow generate a true radio-therapeutic effect, not upon entry in the tissue (as in Photodynamic therapy), but a macroscopic distance within a tissue?* and (*ii*) *Can IR lasers in particular, which emit non-ionizing radiation, replace ionizing radiation (viz radioactive materials) in some cancer treatments?* In other words: can non-linear laser optics be adapted to circumvent the main fundamental problem of dose distribution upon tissue entry, that persistently plagues modern radiation therapy using

ionizing radiation. Conventional high energy ionizing radiation generates radicals, energetic ions and secondary electrons as it travels through tissues. The majority of secondary electrons generated are low energy electrons (LEEs) with energies below 20 eV (~5×10^4 electrons per MeV) (8), which in themselves are genotoxic (9). In living tissue, the interaction of radiation with water, leading to the production of highly reactive and unstable free radicals or reactive oxygen species (ROS), that are responsible for a large part of the deleterious effects of radiation. In turn, the radicals and ROS react with biomolecules (e.g. DNA) in cells, thereby producing mutations and cell death. IR Laser filamentation, as is shown here, produces the same reactive species as the radiolysis of water by ionizing radiation (see below).

Results and discussion

Dosimetry of filamentation. We report that filamentation, produced by intense, ultra-short infrared (800 nm) laser pulses can be used to deposit a large localized energy density at a high dose rate, a macroscopic distance inside a well controlled macroscopic volume. As seen in Fig 1 a, b, the most striking feature of our dose deposition profile is the complete absence of an entrance dose (meaning no damage to healthy tissue in front of the tumor), a characteristic that still eludes conventional radiation sources used for cancer therapy, as clearly seen in fig 1 c. The objective of our contribution here is to demonstrate (a) the radiation-chemical and radiobiological equivalence of IR laser filamentation to ionizing radiation in liquid or tissue equivalent liquid media, and (b) the potential curative utility of femtosecond laser irradiation in an animal breast cancer model. Filamentation is a non-linear optical effect, that is related to a change in the refractive index of a medium in

response to a high electric field (Kerr effect) provided here by the ultra short intense IR laser pulses. The resulting self focusing of the laser beam creates filaments of ionized medium, due to multiphoton and avalanche ionization processes, which act as microscopic wave guides along which the light propagates without divergence.

Firstly, the macroscopic dose-rate of the laser induced filamentation process was determined by two different chemical dosimeters (10); secondly the spatial dose distribution, and hence the microscopic energy density and dose-rate, of the laser-induced filamentation process was captured by a transparent polymer gel dosimeter and visualized by magnetic resonance imaging (MRI) (10). Using this tissue equivalent gel dosimeter, often applied in clinics to test radiotherapy treatment planning, our results clearly show that changing the laser pulse duration enables us to precisely control the distance in the tissue equivalent medium over which the entrance dose is zero (Fig. 1b).

Using the chemical Fricke and the ceric-cerous dosimeters we find that the dose rate by laser filamentation is extremely high along the actual filamentation tracks. Ceric-cerous dosimeters are used for high intensity radiation, because the yield of ceric ions is independent of O_2 concentration and of dose rate (11, 12). Here, the dose absorbed in our macroscopic chemical dosimeter volume (2 ml) varies linearly with irradiation time for femtosecond laser filamentation, and for γ-irradiation using a standard ^{137}Cs source (10). The macroscopic dose rate of the laser filáments and γ-irradiation in the 2 ml volume are 7.8 ± 0.1 and 0.20 ± 0.01 Gy/s, respectively (10). For comparison, the dose rate achieved by clinical proton beam sources (at 60 MeV) is 2.8 Gy/s (13). These results show that laser filamentation can deposit a large macroscopic dose rate in a very local track within the macroscopic sample volume. In addition, the chemical yield of these types of radiation

dosimeters results from reactions of water radiolysis products with metal ions (Fe^{2+} and Ce^{4+}) in aqueous solutions (11,12). Thus, our results also show that the IR laser pulse induced filamentation process generates the same type of radical water radiolysis species than conventional ionizing radiations.

The spatial morphology of the energy-deposition process by laser induced filamentation was evaluated at the microscopic and macroscopic level using a clinically validated tissue-equivalent polymer gel-dosimeter and magnetic resonance imaging (MRI) (Fig. 1); the gels are three-dimensional (14-15) and the tissue equivalent radiation dosimeters (16) used here are used widely in clinical applications. The gel dosimeter is based on radiation-induced polymerization of two monomer species, which is initiated by free radicals derived from water radiolysis (17). The amount of polymerization produced in the dosimeter is directly related to the absorbed radiation dose, i.e. energy deposited. The spatial distribution of the polymer influences the spatial MRI properties of the dosimeter gel. The formation of polymer also alters the initial optical transparency of the dosimeter and this is directly visible to the human eye. Here, the dosimeter sample cells were imaged by MRI as described elsewhere (18). The diameters of filamentation tracks produced here for the MRI micro-dosimetry measurements are estimated to be ~300-400 μm (10). Using the measured values of the macroscopic dose rate of 7.8 Gy/s, discussed above, and the MRI measurements of the filamentation track's dimensions, shows that the actual energy density within the microscopic filamentation track is about 4.6×10^7 to 8.2×10^7 keV/μm, while the effective dose rate within the filamentation track equals ~4.9×10^{11} Gy/s (10). These values surpass those of even the most intense conventional clinical radiation sources to date. Fig. 1a, b shows photographs of a large polymer gel dosimeter irradiated with laser

filamentation. Here, changing the pulse duration leads to changes in the starting point of filaments as shown in Fig. 1b. In case of conventional X-ray irradiation in Fig. 1c, where a clinical irradiator was used, the absorbed dose decrease as a function of depth in the gel dosimeter, from a maximum delivered dose that occurs upon entry into the tissue equivalent medium. Thus, unlike conventional ionizing radiation, such as clinical X-rays, the femtosecond IR laser pulse filamentation process is capable to generate a zero entrance dose, while allowing precise control over the depth and volume shape in which the dose is deposited in the macroscopic medium, at the high microscopic dose rates described here.

Laser filamentation effect on biological systems. Clearly, the laser induced filamentation process, as observed here in chemical and tissue equivalent clinically validated dosimeters, is able to induce similar or identical chemical processes or polymerizations (all related to formation of free radicals) as conventional ionizing radiation; yet, a key questions is if the type of genotoxic damage, induced in DNA or its components, by IR laser induced filamentation is the same as that of conventional ionizing radiation. Here, we use the nucleoside thymidine, and double stranded plasmid DNA as benchmarks to answer this question.

Biological compound damage. Thymidine decomposition resulting from γ-irradiation and laser filamentation is shown here both in the absence and the presence of oxygen (Fig. 2a). The pathway of decomposition of thymidine in solution by γ-radiation involves the generation of an $^{\bullet}OH$ radical and its addition to the 5,6-double bond of thymine or H-atom abstraction from the 2-deoxyribose moiety. The resulting carbon-

centred radicals of thymidine lead to a large number of stable modifications (19). In view of the very similar profiles of products observed here by HPLC-UV of samples exposed in solution to γ radiation and laser filamentation, the mechanism of formation of products involves •OH radicals in both cases. Thymine is a well-known benchmark product of thymidine decomposition by γ-radiation, which arises from initial abstraction of H-atoms from the 2-deoxyribose moiety by •OH radicals generated in the solution (19). The greater release of thymine in oxygenated solution (~ 3 times) compared to that in deoxygenated solution (Fig. 2a) may be attributed to the addition of oxygen to carbon centred radicals at the 2-deoxyribose moiety leading to more efficient cleavage into thymine. Again, the similarities of thymine release and the effect of oxygen on the decomposition of thymidine in both clinical γ-irradiation and IR laser filamentation experiments demonstrate here that •OH radicals are also the damage inducing species in laser filamentation. However, other damage pathways to DNA components, such those mediated by LEEs (20) are also possible.

DNA damage. Supercoiled, double stranded plasmid DNA [pGEM 3Zf(-)], was used to compare the genotoxicity of laser filamentation and γ radiation in aqueous solution. Our results in Fig. 2 b and c clearly show that the damage to double stranded DNA, as indicated by the production of single stand breaks (SSBs, circular form), and double stand breaks (DSBs, linear form), by IR laser induced filamentation is identical to that induced by conventional γ-irradiation; moreover, in both cases this involves the formation of free radical species in the solution, including scavengable solvated electrons in aqueous solutions (21). Here, filamentation also generates a high density avalanche of LEEs (~10^{17}

cm^{-3}) by inverse Bremsstrahlung and multiphoton ionization processes in the aqueous solution (22-26). These LEE, similar to those formed along conventional radiation tracks, have 10 nm range in water (27), and damage DNA even at subionization energies (9). Regardless of their formation mechanism, LEEs will also fragment surrounding molecules, yielding radicals, including ROS, (12, 27-29), which may attack DNA and lead to SSB and DSB that are accepted benchmarks for genotoxic radiation effects.

Animal tumor model. To test the therapeutic curative potential of this fs IR laser irradiation technique, we have begun to study its effects on a well known and validated subcutaneous animal tumor model. Tumors were grown in female Balb/c mice by subcutaneous injection of mouse mammary carcinoma cells (MC7-L1) in both legs, irradiating only one. Our preliminary results, 23 days after treatment show that (a) tumor involution is clearly observed in the treated leg, and (b) while the untreated tumor volume increased on average by 1500% (± 160%), the average reduction in treated tumor volume is at least 50% (± 44%). Most encouragingly, in 1 out of 3 cases the tumor was completely eradicated as shown in Fig. 3. This is likely be due to the fact that the geometric spacing of the five targeted irradiation spots on each tumor was not identical for each mouse, such that tighter spacing could lead to better tumor control. A higher power laser, allowing multiple beam splitting and thus simultaneous irradiation with multiple beams at constant spacing, will remedy this. In any case, our results suggest that the fs IR laser irradiation method used here has a definite curative effect on tumor tissue, and warrants intensive study due to its vast potential to greatly improve cancer therapy.

Conclusion

We have presented evidence that the radiation-chemical and radiobiological mechanisms and outcomes of fs IR laser induced filamentation, even in tissue equivalent dosimetric media, seem equivalent to conventional ionizing radiation. Moreover, we have shown here that this new and conceptually unique approach to cancer therapy, using high-power fs infrared laser pulse filamentation (30) in macroscopic targets, may bring us tantalizingly close to finally achieving the "dream beam" of radiation therapy: maximize the energy dose inside the tumor volume, while keeping the (entrance) dose to healthy tissue zero. In other words, it seems possible to effectively "beam in" radiotherapeutic energy, at a high density, into a well controlled volume, leaving the surrounding medium untouched. Our studies on DNA molecular models and animal tumor models are still underway, particularly regarding the efficiency with which laser filamentation might occur in opaque scattering media such as living tissue, which remains unanswered (31); however the use of adaptive optimization by a spatial light modulator (32) could partly compensate for the scattering of light in actual opaque tissue. While the adaptability of the method described here to very deep seated tumors is not yet clear, we are currently testing specially adapted hollow fiber optic methods to bring the radiotherapeutic pulsed IR laser beam physically closer to specific deep seated target volumes.

Materials and Methods

Laser irradiation. The laser irradiation setup used here for all the experiments in aqueous solutions is shown in Fig. S1 (see supplementary information). Sample solutions were irradiated by femtosecond Ti-sapphire laser beams with the following properties: pulse

duration was 100 fs; pulse energy was 0.3 mJ/pulse; repetition rate was 1 kHz; and the central wavelength was 800 nm. The laser beam was focused by a 30 cm focal length achromatic lens into the sample container (quartz cuvette, $1\times1\times5$ cm^3). The sample cell was located at ~24 cm from the focal lens.

Gamma and X-ray irradiation. The samples were irradiated to a maximum of 300 Gy at 25 °C with ^{137}Cs γ-rays (0.662 MeV) in a Gammacell (Elan 3000, Atomic Energy of Canada Limited). The dose rate for gamma irradiation, ^{137}Cs, was 0.20 ± 0.01Gy/s, as determined by Fricke dosimetry. In some cases gels where irradiated with a clinical X-ray therapy system (Therapax HF150T), at 1, 2 and 3 Gy, to demonstrate typical entrance dose of clinical X-rays.

Chemical radiation dosimeters. We used 1 mM of ammonium ferrous sulfate hexahydrate (≥ 99.99 % Sigma), 0.4 M H_2SO_4 (98 %, Sigma) in saturated oxygen condition, so called the "super Fricke" dosimeter (12). The concentration of Fe^{3+} was measured by UV spectrophotometer at 304 nm (where $\varepsilon = 2196 \pm 5$ $M^{-1}cm^{-1}$) (33). Typically, the production of ferric ions is most sensitive to the radical species produced in the radiolysis of water. Under low linear energy transfer (LET) irradiation conditions, $G(Fe^{3+})$ is equal to 15.6 ± 0.3 molecules/100 eV (12). However, the yield of ferric ions was found to decrease with increasing dose rate above 10^8 Gy/s (33), and was appreciably dependent on the initial concentrations of dissolved oxygen at high absorbed dose (>500 Gy) (33). Since here the microscopic dose rate within the filament volume can exceed such dose rates, a ceric sulfate dosimeter is used here as well.

The ceric sulfate dosimeter has been recommended as a chemical dosimeter for high dose rate radiations (11). The principle of the dosimeter is reduction of Ce^{4+} to Ce^{3+} by radiolysis processes that do not consume oxygen. Here, we used 1 mM cerium (III) sulfate (≥ 99.99 %, Sigma) and 0.25 mM, ammonium cerium (IV) sulfate dihydrate (>99%, Sigma) in 0.4 M H_2SO_4 (98 %, Sigma) (11). The concentration of ceric ions was determined by spectrophotometer at 320 nm which molar absorption coefficient was 5610 ± 7 $M^{-1}cm^{-1}$ (34). At high dose rate (>10^{10} Gy/s), the yield of ceric depends on yield of H_2O_2 which was 1.4 molecules/100 eV (11).

Polymer gel dosimeter. The dosimeter gels were prepared with acrylamide (AA) and N,N'-methylenebisacrylamide (BIS) (99+%, electrophoresis grade, Aldrich), each at 3% w/w dissolved in gelatin (300 bloom, Aldrich) at 5% w/w, and water (de-ionized). The monomers (AA and BIS) were dissolved in an aqueous gelatin matrix. In the manufacture process, gelatin was added to water at room temperature and left to soak for 10 min. The solution was then heated and maintained at a temperature of 45°C. AA and BIS were successively added and magnetically stirred for typically 15 min until complete dissolution. The gels were prepared under a controlled N_2 atmosphere inside a glove box (18). The solution was poured into glass cell (diameter 2 cm × length 5 cm) as shown in Fig. S3a (see supplementary information). For the plastic container as shown in Fig. 2b, the gel was prepared in the glove box with the same recipe but 5 mM of alkaline tetrakis (hydroxymethyl) phophonium chloride (THPC) (80%, Aldrich) as an oxygen scavenger.

Thymidine decomposition. The biochemical reagents used in the experiment were the nucleoside thymidine (>99 %, Sigma), a component of cellular DNA, and de-ionized water.

A 1 mM thymidine solution was prepared, 2 ml were poured into a bubble forming anaerobic cell (1×1×5 cm^3, NSG). The sample cell was purged with nitrogen or oxygen during 15 minutes immediately before irradiation. The samples were irradiated by conventional gamma radiation and laser filamentation. These samples were analyzed by high-performance liquid chromatography (HPLC) with ultraviolet (UV) detection.

Plasmid DNA damage. pGEM-3Zf(-) plasmid DNA (3197 bp, Promega) was extracted form *E. coli* DH5α and purified with the QIAfilter Plasmid Giga Kit (Qiagen). Agarose gel electropholysis was used to show that 96 % of DNA was initially in the supercoiled form, 3 % was in the concatemeric form and 1 % was in the circular form. The DNA was dissolved in de-ionized water. The concentration of DNA was measured by its UV absorption at 260 nm, assuming a molar extinction of 7120 mol^{-1} cm^{-1} at pH7.0 (35). The amount of DNA in each sample that was used for irradiation was 200 ng/ml. The samples were irradiated by conventional gamma radiation and laser filamentation, and analyzed by standard gel electrophoresis.

MC7-L1 tumors implanted in Balb/c mice and laser irradiation. The experimental protocol was approved by the institutional ethical committee and complied with the regulations of the Canadian Council on Animal Care. The mouse mammary carcinoma cell line MC7-L1 was generously provided by Dr Alfredo A. Molinolo of the Instituto de Biologia y Medicina Experimental, Concejo Nacional de Investigaciones Cientificas y Técnicas en Facultad de Medicina, Universidad de Buenos Aires, Buenos Aires, Argentina (36). The MC7-L1 cells were grown in minimal essential medium (MEM) supplemented

with 10 % fetal bovine serum (FBS) (Gibco, Burlington, ON, Canada), 1 mM sodium pyruvate, 2 U/ml penicillin G, 2 μg/ml streptomycin and 250 ng/ml amphotericin B. The MC7-L1 cells (10^6) were subcutaneously injected in both thighs of female Balb/c mice six weeks old. Three to four weeks later, mice bearing tumors with a diameter of 3-5 mm were put under anaesthesia (ketamine/xylazine) and irradiated in one tumor (thigh) only by femtosecond laser pulses, such that the unirradiated tumor (thigh) acted as a control. The laser treatment was performed by irradiating five spots on a tumor and the irradiation time was 10 minutes each spot. The tumor volume was calculated using the equation, L in mm × W in mm × H in mm × 0.5, for measured values of L, W, and H at specific days after the irradiation day.

Acknowledgements. Funding for this research was provided by the Canadian Institutes of Health Research (CIHR), the Canadian Institute for Photonics Innovations of Canada and the Banque National-Centre de Recherche Clinique of the Centre Hospitalier Universitaire de Sherbrooke. RM acknowledges a scholarship from the Ministry of Science and Technology of the Royal Thai Government and Applied Radiation and Isotope Department, Faculty of Science, Kasetsart University, Thailand.

References

1. IAEA (2008) *The Role of PET/CT in Radiation Treatment Planning for Cancer Patient Treatment.* (IAEA, Viena).
2. Intensity modulated radiation therapy collaborative working group (2001) Intensity-modulated radiotherapy: Current status and issues of interest. *Int Radiat Oncol Biol Phys* 51: 880-194.
3. Hall EJ, Phill D (2006) Intensity-modulated radiation therapy, protons, and the risk of second cancers. *Int Radiat Oncol Biol Phys* 65: 1-7.
4. Suit H, et al. (2003) Proton beams to replace photon beams in radical dose treatments. *Acta Oncol* 42: 800-808.
5. Glimelius B, et al. (1999) Potential gains using high-energy protons for therapy of malignant tumors. *Acta Oncol* 38: 137.
6. Goitein M, Jermann M (2003) The relative costs of proton and x-ray radiation therapy. *Clin Oncol* 15: S37-S50.
7. Gibson KF, Kernohan WG (1993) Lasers in medicine: a review *J Med Eng Technol* 17: 51-57.
8. Cobut V, et al. (1998) Monte Carlo simulation of fast electron and proton tracks in liquid water I: Physical and physiochemical aspect. *Radiat Phys Chem* 51: 229.
9. Boudaïffa B, Cloutier P, Hunting D, Huels MA, Sanche L, (2000) Resonant formation of dna strand breaks by low-energy (3 to 20 eV) electrons. *Science* 287: 1658.
10. See supplementary information.
11. Ferradini C, Pucheault J (1983) *Biology of Ionizing Radiation Action "Biologie de l'Action des Rayonnements Ionisants"*, (Masson, Paris) pp 75-77.

12. Spinks JWT, Woods RJ (1990) *An Introduction to Radiation Chemistry*, (Wiley, New York).

13. Goitein M, Abrams M, Rowell D, Pollari H, Wiles J (1983) Multi-dimensional treatment planning: II. Beam's eye-view, back projection, and projection through CT sections. *Int J Radiat Oncol Biol Phys* 9: 259.

14. Maryanski MJ, Gore JC, Kennan RP, Schulz RJ (1993) NMR relaxation enhancement in gels polymerized and cross-linked by ionizing radiation: A new approach to 3D dosimetry by MRI. *Magn Reson Imaging* 11: 253-258.

15. Baldock C, et al. (1998) Experimental procedure for the manufacture and calibration pf polyacrylamide gel (PAG) for magnetic resonance imaging (MRI) radiation dosimetry. *Phys Med Biol* 43: 695-702.

16. Venning AJ, Nitschke KN, Keall PJ, Baldock C (2005) Radiological properties of normoxic polymer gel dosimeters. *Med Phys* 32: 1047-53.

17. Lepage M, Whittaker AK, Rintoul L, Bäck SÅJ, Baldock C (2001) The relationship between radiation-induced chemical processes and transverse relaxation times in polymer gel dosimeters. *Phys Med Biol* 46: 1061-1074.

18. Meesat R, Jay-Gerin J-P, Khalil A, Lepage M (2009) Evaluation of the dose enhancement of iodinated compounds by polyacrylamide gel dosimetry. *Phys Med Biol* 54: 5909-5917.

19. Cadet J, Douki T, Gasparutto D, Ravanat J-L, Wagner JR (2010) in *Radical and Radical Ion Reactivity in Nucleic Acid Chemistry*, ed M. M. Greenberg (Wiley, New Jersey), pp 69-98.

20. Li Z, Zheng Y, Cloutier P, Sanche L, Wagner JR (2008) Low energy electron induced DNA damage: effects of terminal phosphate and base moieties on the distribution of damage. *J Am Chem Soc* 130: 5612.

21. D'Souza JS, Dharmadhikari JA, Dharmadhikari AK, Rao BJ, Mathur D (2011) Effect of intense, ultrashort laser pulses on dna plasmids in their native state: strand breakages induced by in situ electrons and radicals. *Phys Rev Lett* 106: 118101-4.

22. Chin SL, et al. (2005) The propagation of powerful femtosecond laser pulses in optical media: physics, applications, and new challenges. *Can J Phys* 83: 863-905.

23. Couairon A, Mysyrowicz A (2007) Femtosecond filamentation in transparent media. *Phys Rep* 441: 47-189.

24. Chin SL (2006) Some fundamental concepts of femtosecond laser filamentation. *J Korean Phys Soc* 49: 281-285.

25. Goulet T, Bernas A, Ferradini C, Jay-Gerin J-P (1990) On the electronic structure of liquid water: Conduction-band tail revealed by photoionization data. *Chem Phys Lett* 170: 492-496.

26. Vogel A, Noack J, Huttma NG, Paltauf G (2005) Mechanisms of femtosecond laser nanosurgery of cells and tissues. *Appl Phys B* 81: 1015-1047.

27. Meesungnoen J, Jay-Gerin J-P (2005) High-LET radiolysis of liquid water with $^{1}H^{+}$, $^{4}He^{2+}$, $^{12}C^{6+}$, and $^{20}Ne^{9+}$ ions: Effects of multiple ionization. *J Phys Chem A* 109: 6406-6419.

28. Chin SL, Lagacé S (1996) Generation of H_2, O_2, and H_2O_2 from water by the use of intense femtosecond laser pulses and the possibility of laser sterilization. *Appl Opt* 35: 907-911.

29. L. Sanche (2010) in *Radical and Radical Ion in Nucleic Acid Chemistry*, ed M.M. Greenberg (Wiley, New Jersey), pp 239-294.

30. Houde D, Meesat R, Allard J-F, Brastaviceanu T Radiochemistry generator and generator for radiotherapy treatment using filamentation of femtosecond laser. U.S. Provisional Patent Application No 61/313,553 (2010), PCT Patent Application PCT/CA2011/000273 (2011).

31. Jukna V, et al. (2009) Filamentation of ultrashort light pulses in a liquid scattering medium. *Appl Phys B* 94: 175-179.

32. Katz O, Small E, Bromberg Y, Silberberg Y (2011) Focusing and compression of ultrashort pulses through scattering media. *Nature Photon* 5: 372-377.

33. Buxton GV, Stuart CR (1995) Re-evaluation of the thiocyanate dosimeter for pulse radiolysis. *J Chem Soc Faraday Trans* 91: 279-281.

34. Matthews RW (1973) Effect of solute concentration and temperature on the ceric-cerous dosimeter. *Radiat Res* 55: 242-255.

35. Zheng Y, Sanche L (2009) Gold nanoparticles enhance DNA damage induced by anti-cancer drugs and radiation. *Radiat Res* 172: 114-119.

36. Lanari C, et al. (2001) Five novel hormone-responsive cell lines derived from murine mammary ductal carcinomas: *in vivo* and *in vitro* effects of estrogens and progestins. *Cancer Res* 61: 293-302.

Figure 1: Photographs of containers filled with tissue equivalent polymer dosimeter gel and irradiated with fs laser pulses (~400 μm × 400 μm) to draw the logo of Université de Sherbrooke (a) top view and (b) side view. The entrance dose was effectively zero up to a certain depth, which in (b) was wave modulated (yellow arrows) by changing the laser pulse duration (input beam from the right of the container), to show depth control of the zero dose region before the target volume in which filamentation occurs. The length of the filamentation tracks, i.e. their end, is controlled in part by the physical geometry of the optics (lenses, etc), as well as the energy (intensity) per laser pulse, at a given pulse width, *ceteris paribus*, for laser pulse energies above filamentation threshold, and below dielectric breakdown (22,23). In (c), the polymer gel was irradiated with X-rays (150 kVp) from a clinical X-ray therapy system (Therapax HF150T), at 1, 2 and 3 Gy, and clearly shows that the deposited dose is maximum upon "tissue entry" (blue arrows). (d) is a comparison of depth-dose distributions of various conventional radiation modalities related to radiation therapy.

Figure 2: DNA damage induced by ^{137}Cs gamma radiation, and laser filamentation at 800 nm: (a) a graph of the release of thymine (glycosidic bond cleavage) from the irradiation of thymidine in solution versus absorbed dose. Agarose gel electropholysis separating supercoiled plasmid DNA damage (circular and linear DNA conformations correspond to single and double strand breaks) using (b) gamma irradiation and (c) IR femtosecond laser pulse filamentation. The absorbed macroscopic doses to the 2 ml target solution are given in Gy, and the two lanes in (b) after the marker are unirradiated controls.

Figure 3: Femtosecond IR (800 nm) laser pulse treatment (left leg) of the mouse mammary carcinoma MC7-L1 tumor compared to control (right leg) 23 days after laser irradiation. MC7-L1 cells were injected into the right and left thighs of female Balb/c mice. The right side tumor of mice was used as control. Three to four weeks later, mice bearing tumors with a diameter of 3-5 mm were irradiated by femtosecond IR laser pulses. The best laser treatment result here was obtained by irradiating five separate spots (100 – 300 μm diameter, separated by approximately 1 to 1.5 mm) on the tumors, with 10 min irradiation times for each spot; the laser irradiation and dosimetry conditions were identical to those used for filamentation during chemical dosimetry (10).

Figure 1

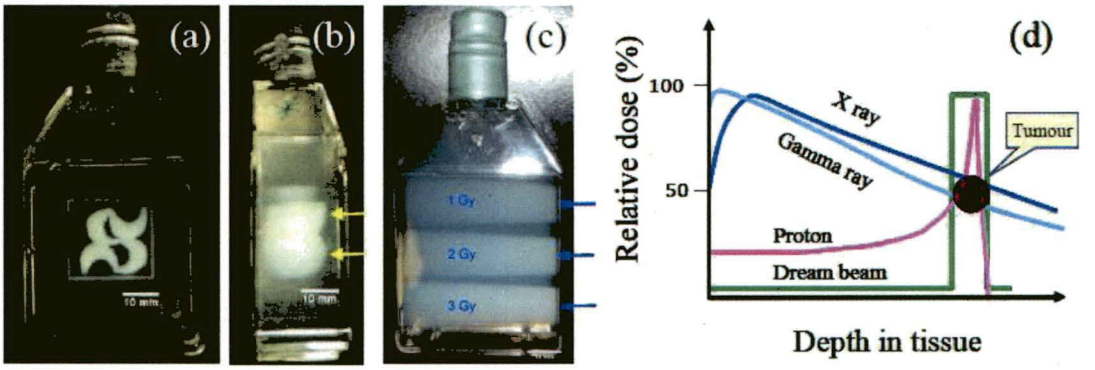
(a)
(b)
(c)
(d)
1 Gy
2 Gy
3 Gy
Relative dose (%)
100
50
X ray
Gamma ray
Proton
Dream beam
Tumour
Depth in tissue

Figure 2

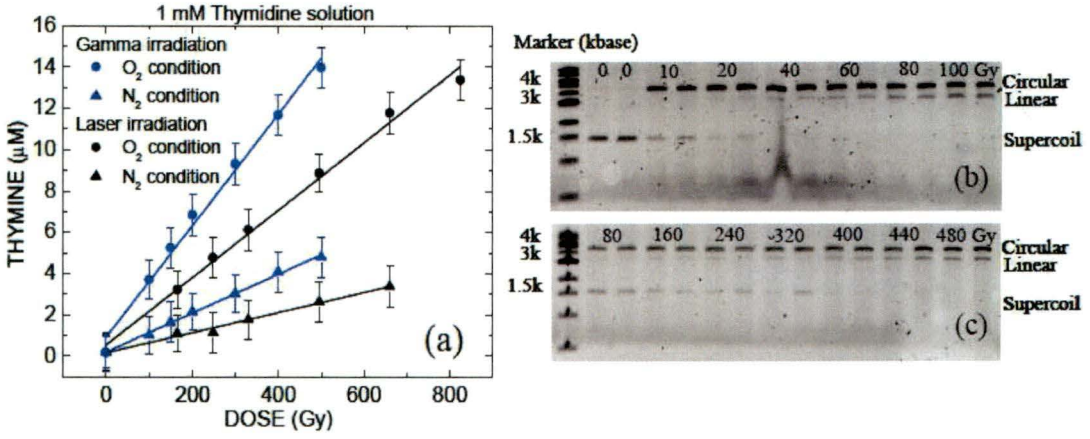
1 mM Thymidine solution
Gamma irradiation
O2 condition
N2 condition
Laser irradiation
O2 condition
N2 condition
THYMINE (µM)
DOSE (Gy)
(a)
Marker (kbase)
4k
3k
1.5k
0 0 10 20 40 60 80 100 Gy
Circular
Linear
Supercoil
(b)
80 160 240 320 400 440 480 Gy
(c)

Figure 3

Supporting information

Experimental setup

We have shown previously that filamentation is produced with these settings (Fig. S1). For chemical dosimeters and the thymidine and plasmid experiments, the aqueous target solution (2 ml) was poured into cuvettes. The sample is then irradiated at the middle of the solution volume during continuous magnetic stirring at 20 °C. The diameter of laser filaments was ~ 300-400 μm, as estimated by polymer gel dosimetry (see below). The total macroscopic absorbed dose of the laser filamentation in the 2 ml volume was estimated by ceric-cerous sulfate and Fricke dosimeter (see section 2 below), yielding a macroscopic dose rate of 7.8 ± 0.1 Gy/s for the above laser filamentation conditions. This dose rate is also used for all other laser irradiation experiments using the gel dosimeters, and mouse tumor models described here.

Dosimetry of laser filamentation and gamma radiation

As shown in Fig. S2, the absorbed dose varies linearly with irradiation time for femtosecond laser filamentation, and for gamma irradiation using a standard ^{137}Cs source. The macroscopic dose rate delivered to the entire sample volume (2 ml) by the laser filaments and the gamma radiation were 7.8 ± 0.1 and 0.20 ± 0.01 Gy/s, respectively. We can thus calculate the ceric effective dose rate (CEDR), which is the CEDR calculated from ceric-cerous dosimeter parameters. The dose per laser shot is estimated to be 7.8×10^{-3} Gy/laser shot (1 kHz), so that the energy deposited by a single laser shot (dose/laser shot × density of dosimeter ($D(H_2O)$) × 2 cm^3) is 1.56×10^{-6} J/laser shot using 2 cm^3 as the volume of the ceric-cerous solution. The CEDR then equals 2.8×10^{11} to 4.9×10^{11} Gy/s (using the effective volume of the filament (from the diameter of 300-400 μm as estimated

by MRI, see below), $D(H_2O)$ and the effective time (ET)). It should be noted that ET is the effective time of deposition which equals the propagation time of light at 800 nm in 1 cm of water (the 1 cm filament length L in the $1\times1\times5$ cm^3 cuvette) which equals $n \times L/c$, neglecting the bandwidth of the laser pulse and the group velocity dispersion; here $n=1.33$ is the index of refraction for 800 nm laser pulses in water, and c is the speed of light in vacuum. This calculated CEDR is in good qualitative agreement with the effective microscopic dose rate (EDR) obtained from the parameters of filamentation theory ($\sim10^{12}$ Gy/s, see discussion below). For the gammacell, the effective dose rate (0.20 ± 0.01 Gy/s) is the same as the average dose rate, which is not the case for the filamentation process. Here, we use fs laser pulses to generate an avalanche of low energy electrons (LEEs) in the filaments by inverse Bremsstrahlung process (22-26).

The process can lead to the formation of molecular and radical species in liquid media. LEEs are generated in massive amounts (in the range of $\sim 10^{17}$ cm^{-3}) (22-23, 26). This is equivalent to the secondary LEEs that are formed by conventional high-energy ionizing radiation like X rays, γ photons or charged particles (accelerated electrons or heavier charged particles) (8). Films of biological molecules in ultrahigh vacuum condition have clearly demonstrated the disruption of DNA plasmids by these electrons (9). In the present work we generate anisotropic concentrations (filaments) of such LEEs in a macroscopic volume ($\sim$ cm^3) of aqueous solutions. In both cases (conventional ionizing radiation or filamentation), the electrons transfer their excess energy to the surrounding water molecules. In filamentation, electrons are generated (22-26) and reaccelerated by the inverse Bremsstrahlung processes (22-26). Chemically reactive species such as e^-_{aq} (37), $H^\bullet$, $^\bullet O^\bullet$ (27, 38), $^\bullet OH$, and $HO^\bullet_2$ (or $O^{\bullet-}_2$, pK_a =4.8) (27, 38) and H^+, OH^-, etc., are thus

produced along the filaments as well as stable species (H_2, O_2, H_2O_2) (28) due to radical recombination. In turn, these chemically reactive species (which are the same as those that are formed by conventional ionizing radiations) react with the Fe^{2+} or Ce^{4+} in the chemical dosimeters used here, or with the monomers in the aqueous gel dosimeters.

As is shown in this work, in terms of their chemical/dosimetric and biomolecular outcome (final damage and induced reaction mechanisms), filaments are an analogue to conventional radiation tracks but some important differences must be noted. The diameter of filaments (multi-filament regime) in liquids is around ~100-250 μm (22) which is much larger than the radial dose deposition (or penumbrae) in a heavy ion track structure (39) produced by conventional ionizing radiation, but smaller than the 4 mm minimum diameter of a collimator of a GammaKnife beam (40) used in Gamma Knife radiosurgery. In our case, the filament diameter that was estimated by MRI was 300-400 μm (see below). Thus, assuming a filament of 300 μm of diameter (Dia) and 6.5 eV (22, 23) per electron with a electron density (ED) of 10^{17} cm^{-3} (22), the effective microscopic LET within the filamentation track is:

$$LET = \pi \times (Dia/2)^2 \times ED \times 6.5\ eV = 4.6 \times 10^7\ keV/\mu m$$

Assuming the same parameters, the effective microscopic dose rate (EDR) within the filamentation track is:

$$EDR = (ED \times 6.5\ eV \times CF)/(D(H_2O) \times ET) = 2.3 \times 10^{12}\ Gy/s$$

Where the conversion factor (CF) is $J/6.242 \times 10^{18}$ eV and $D(H_2O)$ is the water density (1 g cm^{-3}).

Magnetic resonance imaging (MRI)

The samples were irradiated by the pulse filamentation from the femtosecond laser pulse as described above. The spatial distribution of the polymer influences the spatial nuclear magnetic resonance properties of the dosimeter gel by decreasing its spin-spin relaxation time (T_2). The formation of polymer also alters the initial optical transparency of the dosimeter and this is directly visible to the human eye. Here, the samples were imaged using a 7 T small animal magnetic resonance imaging (MRI) scanner as shown in Fig. 3 (see supplementary information). A fast spin-echo protocol to acquire images in the axial (sagittal) planes with the following parameters: TR: 4 400 ms (2 000 ms), echo spacing: 13 ms, echo train length: 8, FOV: 25 × 25 mm^2 (60 × 30 mm^2), matrix: 256 × 256 (512 × 256), slice thickness: 1 mm (3.5 mm), number of slices: 40, number of averages: 4. The in-plane spatial resolution of the axial images was thus ~ 100 μm as shown in Fig. S3c-d. The diameters of filamentation tracks produced here for the MRI micro-dosimetry measurements are estimated to be ~300-400 μm (see Fig S3d).

37. Brastaviceanu T (2004) *M.Sc. Thesis*, Université de Sherbrooke.

38. Meesungnoen J, Jay-Gerin, J-P (2009) High-let ion radiolysis of water: oxygen production in tracks. *Radiat Res* 171: 379-386.

39. Magee JL, Chatterjee A (1987) in *Kinetics of Nonhomogeneous Processes*, G. R. Freeman, Ed. (Wiley, New York), pp. 171-214.

40. Leksell Gamma Knife 4C used in Neurochirurgy in the Centre Hospitalier Universitaire de Sherbrooke (CHUS).

Figure S1. Experimental setup for laser filamentation irradiation of samples in solution.

Figure S2. Graph of macroscopic dose (ceric-cerous and Fricke dosimeter) versus exposure time of laser femtosecond filamentation at 800 nm (●), and gamma radiation (γ-rays from ^{137}Cs) (■).

Figure S3. The filamentation of femtosecond laser radiation fixed in polymer gel dosimeters (a) optical side view of the filamentation and (b) optical image of the cross sections of filamentation (c) MRI image of the tracks of filamentation (d) MRI image of the cross sections of the tracks of filamentation. Note that here the laser was set to produce filamentation immediately upon entry in the gel medium, as opposed to Fig 1a and b in the full text, were the laser pulse width was adjusted to produce a controlled zero entrance dose. Here the filamentation tracks are produced in the single shot mode, one pulse per track.

Figure S1

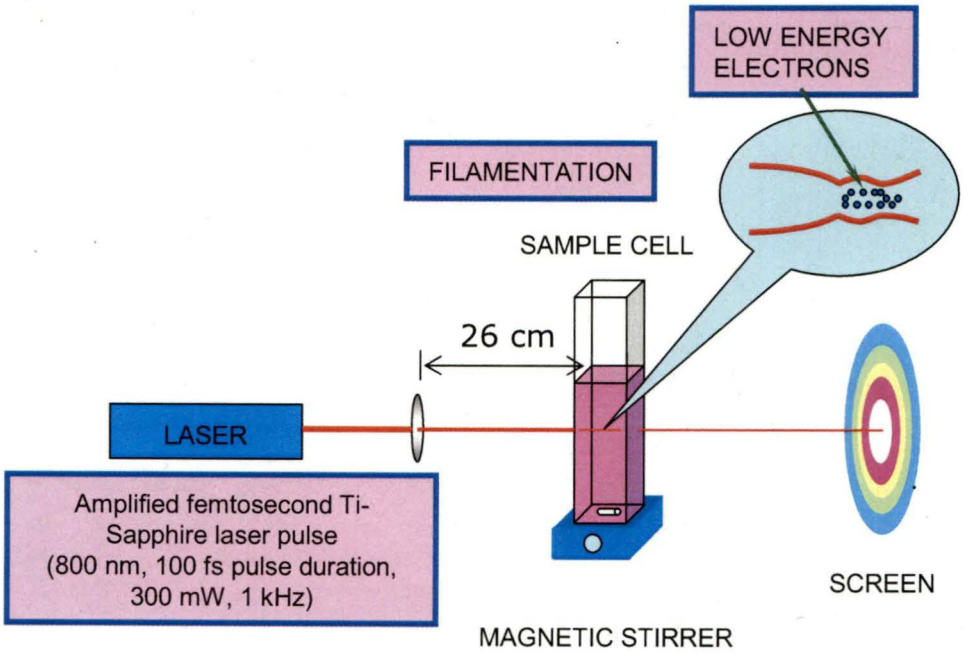
LOW ENERGY ELECTRONS
FILAMENTATION
SAMPLE CELL
26 cm
LASER
Amplified femtosecond Ti-Sapphire laser pulse (800 nm, 100 fs pulse duration, 300 mW, 1 kHz)
SCREEN
MAGNETIC STIRRER

Figure S2

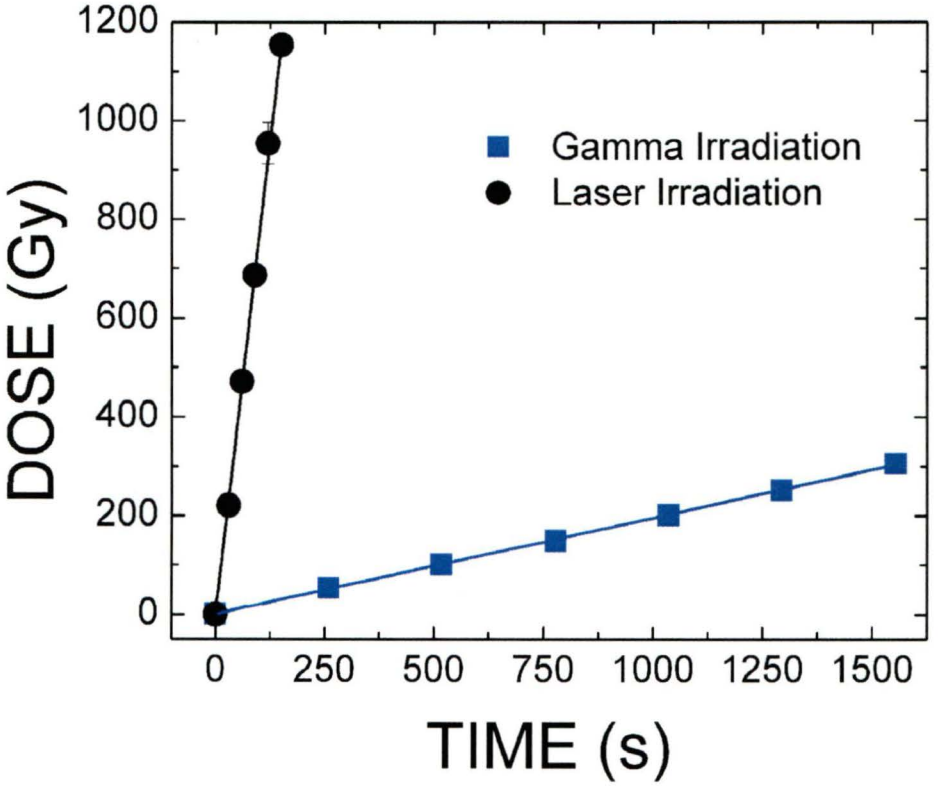
1200
1000
800
600
400
200
0
DOSE (Gy)
0
250
500
750
1000
1250
1500
TIME (s)
Gamma Irradiation
Laser Irradiation

Figure S3

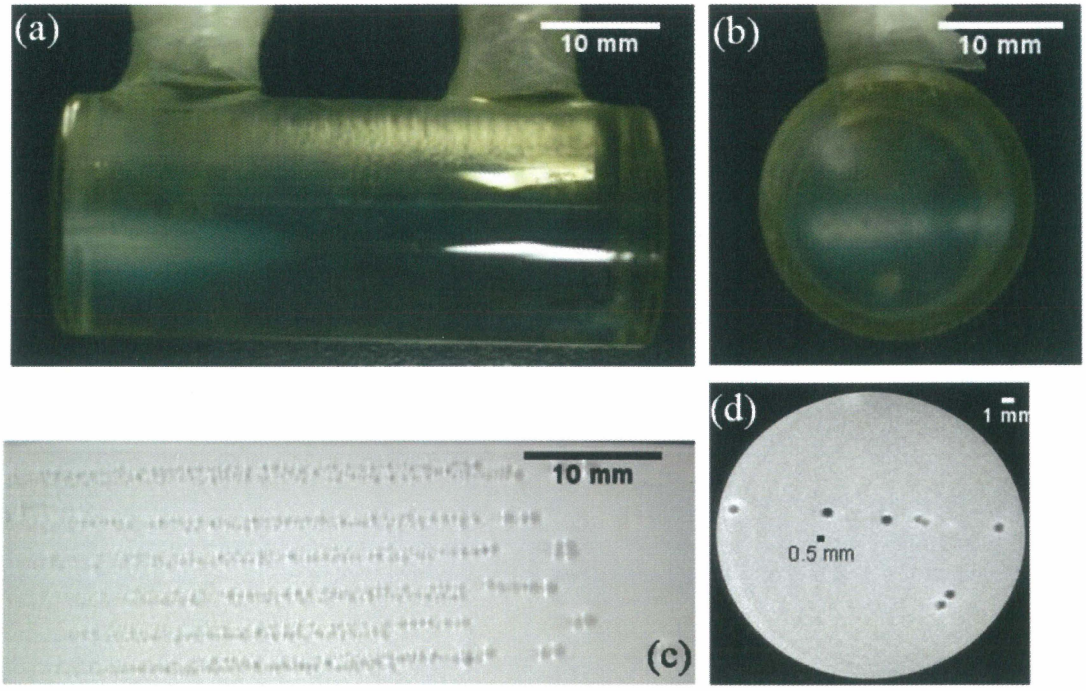

V. Discussion

V. 1 The scope of this thesis

Radiation sensitizers and radiation protectors in clinical therapy have attracted considerable attention during the last decades. Radiosensitizers are intended to enhance tumor cell killing while having much less effect on normal tissues. Chemical radioprotectors are, of course, the reverse of radiosensitizers: the aim is to decrease radiation toxicity, especially of normal tissues. Clonogenic assays have been extensively used to evaluate these compounds, but this only provides information on the addition of these two properties. The aim of this thesis is to develop an alternative method, fast, easy and quantitative to apply, to assess the efficiency and to understand the mechanisms of radiation sensitizers and protectors, based on the use of chemical radiation dosimeters.

In addition, radiation therapy still plays an important role in treatment of cancers. When conventional radiation sources (γ and X radiations, electrons and protons) are directed at the tumor, it is inevitable that normal, non-cancerous tissues surrounding the tumor will also be affected by these radiations and therefore damaged. In this thesis, we showed that using a non-ionizing radiation femtosecond laser pulse can lead to local damage without the deposition of dose before or after a target volume.

In the articles included in this thesis, we have shown that the polyacrylamide gel dosimeter can evaluate the sensitizing effect of halogen compounds and the protecting effect of thiourea and cystamine. The Fricke dosimeter has been used to investigate the protecting effect of cystamine and the mechanisms were understood using simulation studies. Finally, we have studied radiation-chemical and radiobiological effect of femtosecond laser pulse filamentation which may be used for radiation therapy.

V. 2 Radiosensitization quantified by polyacrylamide gel dosimetry

The results of our studies presented in Chapter II show that polyacrylamide gel dosimeter can be used to determine the efficiency of radiation sensitizers. The sensitizing effect is shown in terms of dose enhancement, which is caused by secondary radiations

arising from the photoelectric process of a heavy element (high atomic number (Z)). In this case, we demonstrate that the dose enhancement strongly depends on energy of photon radiation and concentration of the radiation sensitizer. The energy of the radiation should be selected to be close to the absorption energy (absorption edge) of the sensitizer in order to have the highest efficiency of secondary radiation production. When irradiated at the optimal energy, the DER increased with the concentration of sensitizing compound.

In this method, it is important that the radiosensitizer is in neutral condition because the R_2 sensitivity of the polymer gel dosimeter depends on pH (Murphy et al., 2000; McJury et al., 2000). It should be noted that the pH of the PAG solution during preparation is ~5.3. A change in pH modifies the R_2-dose response of the polyacrylamide-based dosimeter because of changing proton concentration. Gochberg et al (Gochberg et al., 2000) have shown that the exchangeable proton concentration in the gel dosimeter affects the spin-spin relaxation time. However, changing the monomers concentration influences the relaxation efficiency by altering chemical exchange (Lepage and Gore, 2004) although the pH is likely to be significant in determining the value (Gochberg et al., 2000; Murphy et al., 2000). In addition, pH can have an effect on chemical and physical properties of gelatin (Fruhner and Kretzschmar, 1989; Hellio and Djbourov, 2006) which is the highest concentration of solute in the gel dosimeter. Consequently, this effect may lead to changing the R_2 relaxation time as well.

V. 2.1 Iodine compounds as a radiation sensitizer

The fundamental goal of radiation therapy is that the delivery of a high therapeutic dose of ionizing radiation to the tumour or treatment volume without exceeding normal tissue tolerance. Conventional radiation therapy does not always meet these criteria because damage to the surrounding normal tissue limits the amount of radiation that can be delivered. One strategy to overcome the tissue radiation tolerance limitation is to use a radiation sensitizing technique. Several *in vitro* and *in vivo* demonstration of the radiation dose enhancement in the presence of iodinated compounds have been reported (Matsudaira et al., 1980; Dawson et al., 1987; Quintiliani, 1987; Mesa et al., 1999; Rose et al., 1999; Adam et al., 2003; Joubert et al 2005). However, in this thesis, we demonstrated that the

sensitizing property depends on the type of iodine compounds. Ionic compounds such as NaI have much less sensitizing effect than compounds that form a covalent bond with iodine atomes, such as iodinated contrast agents (ICAs) (Meesat et al., 2009). It is due to the fact that the ionic compounds can dissociate to form free iodine ions. These ions can react with water free radicals, which would counterbalance the desired sensitizing effect. We showed a decrease in polymerization in the PAG dosimeter. ICAs are among the most frequently used pharmaceuticals for intravascular administration in medical imaging (Christiansan et al., 2000). Thus, ICAs can potentially be used as radiation sensitizers. Many studies have shown that iodinated contrast agents can be used as radiation sensitizers (Quintiliani, 1987; Mesa et al., 1999; Rose et al., 1999; Adam et al., 2003; Joubert et al 2005).

In the radiation therapy perspective, the main idea of a radiation sensitizer technique is that the compound accumulates in a tumor target. Adam et al (Adam et al., 2003) have studied the distribution of ICA in an animal model of glioma. They found that most of the contrast compound was in blood and that the accumulation of the ICA in the tumor of 2.2 mg/ml was about 9 times lower 55 min after injection (Adam et al., 2003). ICA preferentially accumulates in the brain tumor, due to the increased permeability of the blood-brain barrier (Mesa et al., 1999; Adam et al., 2003). The concentration of the ICA in the tumor was quite low, but the concentration of the compound in blood was high enough to cause a sensitizing effect to the tumor blood vessels. It is well known that endothelial cells in tumor blood vessels are proliferating much faster than any normal tissue endothelium (Denekamp, 1984). The process leads to forming permeable vascular structures. Thus, this is an alternative strategy to target and damage newly formed blood vessels with the intention of causing blockage, haemorrhage, thrombosis or collapse of these vessels, leading to ischemic or haemorrhagic necrosis (Denekamp, 1984). In this way, by occluding individual capillaries many thousands of tumour cells can be killed as a result of starvation (Denekamp, 1993).

V. 2.2 **Radioprotection quantified by polyacrylamide gel dosimetry**

We showed in Chapter II that the polyacrylamide gel dosimeter can not only be used to evaluate radiation sensitizers but also can be applied to assess the efficiency of radiation protectors. Basically, the polymerization of PAG dosimeter is initiated by reaction of water radiolysis species with a monomer. As we mentioned in Chapter I, a radioprotector is a free radical scavenger (Bensasson et al., 1993). In the PAG dosimeter in the presence of a radiation protector such as thiourea and halogen ionic compounds, there is a competition between the monomers and the protecting compound, such that the yield of polymer is decreased. In this case, the radioprotector is changed to form protector-derived radicals. Normally, the derived radicals are poorly reactive (Halliwell, 1990). Thus, these radicals can get neutralized after the reaction or react with monomers or gelatin which is in high concentration in the PAG system.

Lepage et al have suggested that an increase in gelatin concentration leads to increase scavenging of water free radicals, initiator fragments and/or increased chain transfer reactions (Lepage et al., 2001), resulting in a decreased sensitivity since less water free radicals become available for reaction with monomers to initiate the polymerization process (Lepage, and Jordan, 2011). The reverse situation may also exist whereby a compound reacting with water free radicals can be transformed into a radical that can initiate polymerization by reacting with monomer. An example of this is cysteine (RSH), an amino acid with the chemical formula $HO_2CCH(NH_2)CH_2SH$ with a thiol side chain (-SH). The sulfide compound is a potential oxygen and radical scavenger and, reacting with oxygen to form a disulfide dimmer according to (Logan et al., 2005)

$$4C_3H_7NO_2SH + O_2 \rightarrow 2C_3H_7NO_2SSO_2NH_7C_3 + 2H_2O\,.$$

In the polyacrylamide gel dosimeter, De Deene and coworkers (De Deene et al., 2002) used cysteine as a oxygen scavenger but the scavenging efficiency was lower than that of tetrakis(hydroxymethyl) phosphonium chloride (THPC). Additionally, under irradiation of cysteine aqueous solution, the thiol compound can rapidly react with e^-_{aq} and $^{\bullet}OH$ radicals with a nearly diffusion-controlled reaction rate constant (6.7×10^9 and 3×10^9

$M^{-1}s^{-1}$, respectively), resulting in the formation of derived radicals as follows (El Samahy et al., 1964):

$$RSH + {}^{\bullet}OH \rightarrow RS^{\bullet} + H_2O,$$

$$RSH + e^{-}_{aq} \rightarrow R^{\bullet} + SH^{-}.$$

These cysteine radicals can initiate polymerization of acrylamide monomer (Bajpai and Bajpai, 1983; Özeroğlu and Kurtoğlu 2001) according to the following reactions:

Initiation: $RS^{\bullet} + M \rightarrow RS + M^{\bullet}.$

Propagation: $M^{\bullet} + M \rightarrow MM^{\bullet}.$

Termination: $M^{\bullet} + M^{\bullet} \rightarrow \text{Polymer}.$

Our results indicate that cysteine leads to increased polymerization in the anoxic-polyacrylamide gel dosimeter as shown in Figure 1. The polymerization increases as a function of cysteine concentration. At the zero dose, the relaxation rate increases as function of concentration which is in agreement with the results of De Deene et al. (De Deene et al., 2002). It should be noted that De Deene and co-workers used 100 mM cysteine in normoxic polyacrylamide gel dosimeter. These results suggested that the thiol compound may initiate polymerization by itself. However, when the concentration of –SH compound increases, the R_2-dose sensitivity increased as a function of absorbed dose. It is due to the fact that the cysteine molecules can be changed to be cysteine radicals as explained above.

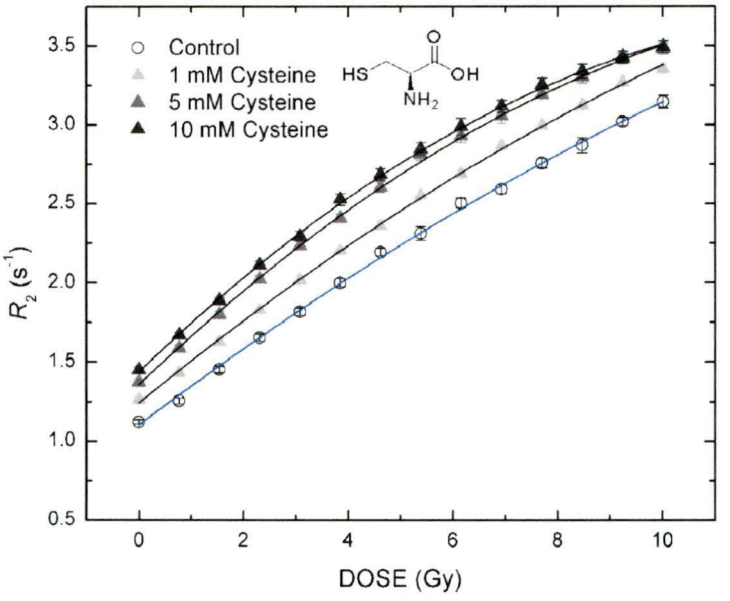

Figure 1. Plot of R_2 against the absorbed dose for PAG dosimeter containing different concentrations of cysteine irradiated with ^{60}Co gamma radiation.

V. 3 Radiation protector quantified by Fricke dosimeter

V. 3.1 Experimental study

As we mentioned earlier, the Fricke system can be used to assess the efficiency of radiation sensitizers (Herold et al., 2000) and radioprotectors (Jayson and Wilbraham, 1968; Lalitha and Mittal, 1971). It also has the merit that it can be simulated by Monte-Carlo techniques (Autsavapromporn et al., 2007; Tippayamontri et al. 2009). By introducing a radioprotector into the solution, a competition is created between the ferrous ions and the radioprotector for the reaction with radical species produced by the radiolysis of water. By inference, appropriately reductive molecular species in biological system will act in the same way, being, in turn, oxidized in the process (Alpen, 1998). However, one obvious disadvantage of the Fricke dosimeter is that it operates under highly acidic conditions (pH 0.46), which may degrade biological compounds. In contrast, the pH of the polyacrylamide gel (PAG) dosimeter is almost neutral (pH 5.3), such that degradation of compounds is much less probable. Accordingly, we have tested whether the PAG dosimeter

could be used to evaluate the radioprotection offerred by cystamine. In order to establish the reliability of the methods, these efficiencies should be tested by using well-known biochemical systems, such as the conjugated diene formation in low-density lipoprotein (LDL) peroxidation. Thus, the lipid peroxidation of LDL extracted from human blood has been used to confirm the protective effect of cystamine (Figure 2). Lipid peroxidation has been broadly defined as the "oxidative deterioration of polyunsaturated lipids containing any number of carbon-carbon double bonds (Halliwell and Gutteridge 1985). The peroxidation process of polyunsaturated fatty acid involves free radical initiation, propagation and termination processes (Halliwell and Gutteridge 1985).

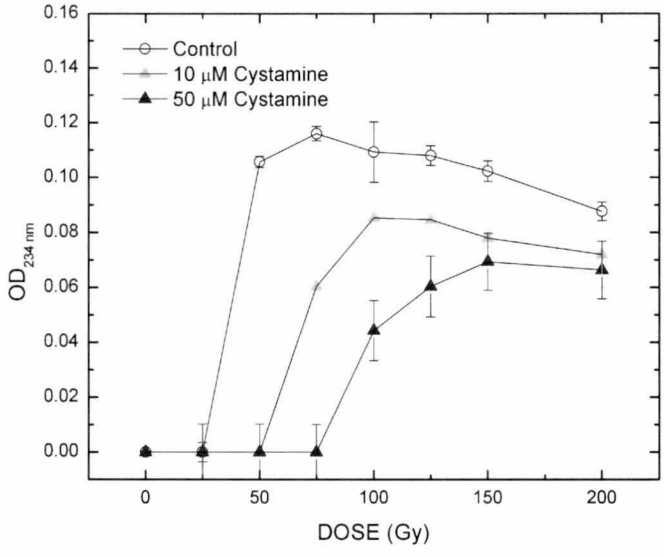

Figure 2. Plot of the optical density at 234 nm as a function of the absorbed dose for low-density lipoprotein peroxidation containing different concentrations of cystamine irradiated with ^{60}Co gamma radiation.

The oxidation process is accompanied by formation of conjugated dienes, which absorb ultraviolet light in the wavelength range 230-235 nm. Figure 2 shows the formation of conjugated diene ($OD_{234\ nm}$) in LDL exposed to free radicals produced by gamma-radiolysis of sample solutions with 0, 10 and 50 mM cystamine as a function of radiation absorbed dose. The results showed that the disulfide compounds can prevent oxidation of LDL. Since the lipid peroxidation results from the reaction of hydroxyl radicals with LDL, this suggests that cystamine mainly scavenges OH radicals. The results were confirmed by

gel electropholysis of lipoprotein (Figure3). These results are in agreement with experimental and simulation data of Fricke system.

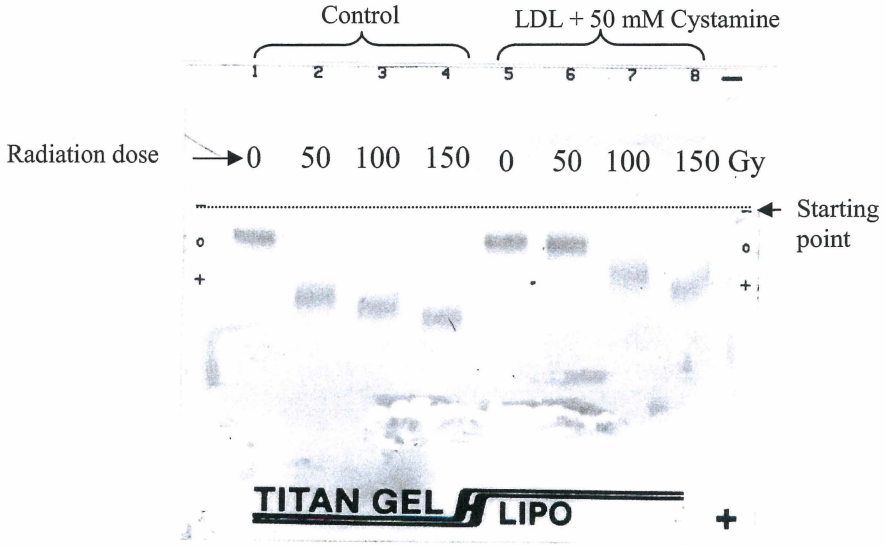

Figure 3. Electrophoresis gel revealing the effect of cystamine upon oxidative modification of LDL. LDL was exposed to water free radicals generated by gamma radiation (dose rate 3.44 Gy/min). Samples contained 0 mM (control) or 50 mM of cystamine.

V. 3.2 Monte-Carlo simulation study

As we mentioned in Chapter II, modeling of chemical reactions that occur during this stage is included in the computer program IRT, which is based on the approximation that reaction time of each pair of reactants is independent of the presence of other particles in the system. In essence, the simulation begins by considering the initial spatial distribution of the reactants. The separation between all the pairs of particles is calculated. Overlapping pairs are allowed to react immediately, and for each potentially reactive, surviving pair, the reaction time is stochastically sampled according to the time-dependent survival function that is appropriate for the type of reaction considered. This function depends on the initial distance separating the species, their diffusion coefficients, their coulombic interactions, their reaction radius, and the probability of reaction during one of their encounters (Mozumder and Magee, 1966; Buxton, 2004; Cobut et al., 1998; Meesungnoen and Jay-Gerin, 2005; Meesungnoen and Jay-Gerin, 2010). The competition

between the various reactions is taken into account by realizing them in the ascending order of sampled reaction times. Thus, the reaction rate constant plays an important role to simulate these reactions in a certain system.

Some reaction rates for cystamine in the Fricke solution have not been reported yet. Fortunately, there is a variety of structurally different sulfur-containing compounds for which the reaction rate constants with radicals are similar (Murry, 1997). For example, some rate constants for the reaction of disulfides with OH radical are shown in Table 1.

Table 1: Rate constants for the reaction of disulfides with hydroxyl radicals

RSSR	**k ($M^{-1}S^{-1}$)**	**Reffernce**
CH_3-CH_2-S-S-CH_2-CH_3	$1.4 \pm 0.5 \times 10^{10}$	Bonifačić et al., 1975
CH_3-CH_2-CH_2-S-S-CH_2-CH_2-CH_3	$2.0 \pm 0.5 \times 10^{10}$	Bonifačić et al., 1975
+NH_3-CH_2-CH_2-S-S-CH_2-CH_2-NH_3+ (Cystamine)	1.7×10^{10}	Mišík et al., 1999
+NH_3-CH_2-CH_2-S-H (Cysteamine)	2.0×10^{10}	Mišík et al., 1999

In this case, we have estimated the rate constants of unknown values from compounds that have a comparable chemical structure to cystamine such as glutathione and cysteine. We used trial and error of the simulation in order to set a proper rate constant of these reactions. The computer simulation has been carried out not only to reproduce the experimental results but also to deduce the reactions that are effectively intervening in the Fricke system.

V. 4 Evaluation absorbed dose of femtosecond laser pulse filamentation by Fricke and PAG dosimeter

V. 4.1 Dosimetry for femtosecond laser pulse filamentation

In high dose rate radiations such as pulsed radiolysis studies, the dosimetry is different from those used with low intensity radiations because of the very much higher absorbed dose rate involved (~10^6 to 10^{10} Gy/s). In this study, the dose rate of laser filametation is similar to pulse radiolysis. Only chemical dosimeters can be used to evaluate the absorbed dose from femtosecond laser pulse irradiation because of their transparency that enables the generation of the filametation process. We therefore used Fricke and ceric-cerous dosimeters to measure the absorbed dose of the laser filamentation. The former was a modified dosimeter to the so-called "super-Fricke dosimeter", which is obtained by saturating the solution with oxygen. The advantage of the super-Fricke solution is that it can be used for high dose rate radiations (~10^8 Gy/s) (Spinks and Woods, 1990). The latter was also recommended to evaluate the absorbed dose for high intensity radiations (Hummel et al., 1953). It is normally crucial to use a dosimeter validated for the dose rate of the irradiation source and the associated *G*-value of the various radiolysis products in order to determine the true absorbed dose. However, the production yields for laser filamentation have not been defined in any dosimter yet. In the Fricke dosimeter, the yield of Fe^{3+} depends on the linear energy transfer (LET) of the incident radiation. For low LET values (~0.37 keV/μm) such as gamma photons from Cs^{137}, $G(Fe^{3+})$ is equal to 15.3 ± 0.3 molecules/100 eV (Spinks and Woods 1990). From the estimated kinetic energy of the electron in filamentation deposited in water, 6.5 eV, the LET is expected to be ~1 keV/μm (Meesungnoen *et al* 2002). The yield of Fe^{3+} should then be 15.3 ± 0.3 (Spinks and Woods 1990). In other words, the same dose of gamma photons or of laser filamentation induced electrons is expected to result in the same production of Fe^{3+} in the Fricke dosimeter. If these assumptions are right, then the dose rate of filamentation in 2 ml of the Fricke solution was 2.8 ± 0.1 Gy/s. If we corrected this value for the time of light propagation in the sample cell and the volume of laser filamentation in the solution (as shown in Chapter IV), the local dose rate in laser filament was 1.0 ± 0.1 × 10^{11} Gy/s. For such a high dose

rate, it is very likely that recombination of radical species will occur before reaction with Fe^{2+}. Consequently, the value provided can merely be interpreted as an underestimation of the yield of Fe^{3+} (Ferradini and Pucheault, 1987). Additional information can be obtained with the ceric-cerouse dosimeter, which is recommended for high dose rate radiations. At very high dose rate (~10^{10} Gy/s), the yield of ceric ions depends on the yield of H_2O_2, which was 1.4 molecules/100 eV (Ferradini and Pucheault, 1987). The dose rate deposited in 2 ml ceric-cerous solution was 7.8 ± 0.1 Gy/s and the calculated dose rate in filamentation volume was 2.8 ± 0.4 × 10^{11} Gy/s (Chapter IV). Obviously, the results suggest that the laser pulse filamentation can be used as a very high dose rate source in irradiated microscopic volume. The validity of these dosimeters at extremely high dose rates has not been reported. Reassuringly, the values we found with both dosimeters are of the same order of magnitude (i.e., 10^{11} Gy/s).

Aqueous solutions of thiocyanate are commonly used as a dosimeter for pulse radiolysis because $(SCN)_2^{\bullet-}$ formed in reaction as following, has a strong absorption band at 475 nm (Buxton, and Stuart, 1995).

$$SCN^- + {}^{\bullet}OH \xrightarrow{SCN^-} (SCN)_2^{\bullet-} + OH^-$$

With the limitation of instruments, we did not use the dosimeter to confirm the dose rate of the laser pulse filamentation.

V. 4.2 Filamentation of ultrashort light pulses in scattering media

The availability of laser pulses with femtosecond duration allows materials to be subjected to higher laser intensity than ever before, opening the door to study of laser/material interactions in a new regime (Schaffer et al., 2001). From a practical point of view, the laser technique offers new challenges and provides new opportunities. In this study, we have shown effect of laser filamentation in transparent media such as chemical dosimeters, thymidine solution, DNA in buffer solution and polyacrylamide gel dosimeter (PAG). In these materials, the laser induced filamentation produces the same effects as ionizing radiations (γ and X-ray), although with a much higher local dose rate. As

mentioned earlier, the filamentation of the ultrashort laser pulses in the nonlinear media (transparent materials) response to the intense light field, resulting in contraction and reshaping of the laser beam accompanied by spectral broadening, plasma generation, temporal reshaping, and sub-diffractive propagation (Couairon and Mysyrowicz 2007; Chin et al., 2005; Vogal et al., 2005). In a transparent medium, there is no linear absorption of the incident laser light because there are no allowed electronic transitions at the energy of the incident photon. Thus, the absorption of light must be a nonlinear effect. However, most biological tissues are characterized by strong optical scattering and hence are referred to as either *scattering media* or *turbid media* (Wang and Wu 2007) because photons traveling within them are predominantly scattered rather than absorbed (Yodh and Chance, 1995). The propagation of laser filamentation in living tissues is not clear yet (Jukna et al., 2009). Here, the PAG dosimeter has been used as a transparent sample to demonstrate effect of laser filamentation in a radiologically tissue-equivalent sample. In fact, the PAG is tissue-equivalent radiological properties for ionizing radiations because the electron density and effective atomic number of the PAG dosimeter are similar to biological tissues (Venning et al., 2005). The optical properties are however different between the gel dosimeter and biological materials as we mentioned above. It has been previously reported that adding a scattering material such as milk (Yodh, and Chance, 1995) or microspheres (Jukna et al., 2009) yields a turbid medium. In fact, milk is an excellent light-diffusing material and a complex biological fluid composed of water, fat, protein, lactose, citric acid, and inorganic compounds (Crofcheck et al., 2002). Light scattering by fat globules and casein micelles causes milk to appear turbid and opaque. These two components scatter light differently based on differences in size, number, and optical properties (e.g., index of refraction) of the particles (Crofcheck et al., 2002). The casein micelles are much smaller than the fat globules. The average particle diameter of casein micelles falls in the range of 100–300 nm and milk fat in the form of globules in the range of 0.1–10 μm for unhomogenized milk, with a mean diameter of 3.4 μm (Crofcheck et al., 2002; Alexander et al., 2002). Accordingly, we have added 2 % fat of milk in PAG gel dosimeter as shown in figure 4. It is shown that the light scattering introduced by the milk (0.1 and 0.2 % in the gel) shifts the nonlinear focus (emergence of the filament) toward further propagation distance and produces somewhat shorter filaments. These results are good agreement with

Jukna et al. (Jukna et al., 2009) even though they used aqueous suspension of 2 μm polystyrene microspheres as a scattering material.

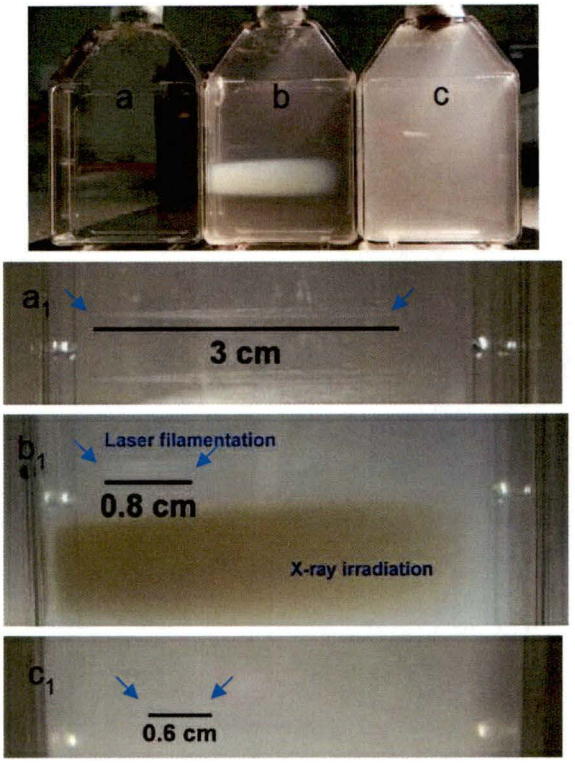

Figure 4. Photographs of containers fill with polyacylamide gel dosimeter (a) without milk, (b) with 0.1 % of milk (2 % of fat), (c) with 0.2 % of milk (2 % of fat). The gels were irradiated by femtosecond Ti-sapphire laser beams in the same condition with the following properties: pulse duration was 100 fs; pulse energy was 0.3 mJ/pulse; repetition rate was 1 kHz; and the central wavelength was 800 nm. The laser beam was focused by a 30 cm focal length achromatic lens. In (b), in order to compare with laser filamentation, the polymer gel was irradiated by X-ray from Therapax HF 150T (x-ray therapy system). Fig. a_1, b_1 and c_1 are zooms of the filamentation track of the sample a, b and c respectively. The scale bars show size of filamentation from starting point to the end (blue arrows) of filamentation.

V. 4.3 Ultrahigh dose rate from femtosecond laser pulse filamentation

When an intense femtosecond laser pulse is focused into transparent media, it will self-focus into a string of intense spots. From each of these intense spots, a strong white light is generated in the forward direction. The phenomenon is so called light bullet (Silberberg, 1990), supercontinuum generation (Chin and Lagacé, 1996; Couairon, and Mysyrowicz, 2007), or filamentation (Weyl, 1989; Chin and Lagacé, 1996; Chin, 2006;

Couairon and Mysyrowicz, 2007) which is believed to be mainly the result of self-phase modulation. In our results, it is obvious that the ultra-fast laser pulse filamentation can be used as a very high dose rate source (Chapter III). The dose rate of laser filamentation is estimated by radiation chemical dosimeters to about 10^{12} Gy/s. High dose rate radiation has been studied before. Dewey and Boag (Dewey, and Boag, 1959) first demonstrated that at ultrahigh dose rate of about 10^{9} Gy/s of X-ray irradiation, the level of oxygen may be depleted, which leads to increased survival of bacteria. When oxygen is present, the oxygen molecules can react with radiation-induced free radicals at diffusion-controlled reaction ($\sim 10^{10}$ $M^{-1}S^{-1}$) (Sonntag, 2006) to cause irreparable biological damage, and their results have been confirmed by many groups (see Town 1967; Berry and Hall 1969; Ling et al., 1978; Hall and Brenner 1991; Tillman et al., 1999). Thus, the ultrahigh dose rate may be exploited in radiation therapy as means of killing cells that is independent of oxygen tension since at sufficiently high dose rate even aerated cells exhibit an anoxic-like response (Hall and Brenner 1991). As such, extremely high dose rates are of potentially great interest in radiotherapy. Unfortunately, with the conventional radiations, the machines which are capable of achieving suitably high dose rates are simply in principle but costly and cumbersome in practical applications (Berry and Hall 1969). Here, we have demonstrated that intense laser pulse filamentation is a source of ultrahigh dose rate irradiation. It is not only non-ionizing radiation, but also it is much cheaper as compared with conventional radiation sources.

V. 4.4 High dose rate for sterilization

Radiosterilization has been extensively used for thermosensitive medical materials such as catheters, syringes, artificial joints, and raw material pharmaceuticals (IAEA, 2008). However, the use of ionizing radiation for drugs in aqueous solution is not even considered. There is a consensus that the radiation sterilization should not be applied to drugs in aqueous solution because of the greater degradation of the drug compared to the solid state (Boess and Bogl, 1996). The degradation of a drug solute in aqueous solution results from free radicals generated by the water radiolysis and depends on several parameters such as the absorbed dose, the dose rate, the temperature and the drug

concentration (Slegers and Tilquin, 2005). In particular, it is very important to investigate how the dose rate can be adjusted to optimize the destruction or the protection of irradiated materials, especially pharmaceuticals in aqueous solution (Slegers and Tilquin, 2005). From simulation method, these authors have shown that a ultrahigh dose rate, of ~10^{12} Gy/s (maximum dose rate for electron beam) can be used to sterilize drugs in aqueous solution. The protective effect of the very high intensity of the radiation could be due to the high radical-radical recombination rate in ionization spurs before radicals have time to diffuse and react with substrate solute molecules. Thus, the very high dose rate of laser induced filamentation process may find an application in drug sterilization.

V. 4.5 Radiation chemistry of femtosecond laser pulse filamentation

Laser pulses generate an avalanche of low energy electrons by the inverse Bremsstrahlung and multiphoton ionization processes in liquid water. Filamentation creates molecular and radical species in aqueous solution. These electrons are generated in massive amounts (in the range of ~10^{17} cm^{-3}). The excess energy of LEEs is transferred to the surrounding water molecules. The process can lead to form radical and molecular species. These chemically reactive species can react with substrates in chemical and biological system as show in Chapter III. A main objective of the study is to investigate the potential of high-power laser filamentation in radiation treatment. So, it is important to know the yield of radiolysis products. Here, we have measured the yield of H_2O_2 and hydroperoxides from irradiated water and 1 mM thymidine solution with and without catalase, respectively (Figure 5). In Figure 5, it shown that the yield of hydrogen peroxide higher than yield of thymidine hydroperoxide. These results can confirm high dose rate of the laser pulse induced filamentation. It is due to the fact that at the high dose rate there are recombinations of radical species before reaction with substrates (thymidine).

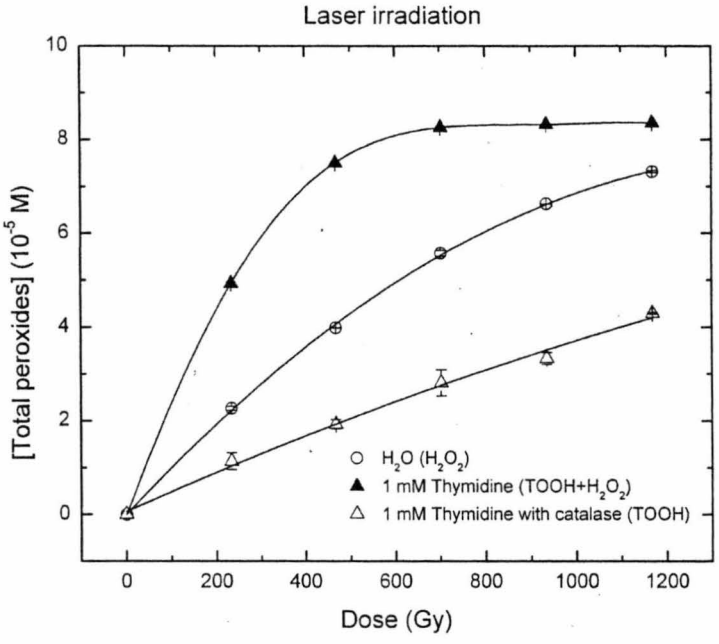

Figure 5. Yield of total hydroperoxides in de-ionized water as a function of dose in the ceric-cerous dosimeter without thymidine (○), with 1 mM thymidine (Δ) and 1 mM thymidine with catalase (▲). The sample solutions were irradiated by femtosecond Ti-sapphire laser beams with the following properties that generated filamentation: pulse duration was 100 fs; pulse energy was 0.3 mJ/pulse; repetition rate was 1 kHz; and the central wavelength was 800 nm. The dose rate was 475 ± 6 Gy/min as measured by the ceric-cerous dosimeter.

We explored further applications of the radiation chemistry of the laser filamentation process. Conventional radiation synthesis is a powerful technique (Henglein, 1993) that can be used to synthesize metal particles without adding reducing agents (Treguer et al., 1998; Gachard et al., 1998; Remita et al., 2005). For example, gold nanoparticles (GNPs) can be synthesized by several radiations such as gamma (Treguer 1998; Gachard et al., 1998;), high intensity of x-ray (synchrotron) (Wang et al., 2008), electrons (Seino et al., 2008), C^{6+} ion (Remita et al., 2005), and high-power laser pulse (Besner et al., 2007).

In the metal colloid radiation synthesis, the solvated electrons and reducing organic radicals play an important role to reduce multivalent metal ions to monovalent state to form nanoparticles (see Treguer et al., 1998; Gachard et al., 1998; Remita et al., 2005). In reality,

the primary species generated by the radiation interaction with the liquid water are (Meesungnoen and Jay-Gerin, 2010):

$$H_2O \rightsquigarrow e_{aq}^-, H^+, H^\bullet, {}^\bullet O^\bullet, {}^\bullet OH, OH^-, HO_2^\bullet (\text{or } O_2^{\bullet-}, pKa = 4.8), H_2, O_2 \text{ and } H_2O_2.$$

At the neutral condition (pH 7), the radiolytic species are: $G(e_{aq}^-) = 2.65$, $G(H^\bullet) = 0.6$ and $G({}^\bullet OH) = 2.8$ elementary species per 100 eV absorbed energy, as we have shown in Chapter I. In gold nanoparticle (GNP) radiation synthesis, gold ions ($Au^{III}Cl_4^-$), are reduced by e_{aq}^- and 2-propanol radicals ($[CH_3]_2{}^\bullet CHOH$) as follows (Treguer et al., 1998; Gachard et al., 1998; Remita et al., 2005):

$$[CH_3]_2CHOH + {}^\bullet OH\ (H^\bullet) \rightarrow [CH_3]_2{}^\bullet COH + H_2O\ (\text{or } H_2),$$

$$Au^{III}Cl_4^- + e_{aq}^-\ (\text{or } [CH_3]_2{}^\bullet COH) \rightarrow Au^{II}Cl_4^{2-} + (\text{or } [CH_3]_2CO + H^+),$$

$$2Au^{II}Cl_4^{2-} \rightarrow Au^{III}Cl_4^- + Au^{I}Cl_2^- + 2Cl^-,$$

$$Au^{I}Cl_2^- + e_{aq}^-\ (\text{or } [CH_3]_2{}^\bullet COH) \rightarrow AuCl_2^-\ (\text{or } [CH_3]_2CO + H^+).$$

Finally, the radiolytic formation of gold atoms ($AuCl_2^-$) can interact with each other and aggregate to form clusters of higher nuclearity surrounded by chloride anions to form GNPs (Gachard et al., 1998). The formation of GNPs can be measured by UV spectrophotometry since the metallic particles absorb UV light at 520 nm.

Here, we used laser pulse filamentation to generate hydrated electrons and the alcohol radicals to synthesize GNPs. It should be noted that the hydrated electrons can also be formed by laser pulse filamentation (Brastaviceanu, 2004). We tested whether laser filamentation could offer advantages in the synthesis of GNPs (Figure 6). Figure 6 show that the optical absorption of GNPs increases as a function of irradiation time. The chemical compositions of solutions in the experiment were the same as gamma irradiation, as reported by Gachard et al (Gachard et al., 1998). These results are consistent with our interpretation that the radiation chemistry of filamentation is similar to conventional radiations. It should be remarkable that in gamma radiation synthesis of GNPs, the induction dose assigned to the start of gold reduction is doubled when the initial gold

compound concentration is doubled (Gachard et al., 1998). Normally, the absorbed dose used for 1 mM initial concentration of gold compound was 5,000 Gy. For example, the dose rate of a gammacell (Elan 3000) of Département de médecine nucléaire et radiobiologie, Université de Sherbrooke is 12 Gy/min. In this case, irradiation during 7 hours would be required to synthesize GNPs. With the high dose rate of laser pulse filamentation, GNPs were synthesized in 10 minutes.

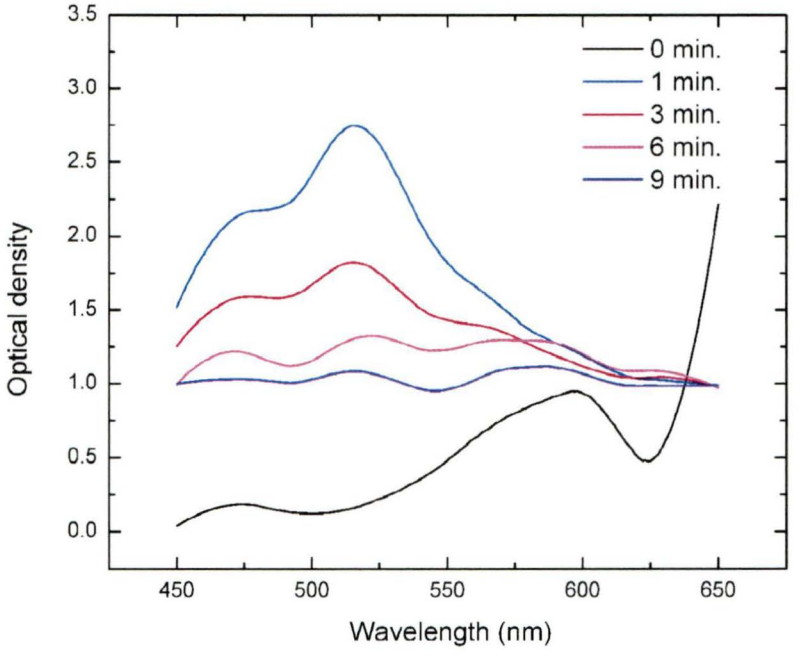

Figure 6. Evolution of absorption spectrum of gold nanoparticles as a function of wavelength for different time of laser filamentation irradiation. The sample solution was composed of 1 mM $HAuCl_4$, 0.1 M polyvinyl acetate and 0.2 M 2-propanal. The samples were irradiated by femtosecond Ti-sapphire laser beams with the following properties to generate filamentation: pulse duration was 100 fs; pulse energy was 0.3 mJ/pulse; repetition rate was 1 kHz; and the central wavelength was 800 nm.

V. 4.6 "Two bullet theory" of femtosecond laser pulse filamentation for cancer therapy

The main principle of radiation therapy is to increase the dose to tumors while minimizing radiation absorbed dose to adjacent normal, healthy tissues. The ideal dose deposition by definition is that which can be deposited in the tumor without killing normal cells. In this study, we have shown that it is possible to use ultrafast laser pulse filamentation to generate low energy electrons and free radicals, confining the high-dose treatment to tumor volume. Here, it is also feasible to use combination effects between low energy electron generation and thermal effect for cancer therapy. The idea is called "two bullet theory" and is based on using femtosecond laser pulse filamentation and gold nanoparticles. A number of biomedical applications of lasers have been established. For cancer therapeutic modalities, the effects of laser on tissue can be separated into chemical and thermal effects (Huang et al., 2008). The former is called "photodynamic therapy" (Wilson and, Patterson, 1986) which involves using a chemical sensitizer that generates reactive oxygen species and results in damage to vasculature or tumor cells. The latter is called "photothermal therapy" (Bown, 1983) whereby light absorption leads to a local temperature increase resulting in damage to tumor cells. In this study, we have shown that using femtosecond laser induced filamentation process leads to create water radiolysis species in view of its potential medical and biological application (Chapter III).

Recently, there have been several reports on a new technique of thermal therapy using gold nanoparticles (GNPs) by laser absorption (see O'Neal et al., 2004; Khlebtsov et al., 2006; Maksimova et al., 2007; Elliott et al., 2008 ; Huang et al., 2008). The use of GNPs has been shown as a method for enhancing the delivery of minimally invasive laser-induced thermal therapy. With nanoscale structure, it has been demonstrated that macromolecules and small particles in the 60–400 nm size range will extravasate and accumulate in tumors without the assistance of antibodies or other targeting moieties (Maeda et al., 2000). This behaviour has been attributed to the leaky nature of tumor vessels, which contain wide interendothelial junctions, an incomplete or absent basement membrane, a dysfunctional lymphatic system, and large numbers of transendothelial

channels (McDonald, and Baluk, 2002). The accumulation of gold nanoparticles in a tumor was found to be maximal 24 hours after injection (James et al., 2007).

In thermal therapy, this class of nanoparticles has a plamon resonance frequency that can be tuned to absorb strongly in near-infrared (750-1100 nm) portion of the spectrum. The optical plasmon resonance is caused by coherent oscillations of free metal electrons under the electric field of the illuminating light (Maksimova et al., 2007; Elliott et al., 2008). These oscillations lead to an enhanced scattering and absorption of light at the resonance wavelengths, resulting in a thermal effect (Maksimova et al., 2007), so called plasmonic photothermal therapy (PPTT) (Huang et al., 2008).

With this principle, we can use not only thermal effect from laser absorption of GNPs, but also water free radicals from generation of interaction of femtosecond laser pulse filamentation for cancer treatment. This is a novel idea which is based on a combination of direct and indirect effect of laser pulse filamentation as well as thermal effect of laser pulse filamentation to GNPs on biological materials. Thus, research in the future will be directed towards testing the hypothesis about this strategy.

VI. Conclusions

In this thesis, we have used fast, easy and quantitative techniques to evaluate efficiency of radiation sensitizers and radioprotectors. These methods are based on the polyacrylamide gel (PAG) dosimeter and the Fricke dosimeter. The radiosensitizing capacity was measured in terms of a dose enhancement in presence of a radiation sensitizer in the PAG dosimeter. Next, we have measured and simulated the radioprotective ability of some compounds at the chemical level. The protecting capacity originates from decreasing of production of Fe^{3+} in presence of radioprotector in the Fricke solution. There is a competition between the protective compound and Fe^{2+} to react with radiolysis species. Monte-Carlo simulation helped understand the mechanism of action of radioprotectors in the presence and absence of oxygen. The results clearly demonstrated that chemical dosimeters can be used to assess quantitatively the efficiency of radiation-sensitizers and protectors. In addition, we reported a very good agreement between the results of the simulations and the experimental production of Fe^{3+} in both aerated and deaerated solution. This is a great advantage of this project when one considers that ultimate objective is to compare, as effectively as possible, the results of our simulations with experiment. The results clearly suggest that the computer simulation approach developed can be useful in a detailed investigation of the action of ionizing radiations upon a system. This methods lead to understand the underlying mechanisms of action of protective compounds.

In addition, we characterized the process of femtosecond laser pulse filamentation in chemical dosimeters and biological solutions. Our measurements from ceric-cerous and Fricke dosimetry showed that the temporal energy-dose deposition rate by laser filamentation was extremely high. Moreover, the femtosecond IR laser pulse filamentation process was capable of generating a negligible entrance dose, while allowing precise control over the depth at which the dose was deposited in the medium. Our results indicated that the type of molecular damage induced by laser filamentation, be it chemical (Fricke and the ceric-cerous dosimeters, or polymerization in gels), or biological (e.g. glycosidic bond cleavage, or SSBs and DSBs in double stranded DNA), was the same as that induced by conventional X or γ rays. Moreover, a clear and substantial radiotherapeutic effect of IR laser filamentation on animal tumor model that was caused by this irradiation

method exclusively inside the targeted volume, was comparable to that of conventional clinical radiation sources used to date. Thus, we showed the feasbility of a new and unique approach to cancer therapy, using high-power infrared laser pulses.

Overall, this thesis proposed possible techniques to improve efficacy of radiation therapy using radiation sensitizers and protectors as well as a "dream beam" treatment by femtosecond laser pulse filamentation.

Acknowledgements

First of all, I would like to express my sincere gratitude to my supervisors, Prof. Jean-Paul Jay-Gerin, Prof. Abdelouahed Khalil and Prof. Martin Lepage, whose encouragement, supervision and support from the preliminary to the concluding level enabled me to develop an understanding of the subject. They are ideal mentors and this dissertation would not have been possible without them.

I am heartily thankful to the Ministry of Science and Technology of the Royal Thai Government for my scholarship. I also wish to express my profound appreciation to all professors and staff of Applied Radiation and Isotope Department, Kasetsart University and Office of Educational Affairs, Royal Thai Embassy, at Washington, DC as well as Office of the Civil Service Commission, the Royal Thai government, for their assistance during my study.

I thank Prof. Leon Sanche, Prof. Yue Zhao, Prof. Kim B. McAuley and Prof. Daniel Houde for having accepted to be on my dissertation committee and for their helpful critical reviews of this thesis.

I also wish to thank my colleagues, especially, Sunuchakan Sanguanmith, Jean-François Allard and Hakim Belmouaddine, for their assistance and interesting discussions. Those help have been very much appreciated.

It is a pleasure to thank the professors of the Department of Nuclear Medicine and Radiobiology for their excellent courses and constructive suggestions, and all the students and members, past and present, of the department, for their kind cooperation and friendship.

Last but not least, my deepest thanks and love go to my family, in particular our son, for his indulgence and understanding during the long time of this study, when I did not adequately take part in family life.

Bibliography

Adam, J.-F., Elleaume, H., Joubert, A., Biston, M-C., Charvet, A.-M., Balosso, J., Le Bas, J.-F., and Estève, F., 2003. Synchrotron radiation therapy pf malignant brain glioma loaded with an iodinated contrast agent: First trial on rats bearing F98 gliomas. *Int. J. Radiat. Oncol. Biol. Phys.* **57**, 1413-1426.

Adams, G.E. 1970. Molecular mechanisms of cellular radiosensitization and protection in *Radiation Protection and Sensitization.* Eds Harold, M., and Quintiliani, M., Taylor & Francis, London.

Adams, G.E., 1979. Prospects and problems with hypoxic cell radiation sensitizers in *Radiosensitizers of Hypoxic Cells* Eds. Breccia, A., Rimondi, C., and Adams, G. E., Elsevier Press, Amsterdam.

Alexander, M., Rojas-Ochoa, L. F., Leser, M., and Schurtenberger, P., 2002. Structure, dynamics, and optical properties of concentrated milk suspensions: an analogy to hard-sphere liquids. *J. Coll. Int. Sci.* **253**, 35-46.

Alpen, E.L., 1998. *Radiation Biophysics 2nd ed.* Academic Press, San Diego.

Anderson, D. W., 1984. *Absorption of Ionizing Radiation.* Baltimore: University Park Press.

Asmus, K.-D., 1993. Recent aspects of thiyl and perthiyl free radical chemistry in *Active Oxygens, Lipid peroxides and Antioxidants.* Eds Yagi K., CRC Press.

Austsavapromprom, N., Meesungnoen, J., Plante, 1., and Jay-Gerin, J.-P., 2007. Monte-Carlo study of the effects of acidity and LET on primary free-radical and molecular yields of water radiolysis - Application to the Fricke dosimeter, *Can. J. Chem.* 85,214-229.

Bajpai, U.D.N., and Bajpai, A.K., 1983. Permanganate/L-cycteine initiated polymerization of acrylamide. *J. Macromol. Sci.-Chem.*, **A19**, 847-500.

Baldock, C., De Deene, Y., Doran, S., Ibbott, G., Jirasek, A., Lepage, M., Mcauley, M. Oldham K.B., and Schreiner, L.J., 2010. Polymer gel dosimetry. *Phys. Med. Biol.* **55**, R1-R63.

Baldock, C., Rintoul, L., Keevil, S.F., Pope J.M., and George, G. A., 1998. Fourier transform Raman spectroscopy of polyacrylamide gels (PAGs) for radiation dosimetry *Phys. Med. Biol.* **43**, 3617-3627.

Barth, R.F., Coderre, J.A., Vicente, M.G.H., and Blue, T.E., 2005. Boron neutron capture therapy of cancer: Current status and future prospects. *Clin. Cancer Res.* **11**, 3987-4002.

Bensasson, R.V., Land, E.J., and Truscott, T.G., Excited states and Free Radicals in Biology and Medicine, Oxford University Press, Oxford.

Berry, R.J., and Hall, E.J., 1969. Survival of mammalian cells exposed to X rays at ultra-high dose-rates. *Br. J. Radiol.* **42**, 102-107.

Besner, S., Kabashin, A.V., and Meunier, M., 2007. Two-step femtosecond laser ablation-based method for the synthesis of stable and ultra-pure gold nanoparticles in water. *Appl. Phys. A.* **88**, 269-272.

Blattmann, H., Gebbers, J.O., Bräuer-Krisch, E., Bravin, A., Le Due, G., Burkard, W., Di Michiel, M., Djonov, V., Slatkin, D.N., Stepanek, J., and Laissue, L.A., 2005. Applications of synchrotron X-rays to radiotherapy *Nucl. Instrum. Meth. Phys. Res. A*, **548**, 17-22.

Boess, C., and Bogl, K. W., 1996, Influence of Radiation Treatment on Pharmaceuticals A Review: Alkaloids, Morphine Derivatives, and Antibiotics. *Drug Devel. Indust. Phar.* **22**, 492-529.

Bonifačić, M., Schäfer, K., Möckel, H., and Asmus, K.-D., 1975. Primary step in the reactions of organic disulfides with hydroxyl radicals in aqueous solution. *J. Phys. Chem.* **79**, 1496-1502.

Bonnett, R., 1995. Photosensitizer of the porphyrin and phthalocyanine series for photodynamic therapy. *Chem. Soc. Rev.* **24**, 19-33.

Boudaïffa, B., Cloutier, P., Hunting, D., Huels, M., and Sanche, L., 2000. Resonant formation of DNA strand breaks by low-energy (3 to 20 eV) electrons. *Science*, **287**, 1658-660.

Boudou, C., Troprès, I., Rousseau, J., Lamalle, L., Adam, J.F., Estève, F., and Elleaume, H., 2007. Polymer gel dosimetry for synchrotron stereotactic radiotherapy and iodine dose-enhancement measurements. *Phys. Med. Biol.* **52**, 4881-4892.

Bown, S.G., 1983. Phototherapy of tumors. *World J. Surg.*, **7**, 700-709.

Brastaviceanu, T. 2004. *M.Sc. Thesis*, Université de Sherbrooke

Brodeur, A., and Chin, S. L., 1998. Band-gap dependence of the ultrafast white-light continuum. *Phys. Rev. Lett.* **80**, 4406-4409.

Bump, E.A., 1997. Introduction in *Radioprotectors:Chemical, Biological, and Clinical perspectives.* Eds. Bump, E.A., and Malaker K.,CRC Press, Boca Raton.

Bump, E.A., and Brown, J.M., 1990. Role of glutathione in the radiation response of mammalian cells *in vitro* and *in vivo*. *Pharmac. Ther.* **47**, 117-136.

Buxton, G. V., and Stuart, C. V., 1995, Re-evaluation of the thiocyanate dosimeter for pulse radiolysis. *J. Chem. Soc. Faraday Trans.* **91**, 279-281.

Buxton, G.V., 2004. The radiation chemistry of liquid water principles and applications. in *Charged Particle and Photon Interactions with Mater.* Eds Mozumder, A. and Hatano, Y., Marcel Dekker, Inc., New York.

Chaudière, J., 1994. Some chemical and biochemical constraints of oxidative stress in living cells in *Free radical Damage and Its Control.* Eds. Rice-Evans, C.V., and Burdon, R.M., Elsevier, Amsterdam.

Chin, S.L., 2006. Some Fundamental concepts of femtosencond laser filamentation. *J. Kor. Phys. Soc.*, **49**, 281-285.

Chin, S.L., and Lagacé S., 1996. Generation of H2, O2, and H2O2 from water by the use of intense femtosecond laser pulses and the possibility of laser sterilization. *Appl. Optic.* **35**, 907-911.

Chin, S.L., Hosseini, S.A., Liu, W. Luo, Q., Théberge, F., Aközbek, N., Becker, A. Kandidov, V.P., Kosareva, O.G., and Schroeder, H., 2005. The propagation of powerful femtosecond laser pulses in optical media: physics, applications and new challenges. *Can. J. Phys.* **83**, 863-905.

Christiansan, C., Pichler, W.J., Skptland, T., 2000. Delayed allergy-like reactions to x-ray contrast media: mechanistic considerations. *Eur. Radiol.* **10**, 1965-1975.

Clifford, P., Green N.J.B., and Pilling, M.J., 1982. Monte Carlo simulation of diffusion and reaction in radiation-induce spurs comparisons with analytic models. *J. Phys. Chem.* **86,** 1322-1327.

Clifford, P., Green, N.J.B., Oldfield, M.J., Pilling M.J., and Pimblott, S.M., 1986. Stochastic models of multi-species kinetics in radiation-induces spurs. *J. Chem. Soc., Faraday Trans.* 1, **82,** 2673-2689.

Cobut, V., Frongillo, Y., Patau, J.P., Goulet, T., Fraser M.J., and Jay-Gerin, J.-P., 1998 Monte Carlo simulation of fast electron and proton tracks in liquid water-I. Physical and physicochemical aspects. *Radiat. Phys. Chem.* **51,** 229-243.

Coderra, J.A., and Morris, G.M., 1999. The radiation biology of boron neutron capture therapy. *Radiat. Res.* **151,** 1-18.

Corde, S., Joubert, A., Adam, J.-F., Charvet, A.-M., Le Bas, J.-F., Estève, F., Elleaume, H., and Balosso J., 2004. Synchrotron radiation-based experimental determination of the optimal energy for cell radiotoxicity enhancement following photoelectric effect on stable iodinated compounds *Br. J. Cancer* **91,** 544-551.

Couairon, A., and Mysyrowicz, A., 2007. Femtosecond filamentation in transparent media. *Phys Rep* **441,** 47-189.

Crofcheck, C. L., Payne, F. A., and Mengüç M. P., 2002. Characterization of milk properties with a radiative transfer model. *Appl. Opt.* **41,** 2028-2037.

Dawson, P., Penhaligon, M., Smith e., and Saunders, J., 1987. Iodinated contrast agent as "radiationsensitizers". *Br. J. Radiol.* **60** 201-203.

De Deene, Y., Hurley, C., Venning, A., Vergote, K., Mather, M., Healy, B.J., and Baldock, C., 2002. A basic study of some normoxic polymer gel dosimeters. *Phys. Med. Biol.* **47,** 3441-3463.

De Deene, Y., Venning, A., Hurley, C., Healy, B.J., and Baldock, C., 2002. Dose–response stability and integrity of the dose distribution of various polymer gel dosimeters. *Phys. Med. Biol.* **47,** 2459–2470.

Denekamp, J., 1984. Vascular endothelium as the vulnerable element in tumours. *Acta. Radiol. Oncol.* **23,** 217-225.

Denekamp, J., 1993. Angiogenesis neovascular proliferation and vascular pathophysiology as targets for cancer therapy. *Br. J. Radiol.* 66, 181-196.

Dewey, D.L., and Boag, J.W., 1959. Modification of the oxygen effect when bacteria are given large pulses of radiation. *Nature Lond.* **183**, 1450-1451.

Draganić, I.G., and Draganić, Z.D., 1971 *The Radiation Chemistry of Water*, Academic Press, New York.

Dugal, P.-C., Huels, A.H., and Sanche, L., 1999. Low-energy (5-25 eV) electron damage to homo-oligonucleotides. *Radiat. Res.* **151**, 325-333.

Dunne-Daly, C.F., 1999. Principles of radiotherapy and radiobiology. *Semin. Oncol. Nurs.* **15**, 250-259.

El Sammahy, A., White, H.L., and Trumbore, C.N., 1964. Scavenging action in g-irradiated aqueous cysteine solutions. *J. Amer. Chem.* Soc. **86**, 3177-3178.

Elliott, A.M., Stafford, R.J., Schwartz, J., Wang, J. Shetty, A.M., Bourgoyne, C., O'Neal, P., and Hazle, J.D., 2008. Laser-induced thermal response and characterization of nanoparticles for cancer treatment using magnetic resonance thermal imaging. *Med. Phys.* **37**, 3102-3108.

Ertl, H.H., Feinendegen, L.E., and Heiniger, H.J., 1970. Iodine-125, a tracer in cell biology: Physical properties and biological aspects. *Phys. Med. Biol.* **15**, 447-456.

Fairchild, R.G., Brill, A.B. and Ettinger, K.V., 1982. Radiation enhancement with iodinated deoxyuridine. *Invest. Radiol.* **17**, 407-416.

Farajollahi, A.R., Bonnett, D.E., Tattam, D. and Green, S., 2000. The potential use of polymer gel dosimetery in boron neutron capture therapy. *Phys. Med. Biol.* 45, N9-N14.

Feinendegen, L.E., 1975. Biological damage from the Auger effect, possible benefits. *Rad. and Environm. Biolphys.* **12**, 85-99.

Ferradini, C. and Pucheault, J., 1983. *Biologie de l'Action des Rayonnements Ionisants.* Masson, Paris.

Ferradini, C., and Jay-Gerin, J.-P., 2000. The effect of pH on water radiolysis: A still open question - A minireview. *Res. Chem. Intermed.* **26**, 549-565.

Fronggillo, Y., Goulet, T., Fraser, M.-J., Cobut, V., Patau J.P., and Jay-Gerin, J.-P., 1998. Monte Carlo simulation of fast electron and proton tracks in liquid water-II. Nonhomogeneous chemistry. *Radiat. Phys. Chem.* **51**, 229-243.

Fruhner, H., and Kretzschmar, G., 1989. Effect of pH on the binding of alkyl sulfates to gelatine. *Colloid. Polym. Sci.* **267**, 839-843.

Gachard E, Remita, H., Khatouri, J., Keita, B., Nadjo, L., and Belloni, J., 1998. Radiation-induced and chemical formation of gold clusters. *New J. Chem.*, 1257-1265.

Garewal, H.S., 1997. *Antioxidants and Disease Prevention.* CRC Press, Boca Raton.

Gilbert, D.L., and Colton, C.A., 1999. *Reactive Oxygen Species in Biological Systems: an Interdisciplinary Approach.*, Kluwer Academic, New York.

Gochberg, D.F., Kennan, R.P., Maryanski. M.J., and Gore, J. C., 1998. The role of specific side groups and pH in magnetization transfer in polymers. *J. Magn. Reson.* **131**, 191–198.

Goulet T., and Jay-Gerin, J.-P., 1992 On the reactions of hydrated electrons with $^{\bullet}OH$ and H_3O^+. Analysis of photoionization experiments. *J. Chem. Phys.* **96**, 5079-5087.

Goulet, T. Fraser, M.-J., Frongillo, Y., and Jay-Gerin, J.-P., 1998. On the validity of the independent reaction times approximation for the description of the nonhomogeneous kinetics of liquid water radiolysis. *Radiat. Phys. Chem.* **51**, 85-91.

Goulet, T., Bernas, A., Ferradini, C., and Jay-Gerin, J.-P., 1990. On the electronic structure of liquid water: conduction-band tail revealed by photoionization data. *Chem. Phys. Lett.* **170**, 492-496.

Hall, E. J., and Brenner, D.J., 1991. The dose-rate effect revisited: Radiobiological considerations of importance in radiotherapy. *Int. J. Radiat. Oncol. Biol. Phys.* **21**, 1403-1414.

Hall, E. J., and Phill, D., 2006. Intensity-modulated radiation therapy, protons, and the risk of second cancers. *Int. Radiat. Oncol. Biol. Phys.* **65**, 1-7.

Hall, E.J., 2000. *Radiobiology for the Radiologist*, 5th edn. Lippincott Williams & Wilkins, Philadelphia.

Halliwell, B., 1990. How to characterize a biological antioxidant. *Free Rad. Res. Comms.* **9**, 1-32.

Halliwell, B., and Gutteridge, J.M.C., 1999. *Free radical in biology and medicine*, 3rd edn. Oxford University Press, New York.

Happen, A., and Mütze, B., 1978. Irradiation of micro-organisms with mono-energetic X-ray; Biological consequences of Auger effect. *Int. J. Radiat. Biol.* **34**, 67-72.

Hellio, D., and Djabourov, M., 2006. Physically and chemically crosslinked gelatine gels. *Macromol. Symp.* **241**, 23-27.

Henglein, A, 1993, Physicochemical properties of small metal particles in solution: "microelectrode" reactions chemisorption, composite metal particles, and the atom-to-metal transition. *J. Phys. Chem.* **97**, 5457-5471.

Herold, D.M., Das, I.J., Stobbe, C.C., Iyer R. V., and Chapman, J.D., 2000. Gold microspheres: a selective technique for producing biological effective dose enhancement. *Int. J. Radiat. Biol.* **76**, 1357-1364.

Hua, H., Chen J., and Vasilik, D.G., 2001. Photon radiation dose enhancement at material interfaces. *Appl. Radiat. Isot.* **55**, 323-326.

Huang, X., Jain, P.K., El-Sayed, I.H., and El-Sayed, M.A., 2008. Plasmonic photothermal therapy (PPTT) using gold nanoparticles. *Lasers Med. Sci.*, **23**, 217-228.

Hubbell, J.H., and Seltzer, S.M., 2010. Ionizing Radiation Division, Physics Laboratory, NIST. http://www.kayelaby.npl.co.uk/atomic_and_nuclear_physics/4_2/4_2_1.html

Hughe, S.G., 1973. *Radiation chemistry*, Claron Press, Oxford.

Humm, J.L., and Charlton, D.E., 1988. Double strand breakage in DNA produced by the photoelectric interaction with incorporated 'cold' bromine in *DNA Damage by Auger Emitters*. Eds. Baverstock, K. F., and Charlton, D. E., Taylor & Francis, London.

Hummel, R.W., Van Cleave, A. B. and Spinks J.W.T., 1953. Betatron irradiation of aqueous ceric sulphate solution. Can. J. Chem. **31**, 1203-1210.

IAEA, 2008. *The Role of PET/CT in Radiation Treatment Planning for Cancer Patient Treatment.* (IAEA, Viena).

IAEA, 2008. *Trends in Radiation Sterilization of Health Care Products*. IAEA, Vienna.

ICRU Report 16, 1970. Linear Energy Transfer. International commission on Radiation Units and Measurements, Washington, DC.

James, W.D., Hirsch, L.R., West, J.L., O'Neal, P.D., and Payne, J.D., 2007. Application of INAA to the build-up and clearance of gold nanoshells in clinical studies in mice. *J. Radioanal. Nucl. Chem.* **271**, 455-459.

Jayson, G.G., and Wilbraham, A.C., 1968. The utilisation of Fricke dosimeter for evaluating the biological radiation-protective potential of water-soluble organic compounds. *Chem. Commun. (London)*, 641-642.

Johannin-Gilles, A., and Vodar, B., 1954. Sur le spectre d'absorption de la vapeur d'eau dans l'ultraviolet de Schumann. *J. Phys. Radium* **15**, 223-224.

Johns, H.E., and Cunningham, J.R., 1969. *The Physics of Radiology 3rd ed.*, Springfield, IL.

Johns, H.E., Hunt, J.W. and Fedoruk, S.O., 1954. Surface back-scatter in the 100 kV to 400 kV range. *Br. J. Radiol.* **58**, 345-356.

Joubert, A., Biston, M.-C., Boudou, C., Ravanat, J.-L., Brochard, T., Charvet, A.-M., Estève, F., Balosso, J. and Foray, N., 2005. Irradiation in presence of iodinated contrast agent results in radiosensitization of endothelial cells: Consequences for computed tomography therapy. *Int. J. Radiat. Oncol. Biol. Phys.* **62**, 1486-1496.

Jukna, V., Tamošauskas, G., Valiulis, G., Aputis, M., Puida, M., Ivanauskas, F., and Dubietis, A., 2009. Filamentation of ultrashort light pulses in a liquid scattering medium. *Appl. Phys. B* **94**, 175-179.

Kamarnisky, L.A., Christopherson, R.J., and Basu, T.K., 2003. Sulfur: Its clinical and toxicologic aspects. *Nutrition.* **19**, 54-61.

Khlebtsov, B., Zharov, V., Melnikov, A., Tuchin, V., and Khlebtsov, N., 2006. Optical amplification of photothermal therapy with gold nanoparticles and nanoclusters. *Nanotech.* **17**, 5167-5179.

Kiefer, J., 1990. Biological Radiation Effects. Springer-Verlag, Berlin Heidelberg.

Klassen, N.V., 1987. Primary products radiation chemistry in *Radiation Chemistry.* Eds Farhataziz and Rodgers, M.A.J., VCH Publishers, Inc.

Knoll, G.F., 2000. *Radiation Detection and Measurement. 3rd ed.* John Wiley, New York.

Kock, C.J., 1998. The mechanisms of radiation protection by non-protein sulfhydryls: Glutathione, Cysteine, and Cysteamine in *Radioprotectors:Chemical, Biological, and Clinical perspectives.* Eds. Bump, E. A., and Malaker, K., CRC press, Boca Raton.

Lalitha, B., and Mittal, J. P., 1971. Electron transfer reaction in the radiation chemistry of some biologically important disulphide compounds. *Radiat. Eff.* **7**, 159-162.

Lampe, F.W., Field, F.H., and Franklin, J.L., 1957. Reaction of gasous ion IV, Water. *J. Amer. Chem. Soc.* **79**, 6132-6135.

Lehnert, S., 2008. *Biomolecular Action of Ionizing Radiation.* Taylor & Francis, New York.

Lepage M., and Jordan, K., 2010. 3D dosimetry fundamentals: gels and plastics. *J. Phys.: Conf. Ser.* 250, 012055.

Lepage, M. and Gore, J.C., 2004. Contrast mechanisms in magnetic resonance imaging. *J. Phys.:Conf. Ser.* **3**,78-86.

Lepage, M., Jayasakera, P.M., Bäck, S.Å.J., and Baldock, C., 2001a. Dose resolution optimization of polymer gel dosimeters using different monomers. *Phys. Med. Biol.* **46**, 2665-2680.

Lepage, M., Whittaker, A.K., Rintoul L., and Baldock, C., 2001b. ^{13}C-NMR, ^{1}H-NMR and FT-Raman study of the radiation-induced modifications in radiation dosimetry polymer gels *J. Appl. Polm Sci.* **79**, 1572-1581.

Lepage, M., Whittaker, A.K., Rintoul, L., and Baldock, C., 2000. ^{13}C-NMR, ^{1}H-NMR, and FT-Raman study of radiation-induced modifications in radiation dosimetry polymer gels. *J. Appl. Polym. Sci.* **79**, 1572-1581.

Lepage, M., Whittaker, A.K., Rintoul, L., Bäck S.Å.J., and Baldock, C., 2001c. The relationship between radiation-induced chemical processes and transverse relaxation times in polymer gel dosimeters. *Phys. Med. Biol.* **46**, 1061-1074.

Ling, C.C., Michaels, H.B., Epp, E.R., and Peterson, E.C., 1978. Oxygen diffusion into mammalian cells following ultrahigh dose rate irradiation and lifetime estimates of oxygen-sensitive species. *Radiat. Res.* **76**, 522-532.

Logan, B.E., Murano, C., Scott, K., Gray, N.D., and Head, I.M., 2005. Electricity generation from cysteine in a microbial fuel cell. *Water Res.* **39**, 942-952.

Maeda, H., Wua, J., Sawa, T., Matsumura, and Hori, Y.K., 2000. Tumor vascular permeability and the EPR effect in macromolecular therapeutics: a review. *J. Controlled Release* **65**,271-284.

Magee, J.L., and Chatterjee, A., 1986. Track reactions of radiation chemistry in *Kinetics of Nonhomogeneous Processes* Ed. Freeman, G. R., John Wiley, New York.

Maksimova, I. L., Akchurin, G.G., Khlebtsov, B.N., Terentyuk, G.S., Akchurin, G.G., Ermolaev, I.A., Skaptsov, A.A., Soboleva, E.P., Khlebtsov N.G., and Tuchin, V.V., 2007. Near-infrared laser photothermal therapy of cancer by using gold nanoparticles: Computer simulations and experiment. *Med. Laser App.* **22**, 199-206.

Maryanski, M.J., Gore, J.C., Kennan R.P., and Schulz, R.J., 1993. NMR relaxation enhancement in gels polymerized and cross-linked by ionizing radiation: A new approach to 3D dosimetry by MRI. *Magn. Reson. Imaging* **11**, 253-258.

Maryanski, M.J., Schulz, R.J., Ibbott, G.S., Gatenby, J.C., Xie, J., Horton D., and Gore, J.C., 1994. Magnetic resonance imaging of radiation dose distributions using a polymer-gel dosimeter. *Phys. Med. Biol.* **39**, 1437–55.

Matsudaira, H., Ueno, A.M., and Furuno, I., 1980. The effect of iodine-based contrast agents on the levels of radiation-induced chromosomal aberrations. *Radiat. Res.* **84**, 144-148.

McDonald, D. M., and Baluk, P., 2002. Significance of Blood Vessel Leakiness in Cancer, *Cancer Res.* **62**, 5381-5385.

Mcjury, M., Oldham, M., Cosgrove, V.P., Murphy, P.S., Doran, S., Leach, M.O., and Webb, S., 2000. Radiation dosimetry using polymer gels: Methods and applications. *Brit. J. Radiol.* **73**, 919-929.

Meesat, R., Jay-Gerin, J.-P., Khalil, A., and Lepage, M., 2009. Evaluation of the dose enhancement of iodinated compounds by polyacrylamide gel dosimetry. Phys. Med. Biol. **54**, 5909-5917.

Meesungnoen, J. and Jay-Gerin, J.-P., 2010. Radiation chemistry of liquid water with heavy ions: Monte-Carlo simulation studies in *Charged Particle and Photon Interactions with Matter-Recent Advances, Applications and Interfaces*, CRC Press, Boca Raton.

Meesungnoen, J., and Jay-Gerin, J.-P., 2005 High-LET radiolysis of liquid water with $^{1}H^{+}$, $^{4}He^{2+}$, $^{12}C^{6+}$, and $^{20}Ne^{9+}$ ions: Effects of multiple ionization, *J. Phys. Chem. A.* **109**, 6406-6419.

Meesungnoen, J., and Jay-Gerin, J.-P., 2009. High-LET Ion Radiolysis of Water: Oxygen Production in Tracks. *Radiat. Res.* **171**, 379-386.

Meesungnoen, J., Jay-Gerin, J.-P., Filali-mouhim, A., and Mankhetkorn, S., 2002. Low-Energy Electron Penetration Range in Liquid Water. *Radiat. Res.* **158**, 657-660.

Mesa, A.V., Norman, A., Solberg, T.D., Demarco J.J., and Smathers J.B., 1999. Dose distributions using kilovoltage x-rays and dose enhancement from iodine contrast agents. *Phys. Med. Biol.* **44**, 1955-1968.

Mišík, V., Miyoshi, N., and Riesz, P. Effects of cysteamine and cystamine on the sonochemical accumulation of hydrogen peroxide-implications for their mechanisms of action in ultrasound-exposed cells. *Free Radic. Biol. Med.* **26**, 961-967.

Mozumder A. and Magee J. L., 1975. The early events of radiation chemistry. *Int. J. Radiat. Phys. Chem.* **7**, 83-93.

Mozumder, A., 1999. *Fundamentals of Radiation Chemistry*, Academic Press, San Diego.

Mozumder, A., and Magee, J.L., 1966. Theory of radiation chemistry. VII. Structure and reaction in low LET tracks. *J. Chem. Phys.* **45**, 3332-3341.

Muroya, Y., Meesungnoen, J., Jay-Gerin, J.-P., Filali-Mouhim, A., Goulet, T., Katsumura, Y., and Mankhetkorn, S., 2002. Radiolysis of liquid water: An attempt to reconcile Monte Carlo calculations with new experimental hydrated electron yield data at early times. *Can. J. Chem.* **80**, 1367-1374.

Murphy, P.S., Cosgrove, V.P., Leach, M.O., and Webb, S., 2000. A modifided polymer gel for radiotherapy dosimeter: Assessment by MRI and MRS. *Phys. Med. Biol.* **45**, 3213-3223.

Murray, D., 1997. Aminothiols in *Radioprotectors:Chemical, Biological, and Clinical perspectives.* Eds. Bump, E.A., and Malaker K., CRC Press, Boca Raton.

Murthy, M., and Lakshmanan, A. 1976. Dose enhancement due to backscatter secondary electrons at the interface of two media. *Radiat. Res.* **67**, 215-223.

Myers, D.K., Childs, J.D. and Jones, A.R., 1977. Sensitization of bacteriophage T4 to ^{60}Co-g radiation and to low-energy X radiation by bromouracil. *Radiat. Res.* **69**, 152-165.

Nair, C.K.K., Parida, D.K., and Nomura, T., 2001. Radioprotectors in radiotherapy. *J. Radiat. Res.* **42**, 21-37.

O'Neal, D.P., Hirsch, L.R., Halas, N.J., Payne, J.D., and West, J.L., 2004. Photo-thermal tumor ablation in mice using near infrared-absorbing nanoparticles. *Cancer lett.* **209**, 171-176.

Özeroğlu, C., and Kurtoğlu, A.E., 2001. The synthesis and characterization of acrylamide polymer containing R-(+)- cystamine end group. *Eur. Polym., J.* **37**, 1053-1059.

Paretzke, H.G., 1986. Radiation track structure theory in *Kinetics of Nonhomogeneous Processes* ed. G. R. Freeman, Wiley, New York.

Pimblott, S.M., and Laverne, J. A., 2007. Production of low-energy electrons by ionizing radiation. *Radiat. Phys. Chem.* **76**, 1244-1247.

Pimblott, S.M., and Mozumder, A., 2004. Modeling of physicochemical and chemical processes in the interactions of fast charged particles with matter in *Charged Particle and Photon Interactions with Mater.* Eds Mozumder, A., and Hatano, Y., Marcel Dekker, New York.

Quintiliani, M., 1987. Physico-chemical basis of radiosensitization by iodine compounds. *Radiat. Phys. Chem.* **30**, 409-422.

Regulla, D.F., Hieber, L.B. and Seidenbusch, M., 1998. Physical and biological interface dose effects in tissue due to X-ray induced release of secondary radiation from metallic gold surface. *Radiat. Res.* **150**, 92-100.

Remita, H., Lamprea, I., Mostafavia, M., Balanzatb, and E., Bouffard, S., 2005. Comparative study of metal clusters induced in aqueous solutions by γ-rays, electron or C^{6+} ion beam irradiation. *Radiat. Phys. Chem.* **72**, 575-586.

Rose, J.H., Norman, A., Ingram, M., Aoki, C., Solberg, T., and Mesa, A., 1999. First radiotherapy of human metastatic brain tumours delivered by a computerized tomography scanner. *Int. J. Radiat. Oncol. Biol.* **45**, 1127-32.

Sanche, L. 1992. Dissociative attachment and surface reaction induced by low-energy electrons. *J. Vac. Sci. Technol. B* **10**, 196-200.

Schaffer, C. B., Brodeur, A., and Mazur, E., 2001. Laser-induced breakdown and damage in bulk transparent materials induced by tightly focused femtosecond laser pulses. *Meas. Sci. Technol.* **12**, 1784-1794.

Seino, S., Kinoshita, T., Nakagawa, T., Kojima, T., Taniguci, T., Okuda, S., Takao A., and Yamamoto, T. A., 2008. Radiation induced synthesis of gold/iron-oxide composite nanoparticles using high-energy electron beam. *J. Nanopart. Res.* **10**, 1071-1076.

Sellakumar, P., Samuel E.J.J., and Supe, S.S., 2007. Water equivalent of polymer gel dosimeters. *Radiat. Phys. Chem.* **76**, 1108-1115.

Shalek, R.J., Sinclair, W.K., and Calkins, J.C., 1962. The relative biological effectiveness of 22 Mevp X-ray, cobalt-60 gamma ray, and 200-Kvcp x-ray. II. The use of the ferrous sulfate dosimeter for x-ray and gamma-ray beams. *Radiat. Res.* 16, 344-35.

Silberberg, Y., 1990. Collapse of optical pulses. *Opt. Lett.* **15**, 1282-1284.

Slavotinek, A., Mcmillan, T.J., and Steel, C.M., 1994. Measurement of radiation survival using the MTT assay. *Eur. J. Cancer* **30A**, 1376-1382.

Slegers, C., and Tilquin, B., 2005. Theoretical approach to the destruction or sterilization of drugs in aqueous solution. *Radiat. Phys. Chem.* **72**, 363-365.

Spinks, W.T., and Woods, R.J., 1990. *An Introduction to Radiation Chemistry*. 3rd ed. Wiley, New York.

Stilts, C.E., Nelen, M.I., Hilmey, D.G. Davies, S.R., Gollnick, S.O., Oseroff, A.R., Gibson, S.L., Hilf, R., and Detty, M.R., 2000. Water-soluble, core-modified porphyrins as novel longer-wave length-absorbing sensitizers for photodynamic therapy, *J. Med. Chem.* **43**, 2403-2410.

Tilikidis, A., Skog, S., and Brahme, A., 1994. Influence of radiation quality changes a microdosimetry variance and dose-response relations. *Radiat. Prot. Dos.*, 52, 43-49.

Tippayamontri, T., Sanguanmith, S., Meesungnoen, J., Sunaryo, G.R., and Jay-Gerin, J.-P., 2009. Fast neutron radiolysis of the ferrous sulphate (Fricke) dosimeter: Monte-Carlo simulations. *Recent Res. Devel. Physical Chem.* **10**, 143-211.

Town, C.D., 1967. Effect of high dose rates on survival of mammalian cells. *Nature Lond.* **215**, 847-848.

Treguer, M., Cointet, C., Remita, H., Khatouri, J., Mostafavi, M., Amblard, J., and Belloni, J., 1998. Dose Rate Effects on Radiolytic Synthesis of Gold-Silver Bimetallic Clusters in Solution. *J. Phys. Chem. B* **102**, 4310-4321.

Tubiana, M., Dutreix, J., and Wambersie, A., 1990. *Introduction of Radiobiology.* Taylor & Francis, New York.

Valko, M., Leibfritz, D., Moncol, J., Cronin, M. T. D., Mazur, M., and Telser J., 2007. Free radicals and antioxidants in normal physiological functions and human disease. *Int. J. Biochem. Cell Biol.* **39**, 44-84.

Vanlier, J. E., Tian, H., Ali, H., Cauchon, N., and Hassession, H.M., 2009. Trisulfonated porphyrazines : New photosensitizers for the treatment of retinal and sunretinal edema, *J. Med. Chem.* **52**, 4107-4110.

Venning, A.J., Nitschke, K.N., Keall, P.J., and Baldock, C., 2005. Radiological properties of normoxic polymer gel dosimeters. *Med. Phys.* **32**, 1047-1053.

Venning, A.J., Nitschke, K.N., Keall, P.J., Baldock, C., 2005. Radiological properties of normoxic polymer gel dosimeters. *Med. Phys.* **32**, 1047-1053.

Viala, J., Vanel, D., Meingan, P., Lartigau, E., Carde, P., and Renschler, M., 1999. Phases IB and II multi-dose trial of gadolinium texaphyrin, a Radiation sensitizer detectable at MR imaging: Priliminary results in Brain metastases. *Radiol.*, **212**, 755-759.

Vogel, A., 1997. Nonlinear absorption: intraocular microsurgery and laser lithotripsy. *Phys. Med. Biol.* **42**, 895-912.

Vogel, A., and Venugopalan, V., 2003. Mechanisms of pulsed laser ablation of biological tissues. *Chem. Rev.* **103**, 577-644.

Vogel, A., Noack, J., Huttman, G., and Paltauf, G., 2005. Mechanisms of femtosecond laser nanosurgery of cells and tissues. *Appl. Phys. B.*, **81**, 1015-1047.

Von Sonntag, C., 1987. *The Chemistry Basic of Radiation Biology.* Taylor & Francis, London.

Von Sonntag, C., 2006. *Free-Radical –Induced DNA damage and its repair.* Springer, Berlin.

Wang, C.-H., Liu, C.-J., Wang, C.-L, Hua, T.-E., Obliosca, J.M., Lee, K.H., Hwu, Y., Yang, C.-S., Liu, R.-S., Lin, H.-M., Je J.-H., and Margaritondo, G., 2008. Optimizing the size and surface properties of polyethylene glycol (PEG)–gold nanoparticles by intense x-ray irradiation. *J. Phys. D: Appl. Phys.* **41** 195301.

Wang, L. V., and Wu H.-I., 2007. *Biomedical Optics.* Wiley, New Jersey

Wardman, P. 1983. Principle of radiation chemistry in *The Biological Basic of Radiotherapy*. Eds Steel, G.G., Adams G.E., and Peckham, M.J. Elsevier, Amsterdam.

Wardman, P., 1987. The mechanism of radiosensitization by electron-affinic compounds. *Radiat. Phys. Chem.* **30**, 423-432.

Wardman, P., 2007. Chemical radiosensitizers for use in radiotherapy. *Clin. Oncol.* **19**, 397-417.

Weiss, J.F., and Landauer, M.R., 2003. Protection against ionizing radiation by antioxidant nutrients and phytochemicals. *Toxicology* **189**, 1-20.

Weyl, G. M., 1989. Physics of laser-induced breakdown: an update in *Laser-induced Plasmas and Application (Optical science and engineering)*. Eds L. J. Radziemski and D. A. Cremers., CRC press.

Wilson, B.C., and Patterson, M.S., 1986. The physics of photodynamic therapy, *Phys. Med. Biol.* **31**, 327-360.

Wishart, J.F., 1998. Accelerator and other sources for the study of radiation chemistry in *Photochemistry and Radiation Chemistry*. Eds Wishart, J.F., and Nocera, D.G., American Chemical Society.

Yablonovitch E. and Bloembergen, N., 1972. Avalanche ionization and the limiting diameter of filaments induced by light pulses in transparent media. *Phys. Rev. Lett.* **29**, 907-910.

Yodh, A., and Chance, B., 1995. Spectroscopy and imaging with diffusing light. *Phys. Today* **48**, 34-40.

Young, S.W., Qing, F., Harriman, A., Sessler, J.L., Dow, W.C., Mody, T.D., Hemmi, G.W., Hao, Y., and Miller, R.A., 1996. Gadolinium (III) texaphyrin: A tumor selective radiation sensitizer that is detectable by MRI. *Proc. Natl. Acd. Sci.* **93**, 6610-6615.